CELLULOSE NANOCRYSTAL/THERMOSET COMPOSITES: A PHYSICAL AND CHEMICAL ROUTE TO IMPROVING DISPERSION AND MECHANICAL PROPERTIES

A Thesis
Presented to
The Academic Faculty

by

Natalie Girouard

In Partial Fulfillment
Of the Requirements for the Degree
Doctor of Philosophy in the
School of Chemical and Biomolecular Engineering

Georgia Institute of Technology
May 2016

CELLULOSE NANOCRYSTAL/THERMOSET COMPOSITES: A PHYSICAL AND CHEMICAL ROUTE TO IMPROVING DISPERSION AND MECHANICAL PROPERTIES

Approved by:

Dr. J. Carson Meredith, Advisor
School of Chemical and
Biomolecular Engineering
Georgia Institute of Technology

Dr. Yonathan Thio
School of Chemical and
Biomolecular Engineering
Georgia Institute of Technology

Dr. Meisha Shofner, Advisor
School of Materials Science &
Engineering
Georgia Institute of Technology

Dr. Joseph Schork
School of Chemical and
Biomolecular Engineering
Georgia Institute of Technology

Dr. Robert Moon
School of Materials Science &
Engineering
Georgia Institute of Technology
The Forest Products Laboratory
USDA Forest Service

Date Approved: December 2015

This work is dedicated to my family.

ACKNOWLEDGEMENTS

To my family, whose way of life is as unique as it is respectable, thank you for teaching me the value of hard work. I remember my uncles and grandfather hunting for the meal that my aunts and grandmother would prepare to feed the entire family. This was a regular scene, not a special occasion. You all, or y'all, are incredible outdoorsmen and survivalists. Growing up around this I had always felt a little different, but now that I can reflect back on my youth, I know where my determination comes from. It is not easy to rely on the land to sustain your family, it is hard, physical work where being tired and not showing up means that you do not eat. It was also not easy being a first generation college student, as I struggled through challenges that seemed to come easy to my friends and colleagues. It is the same motivation that pushes y'all to regularly wake up at 4 AM for a hunt that has pushed me to pursue a PhD and to never give up. I am so proud to consider myself a Cajun, even though I don't talk like y'all or eat crawfish-we are cut from the same cloth.

To my mom and dad: thank you for allowing me to be different and choose my own path. Education was always the top priority for me growing up because you wanted me to have more than you did, and because of your persistence I have the opportunity for that. This is an invaluable gift that I could never fully express my gratitude for other than instilling the same values in future generations of our family.

To my boyfriend, Alex: your measure of support and belief in me is unprecedented. No other person could fill your role of professional advice giver, idea communicator, motivator, someone who will always makes me laugh, co-cat parent, and my best friend. You have the unique ability to take my mind away from stressful thoughts. I look forward to seeing you every day. Thank you for being a constant source of joy and positivity in my life.

I am grateful to my friends and mentors from the University of Louisiana Lafayette who were particularly influential in my decision to go to graduate school. To my friend Jeff LeBlanc, who I studied with for nearly every exam, our academic rivalry motivated me to learn more for the sake of learning. Our frequent discussions on deciding the direction of our careers after undergrad were instrumental in convincing me to get a PhD. You made the process less intimidating because we were in it together. Our work in AIChE and the Chem-E car competition set the precedent to future chemical engineering classes at UL to attend conferences, present their research, and to compete in these competitions that help to get our name out there as a talented engineering school. Of course, our efforts would not have made the impact that they did without the mentorship of Dr. Chirdon who always did more than was required of him for the betterment of his students and our program. And finally, to our department chair, Dr. Garber who gave us advice when we needed it, and asked for our advice when it was needed. Our inclusion in important departmental discussions made us feel valued as students and taught us to speak on issues that are important to us, a lesson that would never be taught inside a chemical engineering curriculum. To Dr. Garber and his wife, Judy Garber, thank you for taking me out to lunch every year since I've been at Georgia Tech, this is only one example of your kindness and exemplifies the fact that you are more than our professor, we also consider you a friend.

To my advisors, Dr. Carson Meredith and Dr. Meisha Shofner, thank you for your leadership and mentorship during my studies. I truly appreciate the opportunity you gave me to do unique research that challenged me throughout my studies. You allowed me to develop and think independently, but were also available when I needed assistance. I especially appreciate the times you gave me valuable career advice as I was considering my career path. I would like to thank my committee members, Dr. Yonathan Thio, Dr. Francis Joseph Schork, and Dr. Robert Moon for

providing me with valuable feedback, support throughout my PhD process, opportunities for collaboration, and access to valuable instrumentation. Additionally, I would like to acknowledge the organizations that provided funding and materials for my project: the U.S.D.A. Forest Products Laboratory and American Process, Inc. I would also like to thank Dr. Greg Schueneman and Dr. Eric Mintz for their regular support and collaboration. I've learned a lot from your creative ideas and helpful suggestions.

I thank the present and some past members of the Meredith and Shofner research groups: Dr. Ismael Gomez, Dr. Jie Wu, Dr. Shanhong Xu, Dr. Haisheng Lin, Dr. Zifu Li, Dr. Oluwatimilehin Fadiran, Yi Zhang, Donglee Shin, Zihao Qu, Songcheng Wang, Chinmay Satam, Cait Meree, Matthew Orr, and Emily Fitzharris, for sharing your knowledge, friendships, and lab equipment with me. I appreciate all the discussions and collaborations we've shared throughout my time in the group.

Lastly, I'd like to thank my friends, who have contributed to my quality of life during my time at Georgia Tech. I would like to thank my classmates Samantha Au and Christine He for not only being great colleagues that were vital to my success in our first few semesters, but also for being great friends.

Table of Contents

LIST OF TABLES

LIST OF FIGURES

LIST OF APPENDIX FIGURES

SUMMARY

Composites have found modern applications in building and construction, automotive technology, electronic materials, and dentistry, and are attractive materials because the combination of the filler and matrix often have improved properties compared to the matrix only. Such properties include but are not limited to: mechanical strengthening, flexibility, color, thermal stability, chemical stability, or cost. As such, composite materials are an active area of research where the theoretical bounds of optimized composite properties are continuously pushed as the discovery of new materials and processing technologies are expanded. Certainly the possibilities for the choice of filler and matrix have not been exhausted, and growing environmental concerns have motivated the investigation of bio-derived fillers as mechanical, optical, and thermal reinforcements in a number matrices. Cellulose nanocrystals (CNCs) offer attractive properties to composite applications such as: high specific strength and modulus, low density, high surface area, and a low coefficient of thermal expansion. The properties of CNCs are analogous to those of common industrial fillers with the additional benefit of renewability and sustainability, however some attributes of CNCs might limit their applications, specifically hydrophilicity and low thermal stability. This research aims to address these issues through insightful processing techniques and a versatile chemical modification route to incorporating CNCs into an epoxy and polyurethane matrix, respectively.

A commercial waterborne epoxy matrix was used to demonstrate the effectiveness of CNCs mechanical reinforcement as a function of loading and order of addition. The epoxy was a two part system that contained a nonionic surfactant stabilized epoxide droplet in water emulsion and a water soluble amine hardner which were crosslinked to form the epoxy thermoset. Composites up to 15 wt.% CNC were synthesized and characterized for their mechanical and

thermal properties, specifically tensile and loss modulus, and glass transition temperature and thermal degradation. CNCs improved the tensile modulus by 64 % compared to the neat epoxy at 15 wt.% CNC, although the CNCs were visualized as micrometer-sized aggregates in the epoxy using polarized light microscopy (PLM). To improve the CNC dispersion, an alternate processing strategy was employed. In one scenario, the CNCs were mixed together with the epoxy emulsion and amine crosslinker and then cured, referred to as 1-step mixing, and in another case, CNCs were premixed with the epoxy emulsion and the amine crosslinker was added some time later and then cured, referred to as 2-step mixing. In the 2-step mixing case, the CNCs were more uniformly dispersed and exhibited improved mechanical properties such as loss modulus, tensile strength, and work of fracture compared to the 1-step mixing case. The proprietary nature of the commercial epoxy resin left unanswered questions about the specific interactions that facilitated the improved CNC dispersion in the 2-step mixing case, although zeta potential measurements hinted that an electrostatic association of the epoxy/water interface with the CNCs was responsible. The mechanism of dispersion and interfacial localization of the CNCs at the epoxy interface was further probed with tensiometry.

In order to better understand the individual component interactions that influenced CNC dispersion, tensiometry was employed. In the tensiometry experiments, the interfacial tension of an epoxy oil similar to the commercial resin was measured as a function of aqueous CNC concentration and also in the presence of CNC/surfactant and CNC/amine aqueous mixtures. In this regard, control over the concentrations and specific components that were added created a clearer picture of the colloidal interactions that were present during the composite synthesis. Contrary to the hypothesis that CNCs were located at the epoxy/water interface, it was found that the CNCs alone did not lower the interfacial tension of the epoxy and that CNCs actually increased

the interfacial tension when used with surfactants, although the increase was not substantial. CNCs also increased the interfacial tension of epoxy when used with the amine crosslinker, and this effect was more pronounced for the CNC/amine mixtures than for the CNC/surfactant mixtures. However, in the CNC/amine case, when the epoxy droplet internal pressure was decreased, the droplet was deformed in an irregular, non-spherical way, revealing that the CNCs were located at the interface. The only scenario where the CNCs were visualized at the epoxy/water interface was with the CNC/amine mixtures, indicating that the amine molecule had a significant influence on the localization of CNCs at the interface. Overall, the tensiometry experiments exposed important findings in the consideration of using CNCs as emulsifiers and identified the component that would be better suited for that application, the surfactant, given that the CNC/surfactant mixtures had the lowest interfacial tension values.

In the second part of this work, a chemical modification of the CNC surface was investigated. A diisocyanate molecule with unequally reactive isocyante groups, isophorone diisocyanate (IPDI), was chosen as the chemical modifier and modified (m-CNC) and unmodified CNCs (um-CNC) were incorporated into a polyurethane matrix based on IPDI and a polyol crosslinker. The unequal reactivity of the IPDI molecule was utilized to render CNC particles with one attached isocyanate group, as a urethane bond, and one free isocyanate group. The chemical structure was confirmed with FTIR, ^{13}C-NMR, and elemental analysis. When the um-CNC and m-CNC were incorporated into the polyurethane matrix, significant differences were observed. First, the um-CNC composites exhibited bulk opacity when compared to the m-CNC composites. When the composites were viewed under cross polarized light, the um-CNC composites revealed significant aggregation of the CNCs while the m-CNCs appeared to be homogeneously dispersed. The

differences in dispersion translated to superior mechanical performance of the m-CNC composites compared to the neat matrix and compared to the um-CNC composites at identical CNC loadings.

Overall, this work presents new considerations for utilizing CNCs in thermoset matrices by exploring in depth a physical and chemical route to improving CNC dispersion in the polymer matrix and the mechanical properties of the resulting composites. This work is also relevant to the research of CNC composites using CNCs produced at pilot-scale quantities versus CNCs produced a few grams at a time which may not have reproducible properties.

CHAPTER 1

INTRODUCTION

1.1 Background

According to the ASTM standard D 883-12, a filler is defined as 'a relatively inert material added to a plastic to modify its strength, permanence, working properties or other qualities, or to lower cost', and a composite is defined as 'solid product consisting of two or more distinct phases, including a binding material (matrix) and a particulate or fibrous material'.[1] This general idea is the motivation behind composite materials, where the desired outcome depends on the application and material property goals. While cost is not considered a material property, it is certainly an important motivating factor. Fillers can reduce cost by reducing the volume of a more costly matrix, or by light-weighting the overall material, resulting in fuel savings.[2] Of course, the criterion for these benefits are that the filler is less expensive and less dense than the polymer matrix which is not always true given the diverse range of fillers and polymers commonly used today.[2] Additional motivating factors could be superior mechanical or thermal performance, or the incorporation of attractive materials such as sustainable and renewable fillers. In this regard, a filler cost increase may be justified if there is a tradeoff between performance and cost. In any case, the optimization of such considerations is an active area of research where filler dispersion and filler-matrix interactions are tuned to achieve optimal composite properties. The focus of this thesis is polymer nanocomposites. This chapter will outline the current filler market and trends, introduce the specific nano-filler and polymers chosen for this research, and the motivation behind their selection and the scientific challenges that this work aims to address.

1.2 Filler Market and Trends

In 2005 the estimated market for filler materials in Western Europe and NAFTA nations was estimated to be between 3.75 and 5 billion USD, including carbon black, and 1.25 billion USD excluding carbon black.[3] The most common types of fillers used industrially are carbon black, calcium carbonate, and silica, with carbon black and calcium carbonate representing approximately 70% of the 7.5 million metric tons of fillers used in 2005. The breakdown of filler use by polymer type was roughly 50% elastomers, 35% thermoplastics, and 15% thermosets, where the elastomer market is dominated by carbon black and silica fillers.[3] The main fillers used in thermoset applications are calcium carbonate and aluminum hydroxide, along with significant use of dispersing and coupling agents which can be costly and time consuming. In addition, these mineral fillers are mined from geological formations formed millions of years ago[4] and are consumed at a faster rate than they are replenished. Such extractions require significant processing (grinding, milling, crushing, etc.) before the filler material would be considered valuable in a given application. These facts have motivated a search for fillers derived from renewable sources, while maintaining performance and process-ability.

The filler market is large but a fair portion of the products fillers are used in are not 'technically sophisticated',[2] which presents an opportunity for substantial progress in this field. The most common applications of fillers include: food, paper, construction materials, paints and coatings, cosmetics and pharmaceuticals. The growth of the filler industry is directly influenced by the growth of the plastics industry and the polymers most commonly used with fillers: polyvinyl chloride, polypropylene, polyamides, and polyesters.[2] As a growing industry, filler technology presents a unique opportunity for scientific advancement. Some of the predicted areas of emerging importance include: nano-, low cost, and conductive fillers, and surface modification technology.[2]

By and large, the composite industry has focused its efforts into advancing carbon fiber and carbon nanotube technology for high performance composite applications such as automotive and aerospace parts. Several attractive properties of carbon fiber and nanotube reinforced plastics have contributed to such interest, namely: high strength, low density, high thermal conductivity, and low coefficient of thermal expansion (CTE).[5–10] As a result, carbon fiber reinforced plastics (CFRP) have become the material of choice for wings and fuselage in commercial aircrafts[8] and are commonly encountered in materials requiring a low CTE for the increasing amount of electronic hardware incorporated into advanced automobiles.[7,9] In fact, NASA's DRAFT nanotechnology roadmap through the year 2030 frequently cites the incorporation of carbon nanotubes into its plans for electronic and lightweight materials.[11] However, some important shortcomings surrounding the utilization of carbon nanotube and carbon fiber materials should be carefully considered. First, the toxicity of carbon nanotubes is known to impact health and occupational safety.[5,12] These added precautions concerning the handling of such materials can impact manufacturing cost and insurance. Second, carbon fiber is manufactured under extreme conditions, requiring temperatures higher than 1000 °C for carbonization,[7,9] resulting in high energy consumption and production costs. Arguably, though, the most appealing property of CFRPs are their equal or superior performance when compared to traditional steel or aluminum automotive bodies at a reduced weight.[11] Replacing metals with polymers would alleviate fuel cost and consumption-an increasing concern for advanced nations addressing climate change with aggressive strategies aimed at reducing CO_2 emissions.[13] This strategy, however, is counter intuitive when considering that the starting material used in carbon fiber production is polyacrylonitrile (PAN), a chemical derived from petroleum based sources.[14] In fact, the cost of carbon fiber is subject to the volatility associated with the crude oil market. The growth of carbon

fiber technologies beyond aerospace is limited by feedstock cost and the increasing cost of PAN.[14] Interestingly, efforts to move away from petroleum based carbon fiber precursors are currently focused on bio-based alternatives, such as lignin.[14–16] The biosphere also offers a direct substitute to carbon fiber and nanotubes: crystalline cellulose. The crystalline form of cellulose theoretically has a higher specific strength than steel, and is 5 times less dense.[17] This idea has excited the polymer composite community and has resulted in a large number of publications and a few review articles detailing the incorporation of nanocrystalline cellulose products into polymer composites.[18,19] Like carbon fiber, cellulose also has important drawbacks when considering composite applications and large scale production. Specifically, their comparatively low thermal stability and hydrophilicity present processing and application obstacles in polymer composites.[20] Sections 1.3 and 1.4 of this chapter will detail the chemistry, properties, and forms of crystalline cellulose.

1.3 Cellulose Chemistry

Cellulose is the most abundant polymer resource on the planet with an estimated production in the biosphere of 90 billion tons annually.[21] Cellulose was discovered in 1838 when Anselme Payen first isolated it by treating plant tissue with acid and ammonia, followed by extractions with water, alcohol, and ether.[22] The chemical structure was then elucidated with elemental analysis.[22] Today cellulose is known as a linear homopolymer composed of ringed anhydroglucose repeat units (AGU). The repeat units are linked together by covalently bonded oxygen to C1 of one glucose ring and C4 of the adjoining glucose ring, referred to as the 1,4 β-glucosidic linkage. The chemical structure of cellulose is given in Figure 1.1 which highlights the six carbon positions and alcohol functional groups. Each repeat unit of cellulose contains three hydroxyl groups, one belonging to C2, C3, and C6. C2 and C3 contain secondary hydroxyl groups and C6 contains a

primary hydroxyl group. C2 and C3 are more reactive to etherification reactions while C6 is more reactive to esterification reactions.[20] As a macromolecule containing oxygen and hydrogen atoms, cellulose is capable of intermolecular hydrogen bonding with itself and other molecules containing electron donor and/or acceptor groups. The ease and strength of cellulose's intermolecular interactions is responsible for its use in many commercial products, and as a result of its abundance it has enjoyed a long history of widespread use in industrial forest products including paper, textiles, ropes, and sails.[18,19]

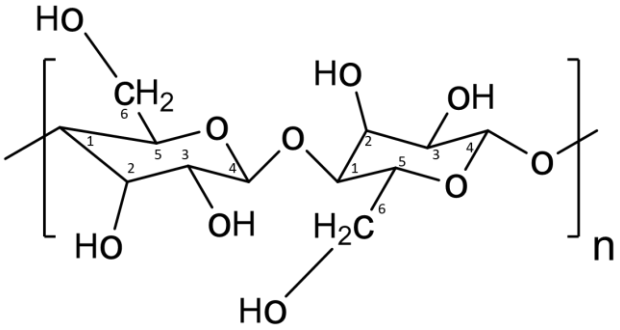

Figure 1.1: Chemical Structure of Cellulose.

Cellulose is produced by the condensation polymerization reaction of glucose monomers and is a product of the photosynthesis process in plants. Native cellulose present in plant cell walls forms a crystalline structure through hydrogen bonding; however it is not a completely crystalline material. Cellulose is biosynthesized in plant and animal sources as individual molecules and assembled into larger units as elementary fibrils (protofibrils), microfibrils, and cellulose fibers. One of the building blocks of hierarchical cellulose structures found in natural materials is cellulose nanocrystals (CNCs), which are individual cellulose crystallites. CNCs are isolated from bulk cellulose by mechanical or chemical treatment of the cellulose fibers to separate amorphous from crystalline regions, common methods include: acid hydrolysis,[18,19] oxidation,[23] homogenization,[24,25] and grinding.[26] The resulting CNCs typically have a rod-like/whisker

morphology. The geometric dimensions, modulus, and surface functionality of the CNC fiber vary depending on the source and preparation conditions.[18,19] Sulfuric acid (H_2SO_4) hydrolysis is one of the most common chemical treatment methods due to a side reaction imparting a negative $–SO_3^-$ charge on the CNC surface, resulting in stable aqueous suspensions through double-layer repulsion between particles.[27] However, several other types of acids may be used for alternate surface functionality such as hydrochloric acid (HCl), which results in –OH functionality, or 2,2,6,6-tetramethyl-piperidinyl-1-oxyl (TEMPO) mediated hypochlorite treatment, resulting in carboxylate (–COOH) functionality.[18]

1.4 Cellulose Nanocrystals

The synthesis of an aqueous cellulose colloidal suspension by sulfuric acid hydrolysis followed by centrifugation and purification was first reported in 1951 by Rånby.[28] The experimental technique used to extract crystalline cellulose of nano-dimensions was then further utilized to characterize cellulose's crystal structure by X-ray diffraction,[29] followed by studies of these particle's unique optical properties manifested as birefringent liquid crystalline phase structures.[30] Since the first reporting of isolated cellulose nanoparticles over 60 years ago, several types of cellulose particles have been extracted and characterized: microfibrilated cellulose (MFC), nanofibrilated cellulose (NFC), microcrystalline cellulose (MCC), and cellulose nanocrystals (CNCs). Additionally, cellulosic particles can be classified by their source which includes bacterial cellulose (BC), tunicate cellulose (TC), and algae cellulose (AC). Applications envisioned for these materials include: drug delivery, batteries, separation membranes, additives for foods and cosmetics, emulsion stabilizers, fire retardants, and reinforcing fillers for polymers- to name a few.[18,31–36] The vast and unique properties of nanocellulose, as well as the variety of particle types available, are responsible for its diverse range of applications. These properties

include, but are not limited to: high specific strength and modulus, low density, optical transparency, biocompatibility, low coefficient of thermal expansion, low production cost, reactive hydroxyl surface, and perhaps most importantly, renewability and sustainability.[18] Since the greatest dimension of a CNC is on the order of a few hundred nanometers, the starting material to produce them can be a relatively worthless material, such as sawdust, which can be transformed into a much more valuable material. For this reason many institutions, both government and industry, are currently interested in commercializing these cellulose based products which has resulted in nanocellulose pilot-scale production facilities across the United States, Canada, and Europe.[37]

1.5 Polymer Composite Mechanical Property Overview

Composites are created with the desire that the particle-filled matrix will perform better than the matrix alone. The matrix and particle are chosen such that the particles have a property (or properties) that the matrix is lacking. It is this very idea that has driven the popularity of polymer composites with the often sought improvement being mechanical in nature since polymers are generally considered to be soft, weaker materials. In order to understand physical limitations and where advances can be made it is important to discuss the mechanical properties that can be improved and how they can be improved by adding particles. The relevant mechanical properties to this work include, but are not limited to: elastic modulus, and tensile strength, and the relevant particle variables include, but are not limited to: particle size, particle loading, and particle/matrix adhesion. Fu *et al.* gives an excellent review of such property expectations with polymer composites and low aspect ratio particles,[38] however the general trends discussed hold for all particle types.

The Young's modulus, or elastic modulus, is the ratio of stress to strain in the linear, or elastic, stage of material deformation. Beginning with the discussion of the elastic modulus dependence on particle properties, it has been repeatedly shown that increasing the loading of particles that are more rigid than the matrix results in increased elastic modulus,[39,40] and that improving particle/matrix adhesion has little to no effect.[41] The increase in modulus with increased particle loading is an intuitive result given that more rigid particles are being added to a less rigid material. Since the elastic modulus is a property of low deformations, the force in the elastic region would be insufficient to result in particle/matrix separation, and therefore, the effect of interfacial adhesion is limited.[38] Finally, particle size will not have an impact on elastic modulus above a critical size, however, below this critical value, the particle size can have a significant effect.[42,43] This critical size depends on the particle, matrix, and particle/matrix adhesion, and is therefore not easily predicted.[38] The underlying mechanism of increased modulus at or below the critical size is governed by the dramatic increase in surface area to volume ratio as particle size decreases at a fixed particle loading.[44] As particles get smaller, their surface area to volume ratio is significantly increased, effectively creating a non-negligible amount of particle/matrix interface.[44] For example, it was predicted that a 3 nm particulate filled composite would have a modulus 200% higher than a 3000 nm particulate filled composite.[44] Clearly, it is advantageous to avoid particle agglomeration in the case of nanoparticles, in order to take advantage of their individual size and high interfacial area.

Continuing with the observed trends in tensile strength, increasing particle size decreases tensile strength, and good particle/matrix adhesion enhances tensile strength. The strength of a material is often defined as the maximum stress that can be sustained under uniaxial tensile loading, therefore the stress transfer between particle and matrix will determine the quality of

particle reinforcement. It was hypothesized that the increased surface area to volume ratio afforded to smaller particles is responsible for a more efficient stress transfer mechanism, resulting in higher strength composites at smaller particle sizes.[38] Additionally, having a good interfacial bond is imperative to efficient stress transfer in composites. When a discontinuity between particle and polymer exists in the form of debonding, the particle cannot carry any of the load experienced by the polymer, resulting in weaker composites.[38] Finally, particle loading has been shown to both decrease and increase the tensile strength. This may be due to the competing effects particle loading has on effective particle size and particle matrix adhesion.[38] For example, as particle loading is increased, larger particle aggregates may be formed, resulting in a larger apparent particle size. If larger aggregates are formed, the particles would have preferential interactions with neighboring particles instead of with the matrix, thus impacting particle matrix adhesion. The effect of particle loading cannot be separated from the particle size and adhesion effects.[38]

It is clear that interfacial adhesion, particle size, and particle loading will play an important role in the mechanical properties of polymer composite. While particle loading is relatively easy to control and interpret, interfacial adhesion and effective particle size are more nuanced and merit discussion. Particle aggregates can actually degrade mechanical and optical properties, and poor interfacial adhesion can lead to inefficient stress transfer, resulting in weaker materials. Therefore, these parameters are often sought to be improved for enhanced composite performance.

1.6 Surface Energy and Adhesion Theories

For uniform stress distribution in composites, monodisperse and uniformly shaped particles are desired.[45] The degree of dispersion will depend on filler surface chemistry, and particle/polymer interactions. Good adhesion is achieved by intimate contact between filler and polymer, sufficient wetting of the particle surface by the polymer, and by optimizing the interfacial

energy of the particle and polymer. The interfacial adhesion can be understood by considering the energy required to create two new interfaces of a homogeneous material (work of cohesion), and the energy required to separate two dissimilar surfaces (the work of adhesion).[46] The first case is primarily relevant to the neat polymer, and the former case is relevant to the particle/polymer interface. Figure 1.2 gives a schematic of these two events, which is expressed by equation 1.1 and 1.2.[47]

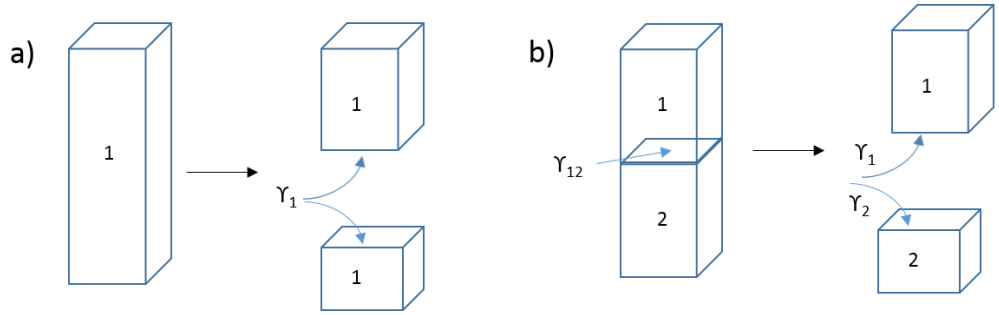

Figure 1.2: Schematic representing the theoretical, reversible, work of cohesion (a) and work of adhesion.

$$W_C = W_{11} = 2\gamma_1 \quad 1.1$$

$$W_A = W_{12} = \gamma_1 + \gamma_2 - \gamma_{12} \quad 1.2$$

In a composite system, γ_1 represents the surface energy of the polymer, γ_2 represents the surface energy of the particle, and γ_{12} gives the interfacial energy of the polymer/particle interface. Equation 1.2 suggests that maximizing the polymer and particle surface energies, γ_1 and γ_2, and minimizing the interfacial energy, γ_{12}, would give a maximum value of the work of adhesion, thus optimizing the interfacial adhesion. Previous studies have determined that equating the surface free energy of the particle and polymer would give the minimum value of the interfacial energy.[48–50]

In addition to maximizing the work of adhesion, the wetting behavior of the polymer solution or melt on the particle surface should also be considered, since sufficient wetting is critical to producing high interfacial contact. The relevant parameter governing the wetting of the particle by the polymer is the spreading coefficient, which is given by equation 1.3.

$$S_{12} = -\Delta G_{wet} = \gamma_2 - \gamma_1 - \gamma_{12} = W_{12} - W_{11} \quad 1.3$$

Here, γ_1 represents the surface tension of the liquid polymer melt or suspension, γ_{12} represents the interfacial tension of the polymer melt or suspension and the particle, which is a liquid/solid interfacial tension, and γ_2 represents the surface energy of the particle. If the spreading coefficient is positive or zero, then spontaneous spreading will occur. Therefore maximizing the surface energy of the particle, and minimizing the interfacial energy of the polymer and particle and the surface energy of the polymer melt would result in the most favorable wetting conditions. Considering equations 1.2 and 1.3, and the criterion for optimizing the work of adhesion and wetting, there exists a tradeoff between maximizing the surface energy of the polymer, to achieve the maximum work of adhesion, and minimizing the surface energy of the polymer, to achieve sufficient spreading of the polymer onto the filler surface. In both cases, though, minimizing the interfacial energy supports favorable adhesion and spreading.

The wetting behavior can also be understood by the liquid contact angle on a solid surface. By substituting Young's equation into equation 1.3, an expression relating the contact angle to the spreading coefficient is obtained (equation 1.4).

$$S_{12} = \gamma_2 - \gamma_1 - \gamma_{12} = \gamma_1(\cos\theta - 1) \quad 1.4$$

In the case of particles and polymers, the filler represents the solid surface (γ_2) and the liquid is the polymer melt or suspension (γ_1). Figure 1.3 gives a schematic of the three possible regimes of wetting.

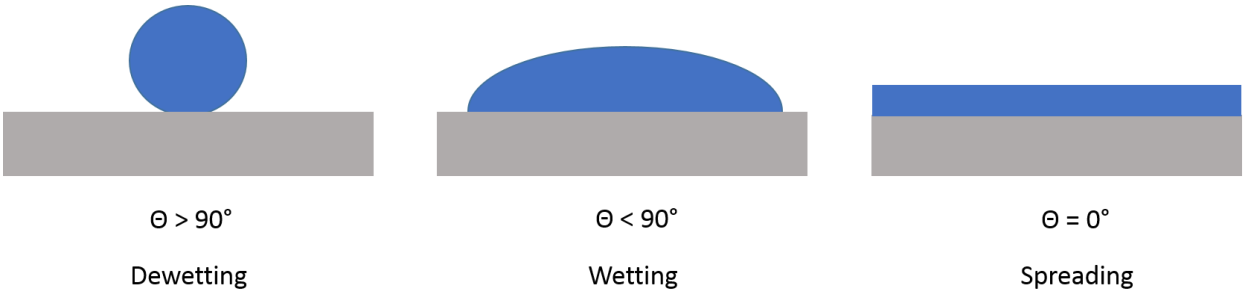

Figure 1.3: The three regimes of wetting as a function of the contact angle.

The ideal case is where the contact angle is 0° and complete spreading of the polymer onto the particle surface occurs.[51] If the solid surface in question is strongly hydrophilic, and the liquid being tested has a contact angle greater than 90°, then that liquid is considered to be hydrophobic, and conversely, if the liquid has a contact angle less than 90°, then that liquid is considered to be hydrophilic. Alternatively, inferences about the solid surface can be drawn by selecting a hydrophilic or hydrophobic liquid probe. Further complicating the contact angle measurement is the reality of surfaces in which no surface is perfectly smooth.[52] Surface roughness is known to influence the measurement of the contact angle. Considering that the solid in this example would be a surface compressed particles, creating smooth surfaces can be time consuming and is often imperfect. Measuring the contact angle of the polymer solution on a single filler particle would be ideal, however, filler particles are typically quite small, on the order of microns or nanometers, thus measuring this contact angle is also quite challenging. Furthermore, the polymer solution is often a complex, inhomogeneous mixture of polymer and solvent, or a polymer melted at high temperature. Surface tension is also a function of temperature and molecular weight, parameters that are often variable during composite synthesis if the polymer is being cooled or heated, or being reacted to increase its molecular weight. Both of these facts render the contact angle and surface energies into vague concepts for such a dynamic system. Therefore, the fundamental interactions governing wetting and adhesion should be considered.

The resulting adhesion between two dissimilar materials is a consequence of mechanical, chemical, and physical forces, or some combination thereof.[20] Each of these forces can influence or overlap one another, and therefore there is no unifying theory that describes adhesion in a comprehensive way.[20] Adhesion has come to be known by physical and chemical processes, such as mechanical interlocking, electrostatic forces, diffusion, absorption, and wetting. Wetting can be related to acid-base interactions, hydrogen bonding, or van der waals forces.[20] In fact, a common method used to quantify the surface energy of solids is by employing the Van Oss Chaudhury-Good theory, which includes a van-der Waals (γ^{vW}), acidic (γ^{+}, electron acceptor), and basic (γ^{-}, electron donor) contribution to the work of adhesion.[20,47,53] This is done by choosing three test liquids and measuring their contact angle on the solid of interest. The liquids should have known surface tensions, one liquid should be apolar, and the remaining two liquids should be bipolar (having similar contributions to the acidic and basic components of surface tension).[53] A common set of liquids include: diiodomethane (van der Waals type), water, and glycerol (bipolar types).[53] Once the contact angle is measured for these three liquids, the following equation is applied to calculate the solid surface energy:

$$W_A = \gamma_l + \gamma_s - \gamma_{sl} = 2(\gamma_s^{vW}\gamma_l^{vW})^{1/2} + 2(\gamma_s^{+}\gamma_l^{-})^{1/2} + 2(\gamma_s^{-}\gamma_l^{+})^{1/2} \quad 1.5$$

Substituting Young's equation into the left side of equation 1.5, the following equation is obtained:

$$\gamma_l\,(1 + cos\theta) = 2(\gamma_s^{vW}\gamma_l^{vW})^{1/2} + 2(\gamma_s^{+}\gamma_l^{-})^{1/2} + 2(\gamma_s^{-}\gamma_l^{+})^{1/2} \quad 1.6$$

From equation 1.6, a system of 3 equations is generated and the dispersive, acid, and base contributions to the surface energy can be determined. The total surface energy is then given by:

$$\gamma_s = \gamma_s{}^{vW} + 2(\gamma_s{}^{+}\gamma_s{}^{-})^{1/2} \quad 1.7$$

This has been done for many types of cellulose, and their acidic, basic, and dispersive contributions to the total surface energy has been quantified. Forsstrom *et al.* evaluated the surface energetic

components of cellulose dissolved in n N-methylmorpholine-N-oxide and dimethyl sulfoxide (DMSO) spin coated onto a glass slide. The films were tested in the neat state, and also in a modified state where the neat cellulose film was treated with propyltrichlorosilane in a gas phase reaction, in order to render the material hydrophobic. It was found that the unmodified cellulose had surface energy components of 40, 2, and 44 mJ/m^2 for the dispersive, acidic, and basic contributions, respectively, and that the modified cellulose had surface energy components of 29, 0.08, and 4 for the dispersive, acidic, and basic contributions, respectively. The total solid surface energy of the unmodified cellulose and modified cellulose was 58.8 and 29.6 mL/m^2, respectively. Similarly, Khoshkava *et al.* found the surface energy components of a nanocrystalline cellulose film to be 41.1, 1.6, and 82.2 mJ/m^2 for the dispersive, acidic, and basic contributions, respectively, and the total surface energy was 64.1 mJ/ m^2.[47] When the cellulose film was modified with alkenyl succinic anhydride, the surface energies were decreased to 35.4, 0.1, and 6.9 mJ/ m^2 for the dispersive, acidic, and basic contributions, respectively, while the total surface energy was decreased to 40.2 mJ/ m^2.[47] These numbers reflect some inconsistencies, likely arising from non-uniform cellulose surfaces, type and origin of cellulose used, test liquids, and general experimental error. However, the general trends are upheld and agree that the largest contribution to the overall surface energy was due to the basic component, the affinity to accept electrons, the dispersive (van der Waals) component was intermediate, the acidic component negligible, and that neat cellulose has a high surface energy.[20,47] Interestingly, when the cellulose was modified with organic compounds all surface energy components decreased, however, the decrease in the polar contributions to the surface energy (acidic and basic) was an order of magnitude greater than that of the dispersive contribution. These results point to the underlying reason cellulose is typically chemically or physically modified for polymer composite applications: cellulose has a higher

polarity and surface energy than most polymers and is therefore inherently compatible.[54] These factors will impact cellulose dispersion and polymer matrix adhesion which in turn will impact composite mechanical properties.

Cellulose is well-known for its capability to form hydrogen bonds with electron donor or acceptor moieties. Indeed, it is the frequency and strength with which cellulose forms hydrogen bonds with itself, both inter- and intra- molecularly, which has given rise to its well-known self-adhesion and use in paper.[20] Hydrogen bonding, along with van der Waals forces, is also responsible for crystalline cellulose's chemical stability and high axial stiffness.[18] However, this feature has limited the use of cellulose in certain applications.[54] For example, nanocellulose is not readily dispersed into common organic solvents such as toluene and tetrahydrofuran (THF). Cellulose can also suffer from agglomeration in polymers that are not water-based or water soluble. A general consensus among the cellulose community attributes this to the cellulose's inherent hydrophilicity and lack of specific interactions (dipole-dipole, electrostatic, hydrogen bonding) with hydrocarbon based solvents and polymers.[54] It is for these reasons that nanocellulose is chemically or physically modified, to render them more compatible with hydrophobic matrices. Ideally, the cellulose nanoparticles would be covalently bonded to the polymer matrix, the strongest form of adhesion.[20] Therefore this research has focused on thermoset –CNC polymer composites, which are capable of forming covalent bonds with the reactive hydroxyl surface of CNCs.

1.7 CNC/polymer composites

CNCs have been incorporated into a wide range of polymer matrices, including both thermoplastic polymers such as polyethylene, polypropylene, and poly(vinyl acetate), and thermosetting polymers such as epoxy and polyurethane, although there has been a heavier

emphasis on thermoplastics and blending techniques.[31–33,55,56]. In many of these studies, the incorporation of CNCs has resulted in increased modulus with respect to the neat polymers, and similar to other nanoparticle systems used in polymer composites, the reinforcing efficacy is higher at temperatures greater than T_g. When considering CNC composites, however, thermosets can offer distinct advantages. Generally thermosetting polymers start out as a low molecular weight, low viscosity pre-polymer resins which then react with a coupling agent to form a molecule of very high molecular weight. In this scenario, the filler can be easily wetted by the pre-polymer resin, resulting in good filler/matrix adhesion or, ideally, covalently bonded to the reacting polymer matrix. Additionally, the crosslinking reaction can be suspended at the point where the fillers are wetted by the polymer matrix, but full cure has not yet occurred. In this scenario, the material can be stored until the molding step. Lower processing temperatures can be used in their synthesis (room temperature-200˚C), potentially lessening the probability of degrading the filler material during processing.[57] Some disadvantages in thermosetting polymers include: required mixing for curing, limited shelf life, long cure times, and the inability to reshape the material once it has been fully cured.[57] In any case, thermosets present a unique opportunity for filler incorporation due to their processing nature which may allow for good filler/matrix adhesion and the opportunity to form covalent bonds with reactive fillers. Therefore, this work has focused on two thermoset matrices: a waterborne epoxy and a polyurethane elastomer. The waterborne epoxy was a commercial product obtained from Air Products, Inc., and the polyurethane elastomer was synthesized by crosslinking two reactive monomers: isophorone diisocyanate (IPDI) and a polyether triol.

1.7.1 Waterborne Epoxies

Given that CNCs are hydrophilic, their incorporation into hydrophobic polymer matrices has presented challenges. These challenges are typically addressed by using CNCs with water soluble polymers, or by performing either chemical or physical modifications of CNCs. This work will consider both routes, first with a waterborne epoxy/CNC composite, and second with a chemical modification step used with a polyurethane matrix. First, the waterborne epoxy will be discussed.

Epoxy resins have been widely used in adhesives, coatings, composites, electric systems, and marine and aerospace applications since their commercial debut in 1947.[58] Epoxy resins can be crosslinked with a variety of curing agents such as amines, hydroxyls, and carboxyls to make flexible or rigid materials. In particular, waterborne epoxy resins have become more important due to the increased legislative restrictions on the emission of organic solvents to the atmosphere.[59] Additionally, waterborne and water-soluble matrices should have a high level of compatibility with water-dispersible fillers, reducing or eliminating the need for chemical functionalization of the filler. The particular resin chosen for this study can be applied as original equipment manufacturing protective coatings, as a floor sealer or paint, and as an anticorrosive primer.[60] One common issue encountered in the coatings industry that this formulation could address is damp concrete, which can only be effectively coated by waterborne resins.[61] It is clear that waterborne epoxies are a relevant class of materials that merit exploration given their low environmental impact and wide array of applications.

Prior to this research, the only existing report discussing CNCs with a waterborne epoxy was published in 2000 by Ruiz *et al.* In that study, tunicate CNCs were mixed with an in-house produced epoxy emulsion and a water soluble amine curing agent. The epoxy droplets were stabilized by a nonionic surfactant, nonyl phenyl polyethylene oxide, and mixed with an overhead

homogenizer, resulting in a 1.7 μm diameter epoxy droplet.[32] The epoxy emulsion, amine hardner, and CNC suspension were mixed together and cured at 40 °C for 6 hours, then at 80 °C for 4 hours.[32] The resulting composites exhibited improved modulus in the glassy, transition, and rubbery region of the dynamic viscoelastic curve at all concentrations tested: 1, 2.5, and 5 wt.% CNC, with the highest reinforcement observed for a 5 wt.% composite.[32] These results showed promise, and a follow up study on the rheological properties of CNC/emulsion mixtures was published in 2001. Here, the emulsion droplet size was optimized by adjusting the surfactant concentration, speed and time of mixing. Once again the tunicate CNCs were shown to improve the mechanical properties compared to the neat, cured matrix.[62] In both papers, the authors postulated that the CNCs could impart stability to their emulsion and stated that ongoing work would investigate specific component interactions, however, these ideas were never realized. These works hinted at key needs in the area of CNC-polymer composites: understanding and optimizing nanoparticle-polymer interactions for enhanced properties. Understanding and controlling the underlying mechanisms of CNC-polymer interactions to produce specific structure and function is clearly still at an early stage. Developing this understanding is critical to future engineering applications of CNC-polymer composites as sustainable materials.

1.7.2 Polyurethanes

Polyurethanes represent a diverse class of polymers that have found applications in foams, adhesives, and coatings.[63] Similar to epoxies, polyurethanes are part of a class of polymers referred to as reactive polymers. Polyurethanes are formed by the reaction of a molecule containing two or more isocyanate functional groups with a polyol containing two of more hydroxyl groups. The extensive choices available for isocyanates and polyols are responsible for polyurethane's wide range of properties and applications.[63]

Given that CNCs have hydroxyl functionality, polyurethanes are a natural choice for CNC composites, and a number of researchers have detailed their findings in the literature. Reports by Saralegi *et al.* and Rueda *et al.* detail the incorporation of CNCs into a segmented thermoplastic polyurethane (STPU) by first synthesizing an isocyanate terminated prepolymer followed by the addition of a chain extender.[64,65] Freeze dried CNCs dispersed in dimethyl formamide (DMF) were then mixed with the DMF-dissolved prepolymers to form the nanocomposites. Both studies reported an increase in the elastic modulus, however this was realized at the expense of the strain at break, maximum tensile strength, and toughness.[64,65] Another report by Rueda *et al.* compared the mechanical properties of a STPU composite with unmodified CNCs and CNCs modified with hexamethylene diisocyanate (HDI), a linear aliphatic diisocyanate. It was found that the modification step resulted in an increase in the elastic modulus while the tensile strength and elongation at break decreased when compared to the unmodified CNCs, this was likely due to the chain extension of the CNCs by the in situ polymerization of the HDI.[66] Finally, a report by Pei *et al.* demonstrated significant mechanical property improvement with a polyurethane elastomer/CNC composite when the polymerization reaction was carried out in the presence of the CNCs.[67] In this scenario, the diisocyaante monomer (diphenylmethane diisocyanate, MDI) can form covalent bonds with the CNCs or the polyol, resulting in uncontrollable reaction sites and uncertain chemistry. Like HDI, MDI can also lead to chain extension of the CNCs given the equal reactivity of the isocyanate groups, which can lead to undesirable aggregation of the CNCs. These studies point to a critical need in realizing the full potential of CNCs in polyurethane composites and controlling their chemistry and dispersion.

1.8 Thesis Overview

This research aims to formulate epoxy and polyurethane CNC composites and characterize their mechanical and thermal properties. A physical and chemical route to improving CNC dispersion and composite mechanical properties pertaining to the waterborne epoxy emulsion and polyurethane elastomer, respectively, will be discussed. These findings will enable the design of high performance CNC/polymer composites through highlighting important processing parameters. The main objectives are as follows:

I. Incorporate CNCs into a commercial waterborne epoxy resin
    a) Develop processing protocol for optimized CNC dispersion
    b) Investigate dispersion mechanism
    c) Characterize nanocomposite thermo-mechanical property

II. Investigate CNCs as emulsifiers using tensiometry
    a) Determine CNC effect on interfacial tension of an epoxy oil
    b) Determine the importance of the image charge effect
    c) Identify CNCs at epoxy/oil water interface

III. Develop formulation for versatile CNC surface modification
    a) Chemically modify the CNC surface
    b) Verify selectivity and versatility of modification step
    c) Formulate polymer composites compatible with modified CNCs

Chapter 2 discusses the formation of epoxy/CNC composites based on a commercial waterborne epoxy emulsion and amine crosslinker. The reinforcing efficiency of the CNCs in the epoxy polymer was determined with dynamic mechanical analysis (DMA) and tensile testing, and a micromechanical model was applied to the data. The elastic modulus of the CNC was an adjustable parameter in the model, and an estimate for its value is given. Chapter 3 will describe an alternate processing method

using the same waterborne epoxy for better control of CNC dispersion. The mechanical properties of the two processing strategies will be compared and a hypothesis for the dispersion mechanism is given. Given the nature of the waterborne epoxy emulsion, and the findings presented in Chapter 3, Chapter 4 will investigate the emulsification property of the CNC particles at an oil water interface using tensiometry. The effect of CNC concentration and type will be discussed, as well as ionic strength and presence of surfactants. Chapter 5 will detail a versatile chemical modification of the CNC surface using hydroxyl/isocyanate chemistry. The efficacy of the chemical modification will be tested by attenuated total reflectance-Fourier transform infrared analysis (ATR-FTIR), elemental analysis, and ^{13}C NMR. The mechanical performance of polyurethane composites made with modified and unmodified CNCs will be compared. Chapter 6 will conclude with a summary of the important findings and provide future recommendations based on this work.

CHAPTER 2

MECHANICAL AND THERMAL PROPERTIES OF WATERBORNE EPOXY COMPOSITES CONTANING CELLULOSE NANOCRYSTALS

This chapter was adapted from a publication in *Polymer*:

Xu, S., Girouard, N., Schueneman, G., Shofner, M. L. & Meredith, J. C. Mechanical and thermal properties of waterborne epoxy composites containing cellulose nanocrystals. *Polymer*. **54,** 6589–6598 (2013).

2.1 Background

As mentioned in Chapter 1, only two studies have been conducted for CNC composites with a waterborne epoxy, using CNCs derived from tunicate precursors.[32,62] To date there are no reports of composites formed from wood-based CNCs in waterborne epoxy. The results of the tunicate CNC studies showed that mechanical percolation of the CNCs occurs at loadings consistent with the CNC aspect ratio, i.e., the filler loading corresponding to the percolation threshold was lower for higher aspect ratio filler. When mechanical percolation occurs in these systems, dynamic moduli increases of greater than one order of magnitude are observed. Trends in the value of T_g also suggested CNC network formation. While it is not clear from these studies if CNC addition increased the matrix T_g by causing changes to the matrix network structure formed during curing and/or by reducing matrix mobility through physical interactions, these results do suggest that some component synergism is at work in these systems that may facilitate higher levels of composite performance. In this work, CNC/waterborne epoxy composites produced using wood-derived CNCs are characterized in order to further the understanding of CNC composites with waterborne polymers available in the literature. This work provides an opportunity to compare CNC/waterborne epoxy composites with CNCs derived from wood to those derived from animal sources.

2.2 Materials

Epoxy resin (diglycidyl ether of bisphenol-A (DGEBA), Air Products and Chemicals Inc., Ancarez AR555, 55 wt.% solid epoxy emulsion in water stabilized by a nonionic surfactant with D_{50}=0.5 μm, epoxide equivalent weight (EEW)=550) was used as received. Amine (polyoxypropylenediamine, Air Products and Chemicals Inc., Anquamine 401, 70 wt.% solute content in water solution, amine hydrogen equivalent weight (AHEW)=200) was diluted with approximately equal weight of DI water to reduce the viscosity. The final solute content in the amine/water solution was approximately 35 wt.%. An 8.75 wt.% aqueous CNC suspension was prepared from mixed southern yellow pine dissolving pulp via 64% sulfuric acid digestion as described elsewhere.[27] The resultant CNCs have sulfate functionality due to residual sulfate esters on their surfaces. The CNCs were determined to contain 0.72 wt.% sulfur on a dry cellulose basis by inductively coupled plasma/mass spectroscopy (ICP/MS). Dried CNC films for nanoparticle characterization were made from CNC suspensions held at 50°C for one week. 95 wt.% octadecyltrichlorosilane (OTS) was purchased from Acros Organics. Toluene, ethanol and cyclohexane were purchased from Sigma-Aldrich. 98 wt.% sulfuric acid and 30 wt.% hydrogen peroxide were purchased from VWR. Silicon wafers (300 mm diameter, double-side polished) were purchased from Silicon Valley Microelectronics Inc.

2.3 Sample Preparation

2.3.1 Substrate Treatment

In order to prevent silanol groups (Si-OH) on the surface of untreated silicon wafers from reacting with the epoxide groups, the silicon wafers were treated with OTS.[68–71] Before treatment with OTS solution, silicon wafers were cleaned by immersing into piranha solution (75% (v/v)

sulfuric acid and 25% (v/v) hydrogen peroxide) for 1 hour at 80°C. Cleaned wafers were immersed into 0.5 mM OTS/cyclohexane solution for 5 minutes followed by washing sequentially with toluene, ethanol, and water.

2.3.2 Film Preparation

Stoichiometric amounts of epoxy and amine were mixed at room temperature with the desired amount of CNC suspension (0-15 wt.%). The mixture was magnetically stirred for 1-5 hours depending on CNC concentration, with higher concentrations mixed for longer times. Then, the nanocomposite mixture was precured for 0.5 to 2 hours at room temperature until the viscosity of the mixture was high enough to barely allow flow. Precuring times were determined by visual inspection and increased with CNC concentration since greater amounts of water, resulting from the CNC suspension, were present thereby diluting the reactive epoxy. The mixture was cast on an OTS treated silicon wafer substrate and dried at room temperature for 1-3 hours until the mixture is not able to flow on the silicon substrate. Then, the coated substrates were transferred to an oven and cured for 2 hours at 100°C, or 120°C (10 and 15 wt.% CNC samples only). Neat epoxy was prepared using the same processing protocol for comparison.

2.4 CNC Characterizations

2.4.1 Transmission Electron Microscopy

The CNC/water suspension as delivered was diluted with DI water to a concentration of 0.1 wt.% and dropped onto a 400 mesh carbon grid with Holey. In order to enhance contrast, samples were stained with a 2 wt.% aqueous solution of uranyl acetate. Samples were imaged using a Philips CM-100 TEM (FEI Company, Hillsboro, OR) at an accelerating voltage of 80 kV.

2.4.2 Zeta Potential

The CNC/water suspension as delivered was diluted with DI water to a concentration of 0.1 wt.%. The zeta potential of the diluted suspension was measured by a Malvern Zetasizer Nano ZS 90. Three consecutive measurements were taken at 23˚C and average values were reported.

2.5 Nanocomposite Characterizations

2.5.1 Field Emission Scanning Electron Microscopy (FE-SEM)

Nanocomposite film samples were freeze fractured by immersing into liquid nitrogen and then sputter coated with gold to prevent charging. The samples' fracture surfaces were imaged by FE-SEM (Zeiss Ultra60).

2.5.2 Polarized Light Microscopy (PLM)

The distribution of CNCs in the epoxy matrix was investigated qualitatively by observation of birefringence with an optical microscope (Olympus BX51) equipped with two polarizers, referred to as the polarizer and the analyzer (Olympus U-AN360P). All films were imaged in transmission mode at full extinction.

2.5.3 Attenuated Total Reflectance-Fourier Transform Infrared Spectroscopy (ATR-FTIR)

The chemical structure of film samples of pure CNC, neat epoxy, and nanocomposites was characterized by ATR-FTIR (Bruker Vertex 80V). Unreacted epoxy emulsion and diluted amine solution were also analyzed by liquid ATR-FTIR. The scan range was 4000 cm^{-1} to 600 cm^{-1} with a resolution of 4 cm^{-1}.

2.5.4 Differential Scanning Calorimetry (DSC)

The values of T_g for the neat epoxy and composite films were measured by DSC (TA Instruments DSC Q200). As a first step, samples were annealed in the instrument at 150°C for 2

minutes and then cooled to 0°C at a rate of 10°C/min. The samples were subsequently heated to 150°C at a rate of 10°C/min. This last heating step was used to obtain T_g of the sample. The value of T_g was assigned as the midpoint of the transition region between the glass and liquid line on the heat flow curve using the instrument analysis software.

2.5.5 Thermogravimetric Analysis (TGA)

Water absorption, thermal stability and changes in degradation patterns associated with CNC addition were assessed with TGA (TA Instruments TGA Q5000). Samples were heated from room temperature to 120°C at a rate of 10°C/min under a flowing nitrogen atmosphere, then held at 120°C for 20 minutes, and then heated to 600°C at a rate of 10°C/min. The water absorbed by samples was measured by the weight loss during the first two steps. The thermal stability and decomposition patterns of the samples were obtained in the temperature range from 120°C to 600°C.

2.5.6 Dynamic Mechanical Analysis (DMA)

Storage and loss modulus of the materials were determined from DMA experiments (Mettler Toledo DMA/SDTA861). Samples were made by cutting films into strips about 3-4 cm long (testing length is 9 mm) and 2.5-3 mm wide. Samples were tested in tension while being heated from 30°C to 150°C at a rate of 2°C/min. The testing frequency used was 1 Hz, and the tests were run within the linear response region of strain for each sample.

2.5.7 Tensile Testing

Uniaxial tensile testing was performed using an Instron 5566. The samples were prepared by cutting films into 100 mm x 10 mm strips following ASTM D882-10. Sample slippage was mitigated by lining the grips with crocus cloth. A minimum of four samples were tested for each material composition, and the average values were reported. Additionally, t-tests were performed

to determine the overall statistical significance (α=0.05) of the change in modulus of composites reinforced with CNCs.

2.6 Results and Discussion

2.6.1 CNC Surface Charge and Dimensions

The dimensions of individual CNCs were measured using TEM. Figure 2.1 shows the TEM image of CNCs. The CNC particles were assumed to be symmetric about their longitudinal axis. The length and diameter of the CNCs estimated from the TEM image were 138 ± 22 and 6.4 ± 0.6 nm, respectively, close to what others have reported.[27] Based on these average dimensions, the aspect ratio of the CNCs was estimated to be 21. The rod-like/whisker morphology and the geometric dimensions were consistent with data reported in the literature for CNCs obtained from wood.[27,72] The zeta potential of CNCs were measured to be -71 mV, indicating that the CNCs were well-dispersed in water and largely isolated from one another. The negative charge is expected due to the sulfate functionality present on the CNC surface and leads to a double-layer repulsion between particles. Due to the high magnitude of the zeta potential, a highly stable suspension is expected, as is observed visually.

Figure 2.1: TEM of wood derived CNCs.

2.6.2 Nanocomposite Morphology

The morphology of the nanocomposites was observed with FE-SEM and optical microscopy imaging. Figure 2.2 shows the FE-SEM images of the cross sections of film samples. No CNC aggregates were observed at this length scale, although it is possible that CNCs were aggregated at a size scale not easily resolved by these images. Additionally, the contrast observed between CNC and epoxy resin with electron microscopy was low due to their similar chemical composition.

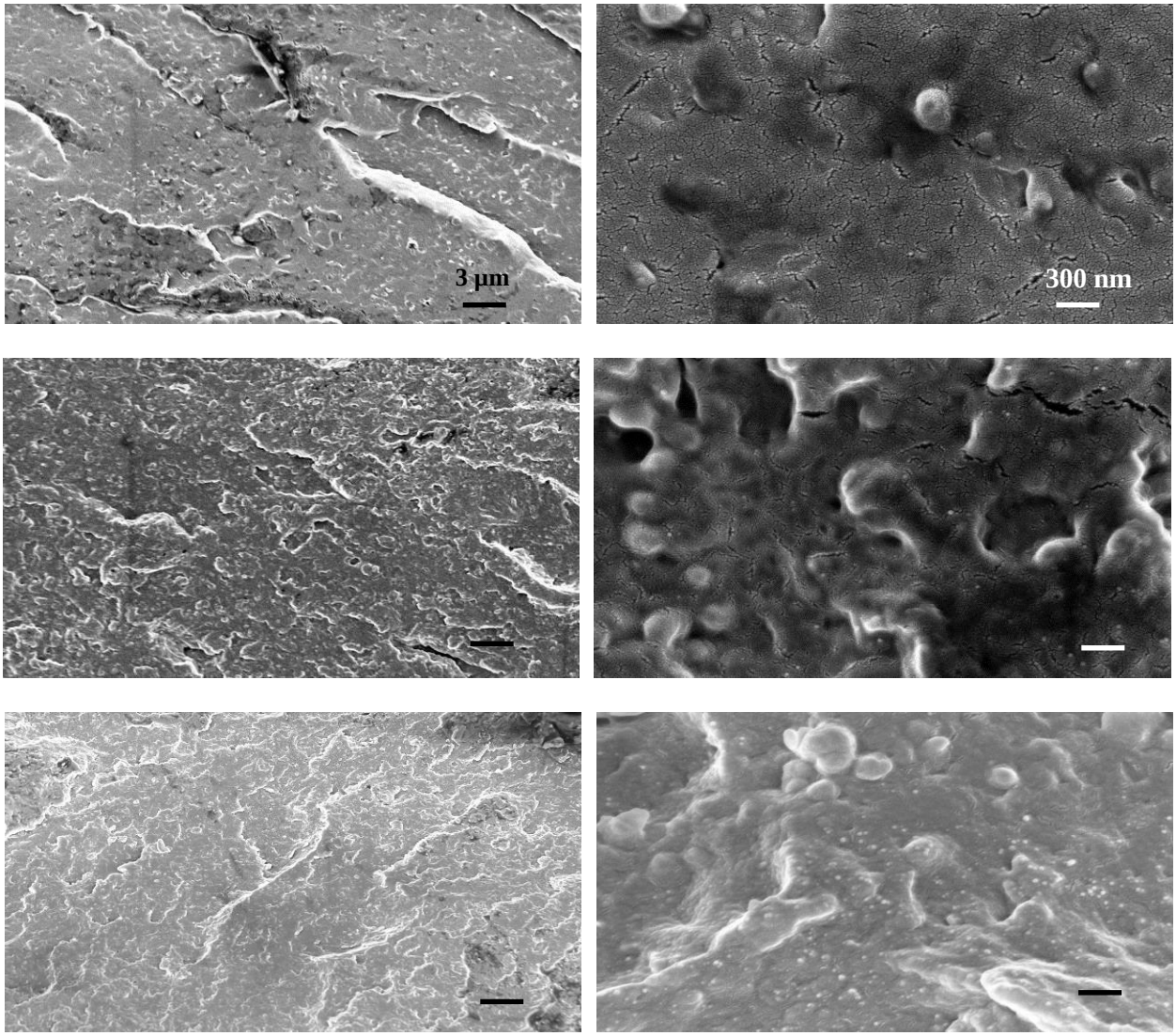

Figure 2.2: FE-SEM images of neat epoxy and composites at two different magnifications. Left column scale bar is 3 µm, right column scale bar is 3 nm. Top: neat epoxy, middle: 5 wt. % CNC, bottom: 10 wt.% CNC.

Therefore, the distribution of CNCs was further investigated by polarized light microscopy. In this method, the presence of optically-resolvable nanofiller-containing regions can be detected based upon birefringence of CNC domains. Exploiting the anisotropic nature of the CNCs, and the isotropic nature of the epoxy matrix, polarized light is capable of distinguishing between these two components. In transmission mode, polarized light travels through the sample along the thickness direction. The birefringent domains observed could be the superposition of the CNC particles/aggregate inside the composite layers perpendicular to the light path. Therefore the birefringent domains represent the three dimensional distribution of CNCs projected as a two dimensional image. It should be noted that when specimens were rotated, the optical properties remained unchanged, suggesting that the CNCs were randomly oriented in the plane of the sample.[73] Figure 2.3 shows the polarized light images of neat epoxy and composites. Pure epoxy exhibited no birefringence, while all composites showed some degree of birefringence in domains on the order of tens of microns. As CNC concentration increased, the size of these domains decreased. This was likely due to longer mixing times required for the higher CNC concentration samples allowing the CNCs to disperse. The presence of birefringent domains in the images suggests that some of the CNCs within the composites were not dispersed as individual particles but were aggregated into optically-resolvable domains.

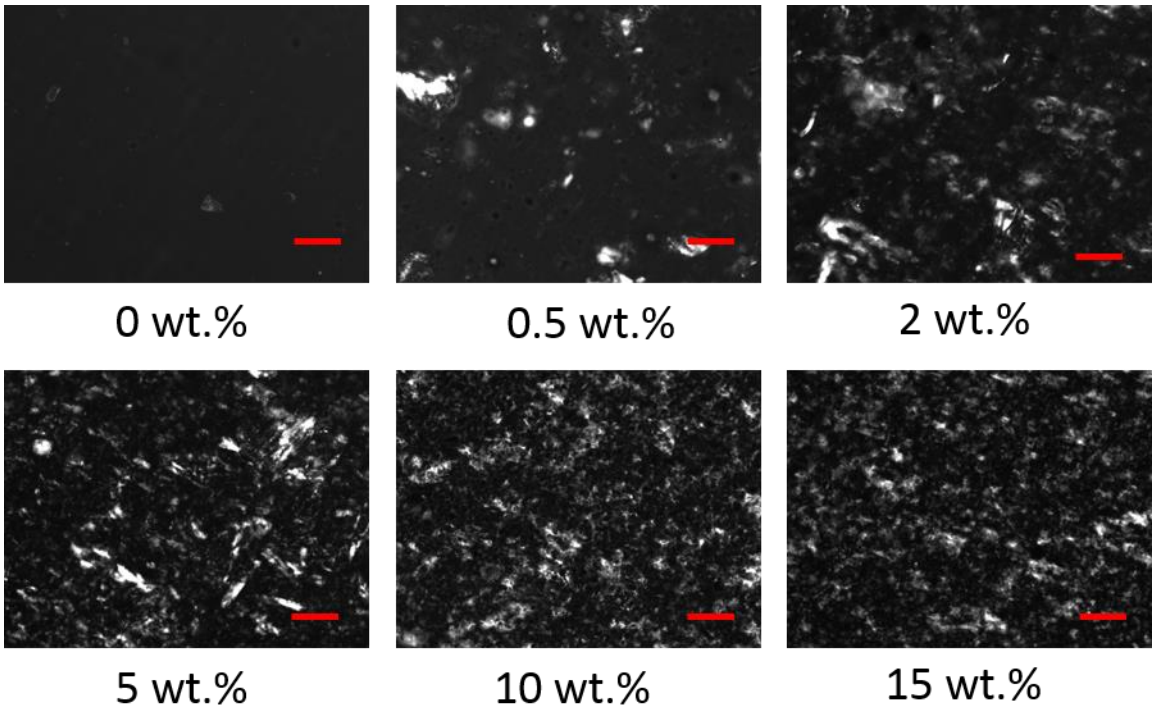

Figure 2.3: Polarized light microscope images of epoxy and epoxy/CNC composites. Scale bar is 80 µm.

Although the CNC aggregates were larger than the wavelength of visible light, all composites up to 15 wt.% remained transparent. Figure 2.4 shows a photographic image of composites and neat film. This was due to similar refractive indices between the epoxy and nanocellulose.[18] Additionaly, work by Yano *et. al.* has shown that bacterial cellulose nanofiber/epoxy composites containing up to 65 wt.% cellulose transmitted 80% of visible light, indicating that even aggregated cellulosic materials appear transparent to the eye.[74]

Figure 2.4: Photographic image of epoxy/CNC films. From left to right: 5, 2, 0 wt.% CNC.

2.6.3 Nanocomposite Chemistry

To assess the degree of cure in the matrix and understand the chemical structure of the nanocomposites more fully, FTIR spectra were measured for the nanocomposite components and nanocomposites. Figure 2.5 shows the FTIR spectra of dried unreacted epoxy, dried amine, and the neat cured epoxy resin. The absorption at 912 cm^{-1} was due to the unreacted epoxide group.[75] Its disappearance in neat cured epoxy indicated that all of the epoxide groups reacted during cure. Figure 2.6 shows the infrared spectra of pure dried CNC, the neat epoxy resin, and a composite with 15 wt.% CNC. Some features were observed in all three spectra. The absorption at 3000-3500 cm^{-1} was due to hydroxyl groups.[76] The absorption at 2925 cm^{-1} was due to CH groups.[76] The strong absorptions between 1000 and 1250 cm^{-1} were assigned to C-O-C (ether) or C-O(H).[76–80]Additionally, the absorption at 895 cm^{-1} observed in the spectra for pure CNC is typical of β-glucosidic linkage.[80,81] In CNC-epoxy composites, the epoxide group can react with $–NH_2$ groups from the amine or the hydroxyl groups on the CNC surfaces. If an epoxide group reacts with a CNC hydroxyl group, the result will be an ether group and a hydroxyl group. These spectra showed that pure CNC, the neat epoxy resin, and the composites all contain hydroxyl groups and ether

groups, and their absorptions overlap in the range of 1000-1250 cm^{-1}. Therefore, infrared spectra cannot provide evidence of CNCs as a chain extender or crosslinking agent in the CNC/epoxy resin composites. However, monitoring of the epoxide group at 912 cm^{-1} indicates that the epoxide group reacted completely in both neat epoxy resin and composites, so the degree of cure attained in all of the samples was likely similar.

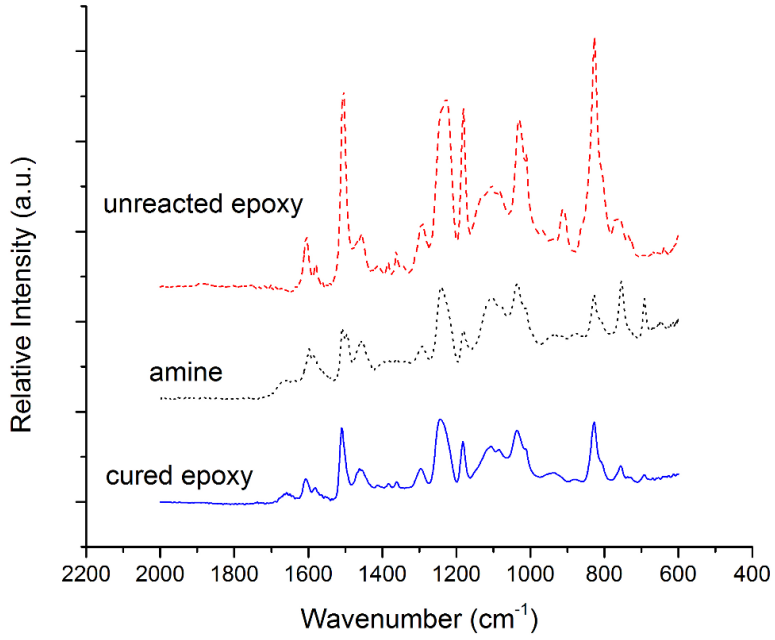

Figure 2.5: FTIR of unreacted epoxy (dashed), unreacted amine (dotted) and neat cured epoxy (solid).

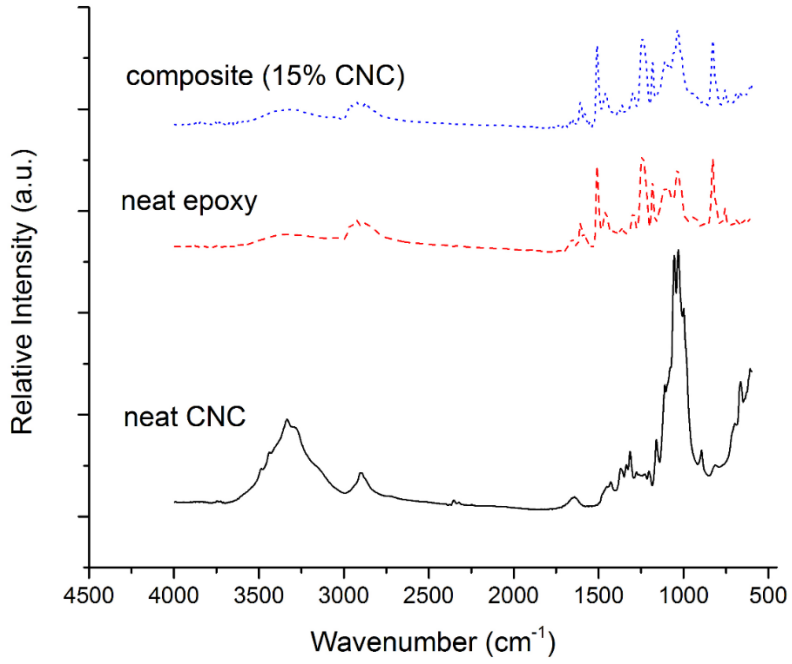

Figure 2.6: FTIR of neat CNC (solid), neat epoxy (dashed) and composite with 15 wt.% CNC (dotted).

2.6.4 Thermal Properties

Further information about the chemical structure and component interactions may be inferred from changes in T_g with CNC addition. Figure 2.7 shows T_g values of the neat epoxy and the CNC/epoxy composites as a function of CNC content. As the CNC content increased, the T_g of the composite increased though the amount of the increase did not follow a linear trend with CNC content at the loadings studied here. At loadings up to 5 wt.% CNC, the increase in the value of T_g was larger as a function of CNC loading than that observed at higher CNC loadings. A maximum increase of approximately 9 ºC was observed at a CNC loading of 15 wt.%. The increase of T_g indicated that the inclusion of CNC particles in the epoxy network inhibited polymer chain movement through either physical or chemical interactions.

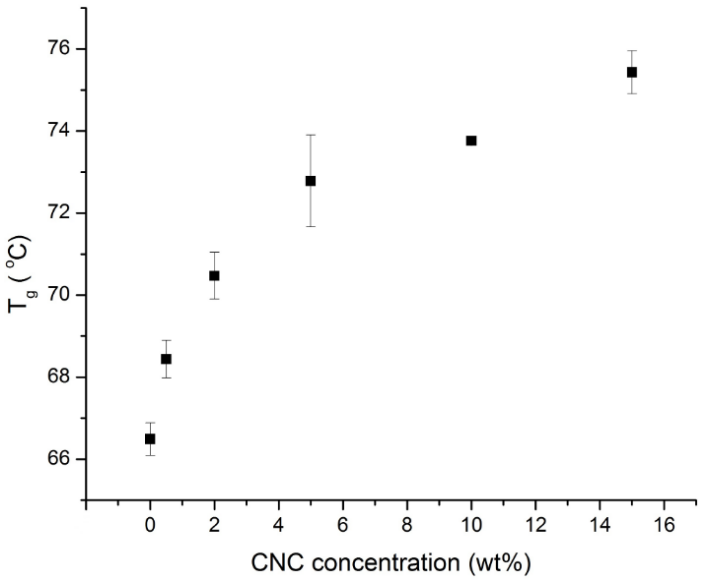

Figure 2.7: T_g of neat epoxy and composites determined from DSC data.

One concern associated with cellulosic fibers is their high moisture absorption and the associated degradation of mechanical properties.[82] Absorbed water can be detrimental to epoxy mechanical properties, and it is therefore important to understand the impact of CNCs on the water content of the composites. Table 2.1 shows the water content of heat cured neat epoxy and composites determined by TGA. Although the water content of neat CNCs was 60% more than that of the neat epoxy resin, it was found that as the CNC content increased, the water content of the composites decreased, though the decrease was not statistically significant. We can conclude however that the CNCs did not introduce additional water to the composites. The unchanged water content suggested that CNC reaction or interaction with the epoxy resin matrix blocks access of water to the hydrophilic hydroxyl groups on the CNC surface. However, two other possibilities should be mentioned. It is possible that the CNCs introduce barriers to water transport that prevent them from becoming saturated with water in the time scale of our measurements. In addition, the aggregation of CNCs within the epoxy might also prevent water access to their surfaces.

Table 2.1: Water content determined by TGA for neat epoxy and composites. Error represents 95% confidence intervals.

	Pure CNC	Neat epoxy	0.5 wt.% CNC/epoxy	2 wt.% CNC/epoxy	5 wt.% CNC/epoxy	10 wt.% CNC/epoxy	15 wt.% CNC/epoxy
Water content (wt.%)	5.6±1.4	3.0±0.7	3.1±0.1	2.6±0.2	2.1±1.6	3.0±1.0	2.3±0.4

Figure 2.8 shows the TGA data for pure CNC, neat epoxy and their composites, including weight loss (Fig. 2.8(a)) and the first derivative of weight loss (Fig. 2.8(b)) versus temperature. The decomposition onset temperature (T_{onset}) and temperature at maximum weight-loss rate (T_{max}) are given in Table 2.2. The decomposition of pure CNCs was similar to that observed in previous work for CNCs from different sources obtained by using sulfuric acid hydrolysis.[83–86] Figure 2.8 shows that the pyrolysis of CNCs occurred in two separate processes. The first process (lower temperature) corresponds to the dehydration of the cellulose chains catalyzed by the acidic sulfate groups present on the CNCs prepared by acid hydrolysis.[83–86] The second process (higher temperature) corresponding to decomposition of the unsulfated crystal interior, and the slow decomposition of solid residues.[83,87] The thermal decomposition of neat epoxy resin consisted of two steps, consistent with that observed by Johnson *et al*.[88] For the CNC-epoxy composites, as the CNC content increased, the onset temperature of thermal degradation for composites decreased compared to neat epoxy, and this change was significant across all concentrations tested (α=0.05). As the CNC content increased, the temperature at the maximum weight loss rate for the first degradation step decreased. However, the change of the temperature at maximum weight loss rate was not significant (α=0.05), except for the composite with 0.5, 10, and 15 wt.% CNC. The temperature at maximum weight loss rate for the second degradation step increased with CNC content, though the change is again not significant (α=0.05).

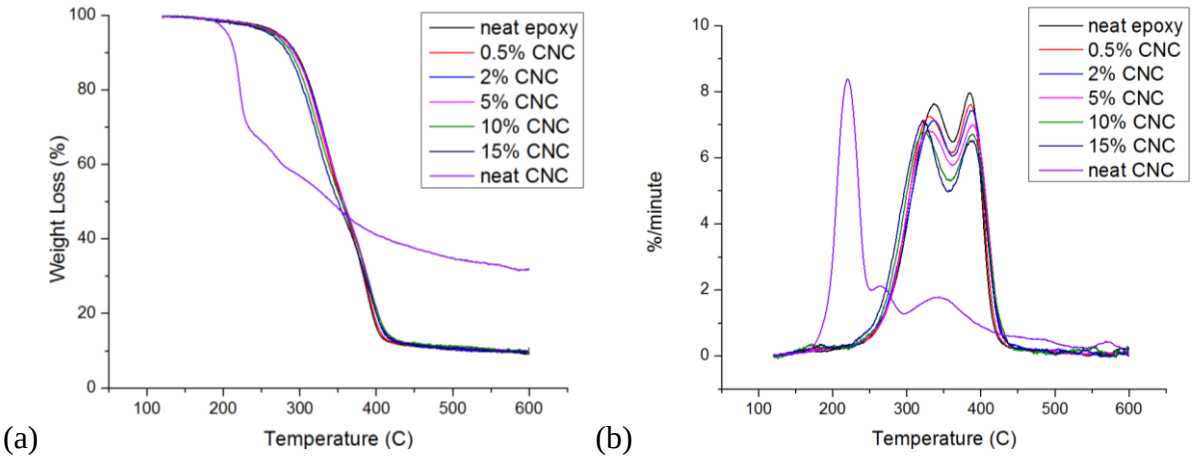

(a) (b)

Figure 2.8: TGA (a) weight loss and (b) derivative of weight loss versus temperature for neat CNC, neat epoxy and composites.

Table 2.2: Onset temperature (T_{onset}), and temperature at maximum weight-loss rate (T_{max}) for TGA data. Error represents 95% confidence intervals.

	Pure CNC	Neat epoxy	0.5 wt.% CNC/epoxy	2 wt.% CNC/epoxy	5 wt.% CNC/epoxy	10 wt.% CNC/epoxy	15 wt.% CNC/epoxy
T_{onset} (°C)	208 ± 5	297 ± 0.3	293 ± 2	293 ± 2	290 ± 1	286 ± 2	287 ± 3
T_{max}^1(°C)	221 ± 1	336 ± 3	331 ± 1	335 ± 1	330 ± 11	325 ± 2	322 ± 2
T_{max}^2 (°C)	267 ± 4	385 ± 1	386 ± 0.4	387 ± 0.3	386 ± 4	389 ± 0.5	388 ± 2

2.6.5 Mechanical Properties

Modulus of the nanocomposites was assessed using two techniques: DMA and uniaxial tensile testing. Figure 2.9 shows the representative DMA data for storage modulus (a) and loss modulus (b) as a function of temperature. The trend in storage modulus observed for the neat epoxy and the nanocomposites was consistent with an amorphous crosslinked polymer. The shape of the storage modulus curves was similar for all of the samples though the amount of reinforcement provided by the CNCs was temperature dependent. The glassy modulus (measured at 30°C) increased by 100% with the addition of 15 wt.% CNC, which is comparable with the CNC/epoxy composites investigated by Tang *et al.* and Ruiz *et al.*[32,89] However, at a 15 wt.% CNC loading, the rubbery modulus was 3 times greater than neat epoxy (measured at 130°C), while Tang *et al.*

reported an increase in the rubbery modulus of 70 times and 12 times the neat polymer for a 15 wt.% tunicate- (aspect ratio = 84) and cotton-derived (aspect ratio = 10) CNC composite, respectively. The increases observed by Tang *et al.* were also dependent on the preparation method of the CNCs where larger increases were observed with tunicate and cotton CNCs prepared by a solvent exchange method versus lyophilization. For example, the composite rubbery modulus measured at 185 °C was increased by 7 times the neat modulus with 15 wt.% cotton CNCs prepared by lyophilization versus a 12 times increase with solvent exchanged CNCs. We provide these values for reference only, in order to present a more comprehensive picture of the properties reported to date with various types of CNCs in epoxy systems. From these data, it is clear that the CNC's reinforcing capability is dependent on the type of CNC fiber used. Several parameters associated with different CNC types will play a role in their polymer composite reinforcing efficiency, such as: aspect ratio, crystallinity, and the axial fiber modulus. Rusli *et. al.* reported on the stiffness of cotton CNCs using the Raman spectroscopy technique and found that the modulus (57-105 GPa) was lower than the value reported for tunicate CNCs (143 GPa).[90,91] The authors attributed this to differences in these material's crystallinity and inherently less efficient stress transfer associated with lower aspect ratio fibers. Given the general metric for the critical volume fraction at which percolation occurs in these systems as $X_c=0.7/A$ (where A is the aspect ratio)[89], it is apparent that a percolation network is achieved at a lower volume fraction given high-aspect ratio fillers. The large difference in polymer reinforcement (at $T>T_g$) between this study and studies performed with tunicate CNCs is likely due to differences in network formation. Another explanation could be that plant-derived CNCs simply have a lower inherent modulus than CNCs derived from tunicates, however few studies on the axial modulus of specifically wood-derived CNCs exist.[18] The Tang *et. al.* study also utilized different epoxy chemistries. For example, in

addition to aspect ratio, some of the difference in the degree of improvement observed in these studies is likely due to the fact that the current epoxy had a higher inherent modulus at temperatures greater than T_g (49 MPa in this study versus 15 MPa in Tang *et al*.) and that the CNC dispersion states were also different than observed in these composites.[89]

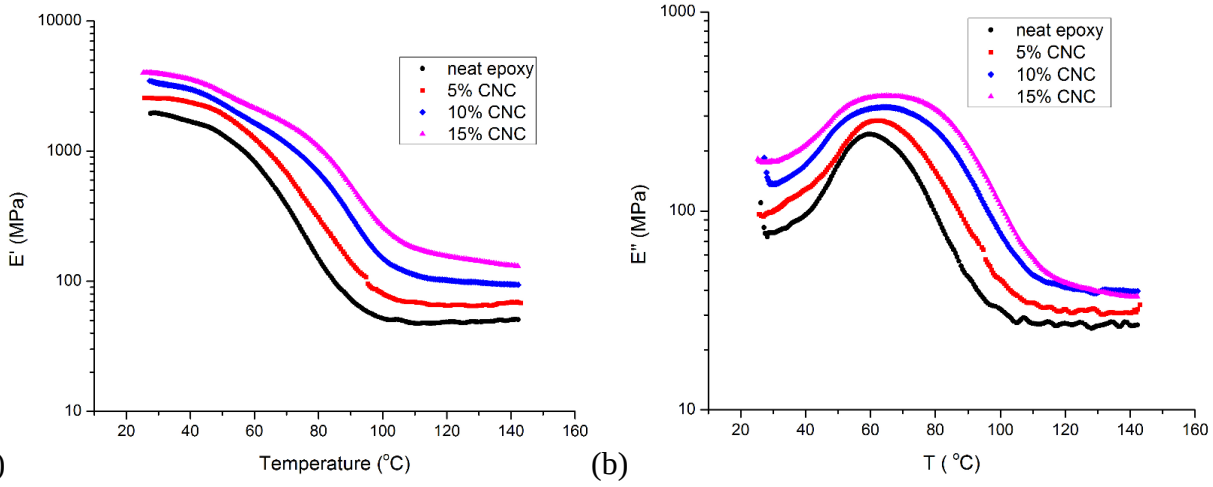

Figure 2.9: Storage modulus (E') and loss modulus (E") for CNC/epoxy composites as a function of temperature.

The value of the loss modulus also increased with CNC addition as compared to the neat epoxy, and the peak of the loss modulus curve was shifted to higher temperature and markedly broader, indicating changes to the matrix relaxation associated with T_g. Using the peak of the loss modulus to assign T_g, a maximum increase of approximately 6 ºC in the 15 wt.% CNC/epoxy composite was observed with respect to the neat epoxy. The trend in T_g change associated with CNC addition was qualitatively consistent with the trend seen in the DSC data, with a nonlinear increase in T_g over the range of CNC loadings used here. However, it is worth noting that the T_g values from DSC measurements were obtained on a second heating cycle, following heating to 150 ºC. Based on the TGA data in this study, the prior heating step could have removed water from the materials, resulting in increased values of T_g relative to the values measured by DMA. It

is not expected that this heating step in DSC resulted in significant post-curing since the time spent above 100ºC was approximately 12 minutes and no exotherm was observed in the DSC data, but the possibility of some post-curing occurring cannot be neglected completely. Beyond changes to the peak value, substantial broadening and reinforcement of the high temperature side of the loss modulus peak indicated that the CNCs hindered the matrix mobility and that this effect was magnified at higher CNC loadings. In the three CNC composite materials measured by DMA, the maximum level of loss modulus reinforcement was observed at temperatures approximately 30 ºC greater than T_g (as measured by loss modulus) due to the high temperature broadening. However, the relative increase in loss modulus due to the addition of CNCs was less than that observed for the storage modulus as shown by the tan(δ) data in Figure 2.10. The value of tan(δ) decreases as the CNC content increases, indicating that the storage modulus is influenced more by the addition of CNCs than loss modulus in the composites. These trends in storage and loss moduli suggest that the primary reinforcement mechanism is physical rather than chemi-physical. Additionally, the peak of the tan(δ) data shifted to higher temperatures, supporting the T_g increases observed in the loss modulus and DSC data.

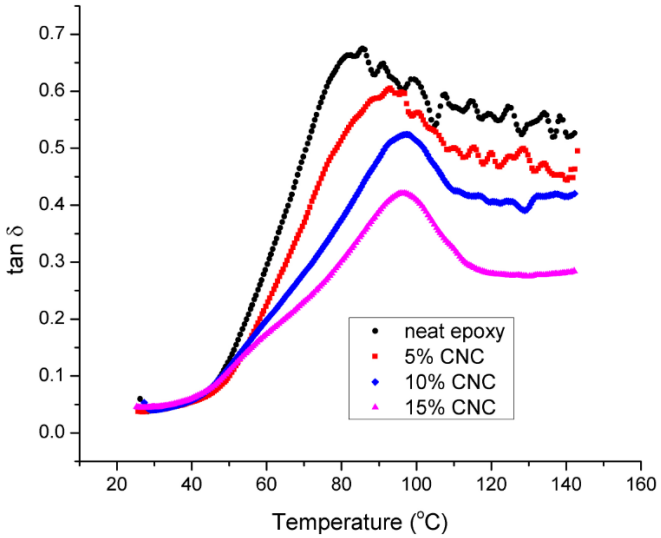

Figure 2.10 Values of tan(δ) from DMA versus temperature for CNC/epoxy composites as a function of CNC composition.

Figure 2.11 shows the storage modulus values at 30°C from DMA (a) and Young's modulus values obtained from tensile tests conducted at room temperature (b) as a function of CNC content. The results of both tests showed that the modulus increased approximately linearly with increasing CNC concentration, indicating that the CNCs serve as a reinforcing phase at all loadings studied here. Additionally, the reinforcement mechanism is likely similar for the CNC loadings used here since the change in modulus scaled roughly with CNC content. The average value of Young's modulus increased from 2200 MPa for neat epoxy to 3600 MPa for a 15 wt.% CNC composite-a 64 % increase, compared to a 100% increase in the storage modulus at 30 ºC measured by DMA. The tensile strength and strain at break from the tensile test decreased for lower CNC content samples (0.5% to 2%) compared to neat epoxy, then increased for higher CNC content samples (5% to 15%). The tensile strength increased from 40 MPa for neat epoxy to 60 MPa for the 15 wt.% composite. This increase in tensile strength was only significant at loadings of 10 and 15 wt.% CNC when compared to the neat matrix. The strain at break remained relatively constant for all loadings tested and did not show significant increases at any CNC concentration compared to neat epoxy, again suggesting a physical reinforcement mechanism. However, we note that the test standard was optimized for measurements of Young's modulus (10 mm/min) and not tensile strength or strain at break (12.5 mm/min and 2.54 cm larger grip separation).

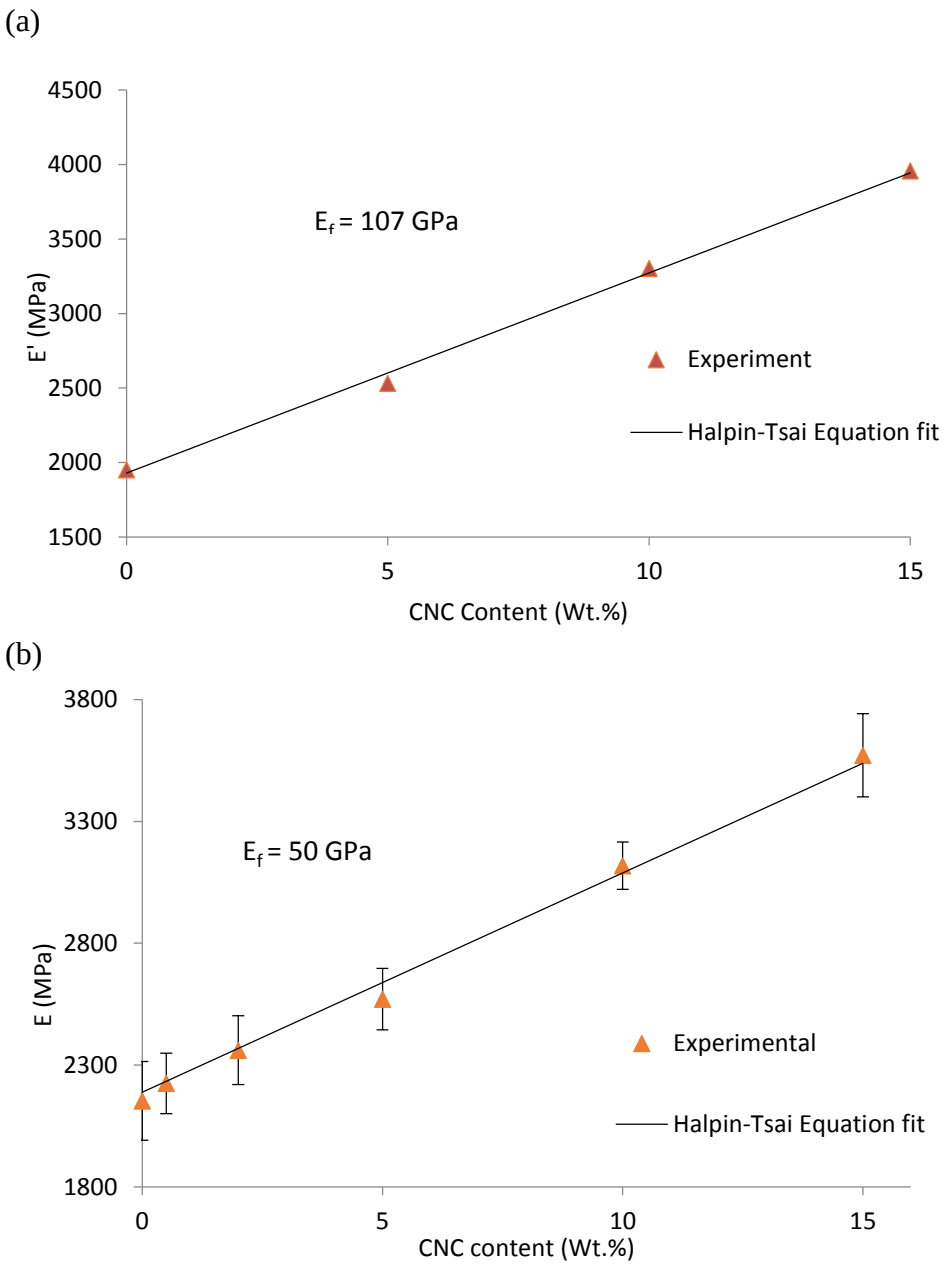

Figure 2.11 Experimental data (symbol) and linear fit (line) of (a) storage modulus (30 °C) and (b) Young's modulus as a function of CNC content.

The glassy modulus values obtained from DMA and the Young's modulus values obtained by uniaxial tensile testing were further analyzed through the use of the Halpin-Tsai and Tsai-Pagano micromechanical model for discontinuously reinforced composites with isotropic filler orientation.[92] The assumptions of the Halpin-Tsai model are uniform distribution of the filler

within the matrix and perfect adhesion between the filler and matrix.[93] The Tsai-Pagano equation averages the longitudinal and transverse composite modulus by the following equation:

$$E_c = \frac{3}{8}\mathrm{E_l} + \frac{5}{8}\mathrm{E_t} \quad (2.1)$$

where E_c is the predicted modulus of the composite, E_l is the longitudinal elastic modulus and E_t is the transverse modulus for the composite material. E_l and E_t are obtained from the Halpin-Tsai equations as follows:

$$\mathrm{E_l} = \left[\frac{1+2\left(\frac{l}{d}\right)\mathrm{n_l V_f}}{1-\mathrm{n_l V_f}}\right]\mathrm{E_m} \quad (2.2)$$

$$\mathrm{E_t} = \left[\frac{1+2\mathrm{n_t V_f}}{1-2\mathrm{n_t V_f}}\right]\mathrm{E_m} \quad (2.3)$$

The value *l/d* represents the aspect ratio of the CNCs, determined experimentally to be 22 by TEM (Figure 2.1) and V_f is the volume fraction of CNCs. Using the reported density of CNCs as 1.6 g/cm^3 and the measured density of neat epoxy as 1.18 g/cm^3, weight fractions were converted to volume fractions. n_l and n_t have the following expressions:

$$\mathrm{n_l} = \frac{\left(\frac{\mathrm{E_f}}{\mathrm{E_m}}\right)-1}{\left(\frac{\mathrm{E_f}}{\mathrm{E_m}}\right)+2\left(\frac{l}{d}\right)} \quad (2.4)$$

$$\mathrm{n_t} = \frac{\left(\frac{\mathrm{E_f}}{\mathrm{E_m}}\right)-1}{\left(\frac{\mathrm{E_f}}{\mathrm{E_m}}\right)+2} \quad (2.5)$$

E_f and E_m represent the axial fiber and matrix modulus, respectively. The value chosen for E_m was the experimentally-determined modulus value for the neat epoxy. The Halpin-Tsai equations give a prediction for the composite modulus of a material containing uniaxially-oriented discontinuous fibers, or 1-D orientation. The Halpin-Tsai equations combined with the Tsai-Pogano equation yield an approximation of the composite modulus for a random orientation of the fibers within the plane, or 2-D orientation.

The model was fit to the experimental data by a least-square regression, by using E_f as an adjustable parameter. The fitting results for the DMA (a) and uniaxial tensile testing data (b) are shown in Figure 2.11. In the literature, the axial Young's modulus of CNC has been reported to be as low as 57 GPa, and as high as 220 ± 50 GPa.[91,94] The Halpin-Tsai model applied to our data gives a value for the CNC modulus of 107 GPa and 50 GPa, for the DMA and uniaxial tensile testing data, respectively. These values fall on the low end of the range reported in the literature. A possible explanation for the low estimate of CNC modulus is that individual CNC dispersion was not achieved in these composites and that the primary reinforcement mechanism is physical. The aggregates seen in polarized light microscopy would decrease the expected reinforcing effect provided by the incorporation of individually dispersed CNCs within the composites. Another possible explanation could be that the CNC/epoxy interface was not ideal as assumed by the model. In any case, the Halpin-Tsai analysis provides an estimate of the modulus of wood based CNC for comparison with current literature values, and it provides an expectation of the effective filler modulus for the CNCs in this epoxy composite.

While the Halpin-Tsai model provides an estimate of the effective filler modulus, some drawbacks that might hinder its interpretation are the assumptions of uniform dispersion and a perfect interface between CNC and epoxy. From the PLM analysis, it is clear that these samples did not have uniform CNC dispersion, and determining the quality of the interface is extremely challenging for nanocomposites. Additionally, the Halpin-Tsai with the Tsai Pagano equation give composite modulus predictions of composites containing short fibers randomly oriented within the plane (2-D), and the fiber distribution in this case was likely 3-D given that the sample thickness was approximately 3 orders of magnitude greater than the length of the CNCs. Therefore, it is

important to consider the theoretical limitations on the elastic modulus of this epoxy/CNC composite, i.e. the theoretical upper limit.

For a composite where all orientations of the CNC phase are equally probable (3D random), as is the case for the epoxy/CNC composites studied here, the upper and lower bound properties are calculated by averaging stiffness and compliance matrix elements over all possible orientations for the axial direction of the CNC crystal.[18,95,96] A model derived by Christenson,[96] and Watt and Peselnick[95] describe the upper and lower bounds on the bulk, K, and shear, G, modulus, respectively. The equations are as follows:

$$\left(\frac{V_f}{K_T}+\frac{V_m}{K_m}\right)^{-1} \leq K_c \leq \frac{V_f}{9}(E_A + 4K_T + v_A^2 + V_m K_m) \quad 2.6$$

$$\left(\frac{V_f}{15}\left(\frac{1}{K_T}+6\left(\frac{1}{G_A}+\frac{1}{G_T}\right)+\frac{3(1+4v_A)}{E_A}\right)+\frac{V_m}{K_m}\right)^{-1} \leq G_c \leq \frac{V_f}{15}(E_A + 6(G_A+G_T) + K_T(1-2v_A)^2) + V_m G_m \quad 2.7$$

Here, the subscript 'A' refers to the parameter measured in the axial direction, 'T' refers to the parameter measured in the transverse direction, the subscript 'f' refers to the filler property, 'c' refers to the composite property, and 'm' refers to the matrix property. As mentioned previously, K is the bulk modulus and G is the shear modulus, E is the elastic modulus, and v_A is the axial Poisson ratio. For a glassy polymer, like epoxy, a good estimate of the Poisson ratio is 0.33. The bulk and shear modulus can be calculated from the theoretical relationships between elastic parameters, where the elastic modulus, E, and the Poisson ratio, v_A, is known.[97] For CNCs, the following estimates for material properties were used: E_A = 150 GPa, K_T = 7.6 GPa, v_A = 0.25, G_A = 15 GPa, G_T = 3.8 GPa.[18] From equations 2.6 and 2.7, the upper and lower bounds of the elastic modulus can be estimated as follows[18]:

$$\frac{9K_C^l}{1+\frac{3K_C^l}{G_c^l}} \leq E_c \leq \frac{9K_c^u}{1+\frac{3K_c^u}{G_c^u}} \qquad 2.8$$

Here, the superscript 'l' refers to the lower bound of the parameter as estimated by the left hand side of equations 2.6 and 2.7, and 'u' refers to the upper bound parameter as estimated by the right hand side of equations 2.6 and 2.7. Equation 2.8 was used to calculate the upper and lower bounds on the composite modulus and the results are given in Figure 2.12.

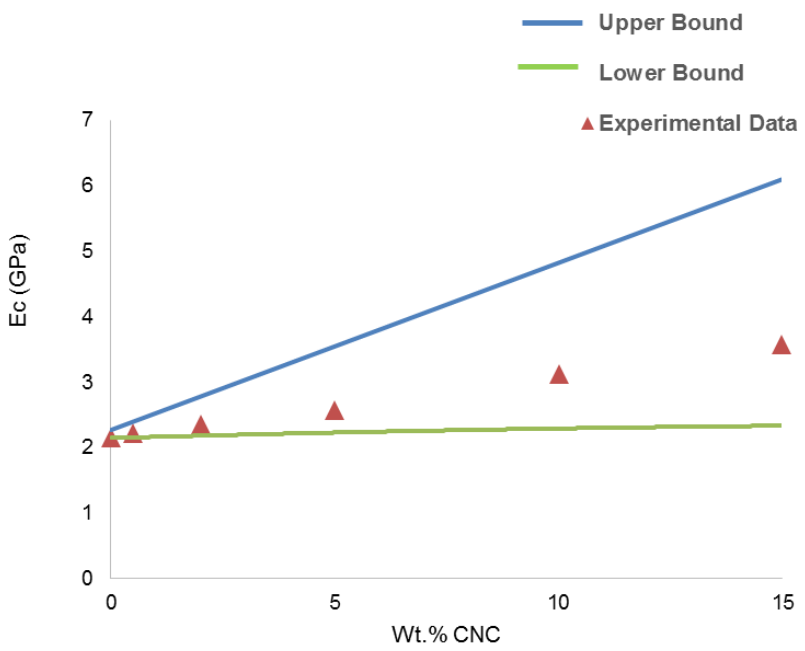

Figure 2.12 Upper and lower bound composite modulus in GPa for an epoxy/CNC composite.

Although equations 2.6-2.8 contain some estimates and assumptions, Figure 2.12 illustrates an important point: the epoxy/CNC composite modulus fell between the elementary upper and lower bounds for a glassy polymer. The increase in modulus with increasing CNC concentration observed here is notable, but not optimal, and improvements can be realized. Chapter 2 proposes an alternate processing method for enhanced CNC dispersion and improved composite mechanical property.

2.7 Conclusions

We report the preparation of wood-derived CNC-reinforced waterborne epoxy nanocomposites. The storage and loss modulus, Young's modulus, T_g, and tensile strength all increased with increasing CNC content, indicating good reinforcement of the epoxy resin matrix. While these increases were observed even though some aggregation of CNCs was seen, the investigation of methods to improve is worthy of future study. Water content and thermal stability were not degraded with the addition of CNCs. Overall, these results indicate that high loadings of CNC can be incorporated into waterborne epoxy matrices to improve their mechanical properties without compromising the neat matrix properties. When taken in the context of the results available in the literature for CNC nanocomposites, as well as other types of polymer nanocomposites, these results support the assertion that the processing-structure-property relationships in such nanocomposites are diverse and can be used to design materials for a broad range of applications.

CHAPTER 3

EXPLOITING COLLOIDAL INTERFACES TO INCREASE DISPERSION, PERFORMANCE, AND POT LIFE IN CELLULOSE NANOCRYSTAL/WATERBORNE EPOXY COMPOSITES

This chapter was adapted from a publication in *Polymer*:

Girouard, N., Schueneman, G. T., Shofner, M. L. & Meredith, J. C. Exploiting colloidal interfaces to increase dispersion, performance, and pot-life in cellulose nanocrystal/waterborne epoxy composites. *Polymer* **68,** 111–121 (2015).

3.1 Overview

In this study, cellulose nanocrystals (CNCs) are incorporated into a waterborne epoxy resin following two processing protocols that vary by order of addition. One approach towards controlling the interactions of CNCs with polymers is to take advantage of liquid-liquid or liquid-solid interfaces where CNCs may preferentially adsorb. CNCs contain both hydrophobic and hydrophilic domains[34] and can adsorb at oil-water interfaces to stabilize emulsions.[98] Several studies have detailed the phenomenon of colloidal haloing[99,100] and a large body of literature has defined and explored the broader field of Pickering emulsions.[35,98] In Pickering emulsions, stabilization of a liquid droplet involves particles that are strongly adsorbed to the liquid-liquid interface, which provide a mechanical barrier to droplet coagulation. Colloidal haloing is the stabilization of large drops or particles by much smaller particles, where the two particles have high charge asymmetry. The smaller particles are not directly adsorbed on the larger particle interface, but maintain a separation distance a few nanometers from the particle or drop surface.[100]

The adsorption or association of CNCs at interfaces offers intriguing possibilities for control of CNC-polymer interactions by changing the order of CNC addition, especially in multicomponent systems. The current study examines the effect of CNC order of addition on colloidal stability, CNC dispersion, and composite performance in a waterborne epoxy system.

Here we report that a simple change in the order of CNC addition, involving adding the CNCs either before or during the diamine addition, alters significantly the manner in which the CNCs interact with the epoxide. The formulations resulting from pre-addition of CNCs prior to diamine have long pot lives, suggesting that they may be candidates for one-part coatings with long shelf-life (> 1 month instead of a few hours).

3.2 Materials

The materials used in this Chapter are identical to those used in Chapter 2. Specifically, the 55 wt.% solid epoxide emulsion was crosslinked with a water soluble amine, and the 8.75 wt.% aqueous CNC suspension was used as received. The aqueous CNCs were used in all of the composite film samples. The aqueous CNC/epoxy composite suspensions were cast onto treated silicon wafers for the final curing step. A sample of freeze dried CNC material was also obtained from the U.S.D.A. Forest Products Laboratory. These particles were determined to contain 0.96 wt.% sulfur on a dry cellulose basis by ICP/MS. The freeze dried CNC particles were only used in the pot life experiment. Both CNC samples, aqueous and freeze dried, contain Na^+ as the counterion to the negative sulfate charge.

3.3 Sample Preparation

Film samples were prepared by two methods. In the first method, the epoxide emulsion, amine crosslinker, and aqueous based CNCs were combined and magnetically stirred together at medium speed (Corning PC-200 stirrer), referred to as ‘one-step mixing’. In the second method, the epoxy emulsion and aqueous based CNCs were combined and magnetically stirred at medium speed for 1 hour prior to crosslinker addition, referred to as ‘two-step mixing’. In both cases, stoichiometric amounts of epoxy and amine were used, and mixing was carried out at room temperature. Subsequent steps leading to film formation were the same for both methods. The nanocomposite

mixture was precured for 0.5 to 2 hours at room temperature until the viscosity of the mixture increased enough to barely allow flow. Precuring times were determined by visual inspection and increased with CNC concentration since greater amounts of water, resulting from the CNC suspension, were present thereby diluting the reactive epoxy. The mixture was then cast onto the OTS treated silicon wafer substrate and dried at room temperature for 1-3 hours until the mixture was not able to flow. The coated substrates were then transferred to an oven and cured for 2 hours at 100°C, or 120°C (10 and 15 wt.% CNC samples only). Neat epoxy samples were prepared using the same processing protocols for comparison. As a control for the two-step mixing procedure, the neat sample was prepared by first magnetically stirring the epoxy emulsion for 1 hour followed by addition of the amine crosslinker and additional mixing. The final thickness of the neat epoxy and nanocomposite films was approximately 150 to 200 μm. Optical, thermal, and mechanical characterization described below was carried out on nanocomposite films made with the aqueous based CNCs.

3.4 Composite Characterization

3.4.1 PLM

The level of CNC dispersion achieved by the two processing methods in the epoxy matrix was investigated qualitatively by the observation of birefringence with an optical microscope (Olympus BX51) equipped with two polarizers (Olympus U-AN360P). Images were captured with an Olympus camera (U-CMAD3) and processed with PictureFrame software. All films were imaged in transmission mode with a 20X objective and at full extinction of the polarizers.

3.4.2 ATR-FTIR

The chemical structure of cured film samples was characterized by Fourier transform infrared (FT-IR) spectroscopy using an attenuated total reflectance (ATR) accessory (Bruker

Vertex 80V, equipped with Hyperion 20X ATR objective). The spectra were corrected to subtract the background signals and flatten the baseline. The wavenumber scan range was 4000 cm^{-1} to 600 cm^{-1} with a resolution of 4 cm^{-1} and a total of 64 scans. The epoxy precursor contains aromatic rings which were assumed to not participate in the reaction. Aromatic rings absorb in the 1600-1470 cm^{-1} region, specifically at 1600, 1580, 1470, and 1510 cm^{-1}.[101] All of these peaks were present for both the epoxy precursor and the cured neat polymer thus confirming that these functional groups do not react in this system. The FTIR spectra were normalized by the absorbance at 1510 cm^{-1}, a peak common to all samples and unaffected by the chemical reactions or interactions. All figures represent normalized data.

3.4.3 Zeta Potential

The epoxy emulsion and aqueous CNC suspension were mixed together for several hours and then diluted. The volume fraction of epoxy was held constant while the volume fraction of CNC was varied. The zeta potentials of neat CNCs and neat epoxy emulsion were also measured. The measurements were performed using a Malvern Zetasizer Nano ZS 90. Measurements were performed in triplicate at 25 °C, and the average values were reported. The same instrument was used to measure the size of the epoxy particles in light scattering mode.

3.4.4 FE-SEM

To observe the component interactions in the two-step processing method, the CNC/epoxy emulsion suspension were imaged with field emission scanning electron microscopy (FE-SEM). To prepare the sample, the epoxy emulsion and aqueous CNC suspension were mixed together for several hours and then diluted. The sample was then lyophilized for suitable imaging. The resulting product of the freeze drying process was adhered to carbon tape and sputter coated with a thin layer of gold. The samples were imaged by FE-SEM (Zeiss Ultra60). The morphology of cured

polymer fracture surfaces were also examined with FE-SEM (Hitachi SU8010). These samples were not sputter coated and imaged at 0.9 kV.

3.4.5 DSC

The values of the glass transition temperature (T_g) for the fully cured neat epoxy and composite films were measured by differential scanning calorimetry (DSC) (TA Instruments DSC Q200). In the first step, samples were heated from 30 °C to 150 °C at a rate of 10 °C/min and then held at that temperature for 2 minutes. The samples were then cooled to 0 °C, held for 2 minutes, and subsequently heated to 150 °C at a rate of 10 °C/min. Data from the first and second heating step were used to obtain the T_g of the sample. The value of T_g was assigned as the midpoint of the transition region between the glass and rubber line on the heat flow curve using TA Universal Analysis Software. An exothermic/cure peak was not observed for any of the samples tested here, only a broad evaporation peak around 100 °C which was due to residual moisture left in the samples. The moisture content of the samples was quantified with thermogravimetric analysis (TGA). Measurements were performed three times on fresh samples for each material composition, and average data were reported.

3.4.6 TGA

Water absorption, thermal stability and changes in degradation patterns associated with CNC addition and processing were assessed with TGA (TA Instruments TGA Q5000). Samples were heated from room temperature to 120 °C at a rate of 10 °C/min under a flowing nitrogen atmosphere and then held at that temperature for 20 minutes. In the final step, samples were heated to 600 °C at a rate of 10 °C/min. The water absorbed by samples was measured as the weight loss during the first two steps. The thermal stability and decomposition patterns of the samples were obtained from the last step. The onset temperature and temperature at maximum weight loss were

determined with TA Universal Analysis software. Measurements were repeated three times, and average values were reported.

3.4.7 DMA

The storage and loss moduli of the materials was determined from dynamic mechanical analysis (DMA) experiments (Mettler Toledo DMA/SDTA861). Samples were made by cutting films into strips a few centimeters long and 2.5-3 mm wide. The sample length was trimmed after the samples were mounted, resulting in a testing length of 9 mm. Samples were tested in tension mode in the linear viscoelastic regime for the materials. The linear viscoelastic regime was determined by strain sweep tests at the lowest and highest temperatures to be used during the test. The tests were conducted at a frequency of 1 Hz, over a temperature range of 30 °C-150 °C, and at a heating rate of 2 °C/min. Measurements were repeated three times, and average values were reported. Additionally, T_g values were obtained from the peak of the loss modulus curve.

3.4.8 Tensile Test

Uniaxial tensile testing was performed using an Instron 5842 testing frame equipped with a 100 N load cell. The samples were prepared by die cutting the films with a dog bone template based on the ASTM standard D1708-13. The specimens were strained at a rate of 0.5 mm/minute. Tensile strength, % elongation, and toughness data were obtained. A minimum of four samples were tested for each material composition, and the average values were reported where the error bars represent 95% confidence intervals.

3.5 Results and Discussion

3.5.1 Nanocomposite Morphology

Composites up to 15 wt.% CNC were produced, and across all concentrations tested and for both mixing procedures, the materials retained a similar level of transparency to the neat matrix.

Figure 3.1 highlights this result, showing that films made by the one-step and two-step mixing methods were colored but transparent.

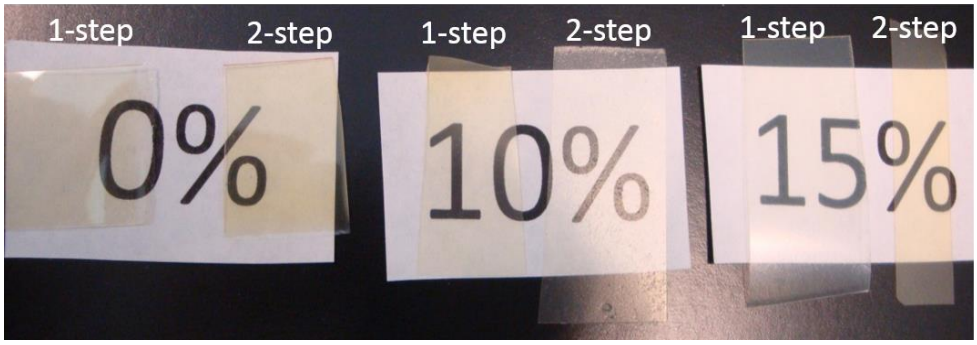

Figure 3.1: Image of neat epoxy and nanocomposite films containing 0, 10, and 15 wt.% CNC following curing. The films made by both methods appear transparent but colored.

The dispersion level of the CNCs within the cured epoxy matrix for both processing methods was assessed with polarized optical microscopy. The images are given in Figure 3.2. The neat material displayed limited birefringence, so birefringent domains observed in the composites were attributed to CNC aggregates. Composites with CNC loadings up to 15 wt.% showed varying degrees of birefringence and different domain sizes for the birefringent regions. These differences in birefringence were related to the processing method and the CNC loading. For the samples made by one-step mixing, the size of the CNC domains was on the order of tens of microns. Larger aggregates were present in lower concentration samples compared to higher concentration samples. This effect was attributed to the longer mixing times used to prepare the 10 and 15 wt.% samples. Since more water was introduced into these samples with CNC addition, longer mixing times were required to attain the viscosity needed for proper precuring. The longer mixing times resulted in a better level of CNC dispersion. For films made by the two-step process, the CNCs had improved dispersion at all loadings tested with respect to those made by the one-step process. The 2 wt.% composite produced by the two-step method displayed almost no birefringence while

higher loadings contained CNC domains. These domains were smaller in size and their brightness was less intense than the domains seen in composites made by one-step mixing.

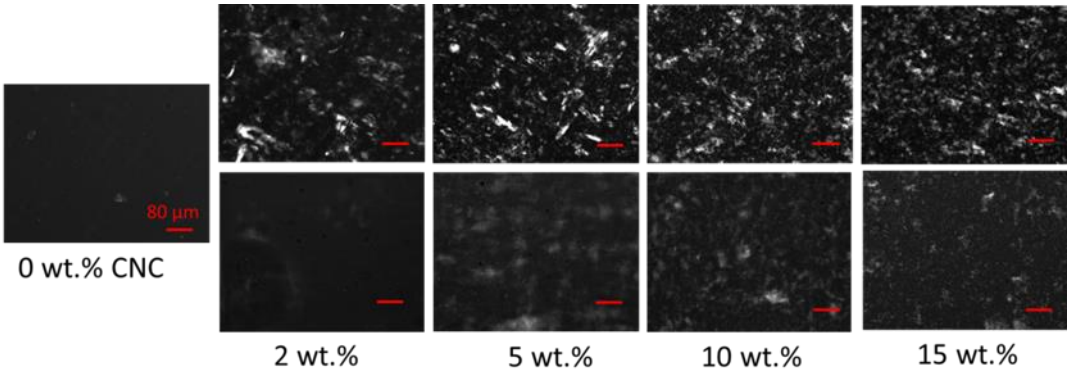

Figure 3.2: Polarized light microscopy images of epoxy/CNC composites. Top: one-step mixing, bottom: two-step mixing.[102]

Although domains of CNCs larger than the length of visible light were observed in polarized light, all composites had a similar level of transparency with respect to the neat epoxy as shown in Figure 3.1. This attribute was due to refractive index matching of the epoxy and CNCs. Landry *et al.* reported that the refractive index of sulfuric acid hydrolyzed cellulose was 1.499[103] and Cranston *et al.* reported the refractive index of cotton-derived CNCs to be between 1.51 and 1.55, depending on the measurement method and number of bilayers of alternating cellulose and poly(allylamine hydrochloride).[104] Epoxy polymers typically have a refractive index ranging from 1.515 to 1.565.[105] Thus, it is expected that the refractive index of this epoxy polymer is within this range and similar to that of the CNCs.

To assess the degree of cure and understand the chemical structure of the nanocomposites, FTIR spectra were measured for the nanocomposite components and the nanocomposites. For the epoxy prepolymer, the absorption band at 912 cm^{-1} was associated with the unreacted epoxide group.[75] The disappearance of this band in the neat epoxy and all composites tested here indicated that all of the epoxide groups reacted during the curing cycle.

CNCs have the potential to react with the epoxide group. If this event does occur, an ether bond will form, a hydroxyl group from cellulose will be consumed and a different hydroxyl group will be created, linking the epoxide monomer to the CNC surface. Additionally, the hydroxyl groups from cellulose can form hydrogen bonds with the epoxide group.

Differences in the FTIR spectra were observed for films made by the one-step and two-step methods. Portions of the spectra highlighting these differences are shown in Figure 3.3. First, an increase in intensity was observed in the 3200-3600 cm^{-1} region for the composites produced by the two-step method. The composites with improved CNC dispersion will inevitably have more interfacial area with the polymer matrix, and the exposed CNC surface hydroxyls likely have different infrared absorption characteristics (extinction coefficient, shift in wavenumber) than hydroxyls that are buried within CNC aggregates. For example, in addition to the increased intensity, a shift in the peak maximum was observed from 3400 cm^{-1} for the one-step method to 3330 cm^{-1} for the two-step mixed. A peak shift towards lower wavenumbers could indicate the presence of increased hydrogen bonding between CNCs and the polymer matrix in the two-step samples, which appears to correspond with the enhanced CNC dispersion.[106]

Second, a new peak was observed at 1060 cm^{-1} for the two-step mixed samples. This band appears to be evidence of a new ether bond. Two other possible assignments for this band include a primary aliphatic alcohol, which would be present in this system before and after an epoxy/cellulose reaction, or the glycosidic bond in cellulose, which is sometimes obscured in the infrared spectrum.[101] The evolution of this band as a function of time was monitored with liquid ATR-FTIR, and it was found that the intensity increased as reaction time increased. This observation indicates higher concentrations of this bond as the reaction progressed. This absorption was not present for the neat sample tested under the same conditions thus indicating that the

presence of CNCs was responsible for these changes. While these changes are obvious, it is difficult to discern the functional group(s) responsible since absorbance in this region of the spectrum is likely due to a number of functional groups present in the cured composites.

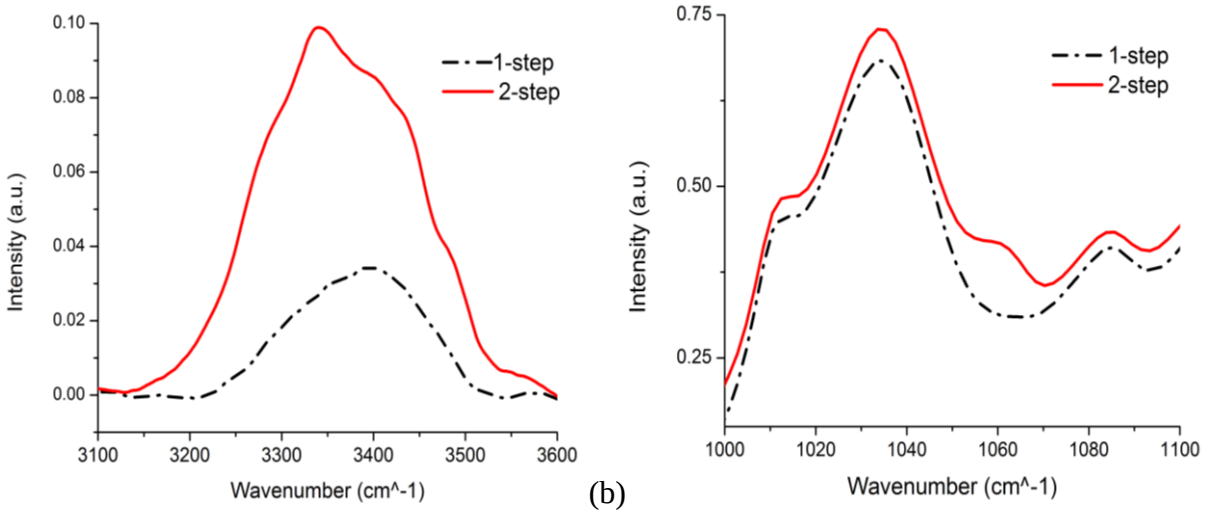

Figure 3.3: ATR-FTIR spectra of films made by one-step (-•-•-) and two-step (—) mixing for a 5 wt.% cured composite, (a) 3100-3600 cm^{-1} (b) 1000-1100 cm^{-1}.

Chemical analysis of this CNC/epoxy system was not trivial since most of the absorbances present in the reactants were also present in the final cured composite, and similar functional groups were present in all components. Nevertheless, the possibility of hydroxyl-containing CNC particles reacting with the epoxide group was ruled out when no change in the intensity of the oxirane vibration at 912 cm^{-1} was observed before and after heating the epoxy-CNC suspension at 100 °C for 1 hour. Therefore, an altered stoichiometry is not responsible for the changes reflected in the composites made by the two processing methods, the effect is purely a physical one.

3.5.2 Size and Charge Measurements

The zeta potential of a 0.01 wt.% CNC suspension was measured to be -71 mV, indicating that the CNCs were well-dispersed in water and largely isolated from one another. The negative charge was expected due to the sulfate ester functionality present on the CNC surface, leading to

double-layer repulsion between particles. Due to the high magnitude of the zeta potential for the CNC suspension, a highly stable suspension was expected. The zeta potential of a 0.05 wt.% aqueous epoxy prepolymer suspension was measured to be -20 mV, a low charge that indicated a significantly lower kinetic stability than the -71 mV measured for the CNCs, and -68 mV for the $V_{CNC}=1x10^{-4}$ CNC-containing epoxy droplets. Additionally, the size of the epoxy drop was measured with this instrument, indicating that the average diameter was 484 ± 63 nm, in agreement with the manufacturer's data.

The zeta potential of the aqueous suspension consisting of the epoxy prepolymer with varying amounts of CNC is shown in Figure 3.4. The volume fraction of epoxy remained constant at $5x10^{-5}$, while the CNC volume fraction was varied. At low volume fraction of CNCs, the zeta potential of the binary mixture remained close to the zeta potential of neat epoxy. As the CNC concentration increased, the zeta potential also increased, approaching the value for neat CNCs when the CNC volume fraction was $1x10^{-4}$. This result indicated that the CNC particles shielded the epoxy particles through either nanoparticle adsorption (Pickering emulsion) or a nanoparticle haloing effect. Since electrophoretic mobility is independent of size, this result implied that the epoxy particles and the CNCs moved in unison in response to the applied voltage, indicating that the two were associated.[99] This result supports the previous hypothesis that the CNCs associate around the epoxide droplet to hinder particle coalescence. Based on this information, it was also concluded that the CNCs imparted additional stability to the epoxy emulsion. Similar results have been reported for silica microspheres stabilized by zirconia nanospheres,[99] a poly(butylmethacrylate) emulsion stabilized with cellulose whiskers,[107] and $CaCO_3$ nanoparticles stabilized by sodium dodecyl sulfate.[108] Two possible explanations are colloidal haloing or

nanoparticle adsorption directly at the epoxide-water interface (as in a Pickering emulsion), which are known to create the same behavior in zeta potential found to occur in the two-step samples.

It is important to note that while this result indicated that CNCs and epoxy precursors certainly had some interactions, it is difficult to specify those interactions for this system. This epoxy formulation is proprietary and thus some chemical information about the components is unknown. The molecular formula for the surfactant used to emulsify the epoxy is not given, so it is important to clarify that the CNCs may be interacting with the epoxy itself, the surfactant, or both.

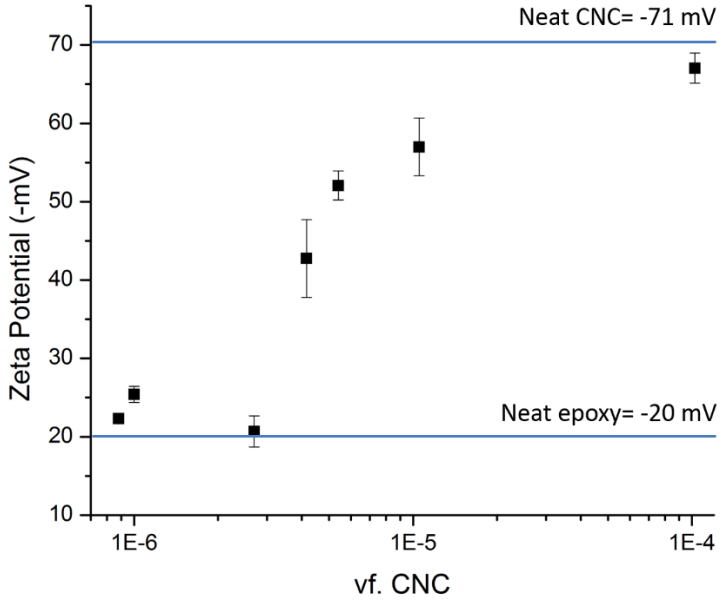

Figure 3.4: Zeta potential curve for epoxy precursor and CNC dispersions as a function of volume fraction of CNC (vf. CNC).

3.5.3 Polymer Morphology

The morphology of this CNC/epoxide configuration was further investigated with FE-SEM. A mixture of CNCs, epoxy, and water was mixed together for several hours, freeze dried, and imaged. This result is given in Figure 3.5. The imaging indicated that a sphere consistent in

size with the epoxy precursor was coated with a layer of CNCs. This result support the hypothesis that the CNC/epoxy premixing step leads to improved dispersion due to a more intimate association between the CNC and surfactant coated-epoxy particle.

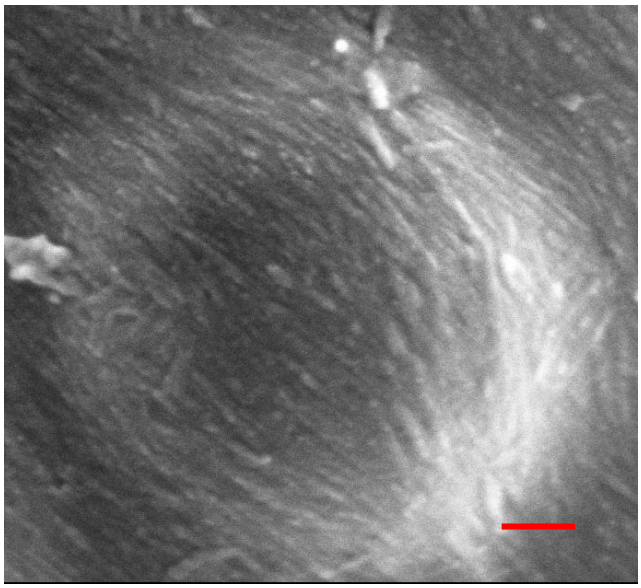

Figure 3.5: FE-SEM image of an epoxy particle coated with CNCs. Scale bar is 100 nm.

The morphology of the composite interface was also investigated with FE-SEM. The samples were fractured in ambient conditions, below T_g for the cured epoxy. Figure 3.6 shows the fracture surfaces of 5 wt.% composites made by one-step and two-step mixing. The interface of the composite made by one-step mixing appeared smooth and represented that of a typical polymer surface which experienced brittle fracture. It should be noted that the micron-sized CNC domains did not appear in these images. The contrast observed between the CNCs and the epoxy resin with electron microscopy was low due to their similar electron density. The interface of the composite made by two-step mixing showed some noteworthy features. First, the two-step mixed sample was rougher than the one-step mixed sample. Second, this surface appeared to feature spherical particles. These particles were consistent in size with that of the epoxy precursor. Thus, for the

two-step mixing case, the CNC particles appear to have preserved the epoxy as a separate phase rather than becoming a homogeneous matrix upon reaction with the amine. We hypothesize that the CNCs are the cause of this effect with the likely mechanism being their surrounding the epoxy particle to form a barrier to epoxy droplet coalescence until the water has evaporated, preserving the shape of the original droplet. Another difference between these two interfacial morphologies was that the fracture surface of the sample produced by one-step mixing was relatively homogeneous throughout the observed area, whereas the fracture surface of the sample produced by two-step mixing was inhomogeneous with some areas containing spherical features while other areas are consistent with the sample produced by one-step mixing. This blend of morphologies is indicative of a transitional or intermediate state where most but not all of the epoxy particles have strong interactions with CNC prior to cure.

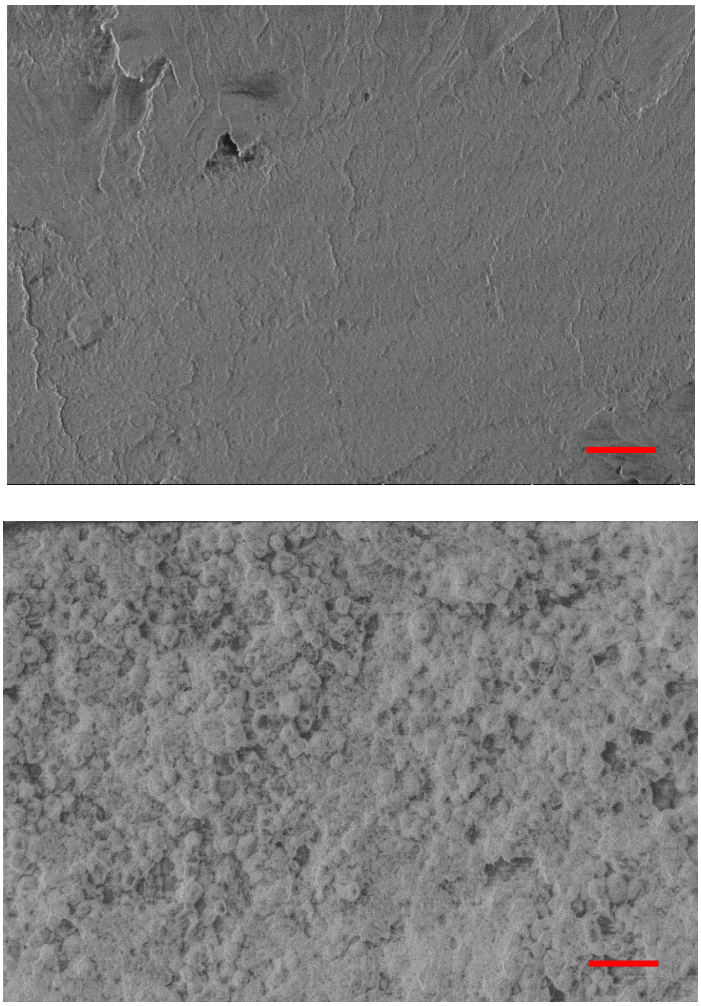

Figure 3.6: FE-SEM images of a 5 wt.% composite fracture surface. Top: one-step mixing Bottom: two-step mixing, scale bar is 1 µm.

3.5.4 Thermal Properties of Nanocomposites

The values of T_g for composites made by the two processing protocols were determined with DSC experiments, and the results are shown in Table 3.1. The values of the T_g observed during the first heating cycle for all concentrations and processing methods were similar when considering confidence intervals. Thus, it was concluded that the mixing method and CNC content did not significantly affect the T_g of the samples following preparation. However, the measured T_g value obtained from a second heating cycle was affected by CNC content for samples prepared by

the one-step mixing method. Similar to data reported previously by the authors,[17] T_g increased by approximately 7 °C at a CNC loading of 10 wt.% after being heated to 150 °C during the first heating cycle. In contrast, the T_g values obtained for the samples produced by the two step mixing method were not appreciably affected by CNC content, though these values were higher than those measured from the first heating cycle. These differences are difficult to interpret precisely because of the larger confidence intervals for the materials produced by the 2-step method.

Table 3.1: Glass transition temperature values with varied CNC concentration and processing method. Error represents 95% confidence intervals.

	0 wt.% CNC		5 wt.% CNC		10 wt.% CNC	
	1-step	2-step	1-step	2-step	1-step	2-step
First Heat	48.6 ± 5.9	46.7 ± 0.7	46.1 ± 3.4	45.9 ± 3.5	50.6 ± 2.4	49.2 ± 1.8
Second heat	63.0 ± 1.8	60.6 ± 4.2	63.6 ±1.5	62.0 ± 5.4	69.8 ±1.1	61.9 ± 5.5

The thermal stability of the composites was tested with TGA, and the results are shown in Figure 3.7. The onset temperature of thermal degradation was reduced with increasing CNC concentration. The bounding thermal degradation temperatures were established by the composite components. Neat epoxy began degrading at 297 °C, and neat CNC began degrading at 208 °C. There were no differences in degradation between composites made by one-step and two-step mixing. Compared to neat samples, while the CNCs did affect the initial degradation profile, the extent of the impact was not as great as expected at the higher CNC loadings. Employing the rule of mixtures model, it was found that the onset degradation temperatures for the composites containing lower CNC loadings (< 10 wt.%) were consistent with the prediction; however, this

model predicted that the composites containing 10 and 15 wt.% CNC would have a lower onset degradation temperature than the experimentally measured value. This departure from the rule of mixtures suggested that the CNCs were integrated within the epoxy matrix, possibly through chemical bonds, for both processing scenarios.

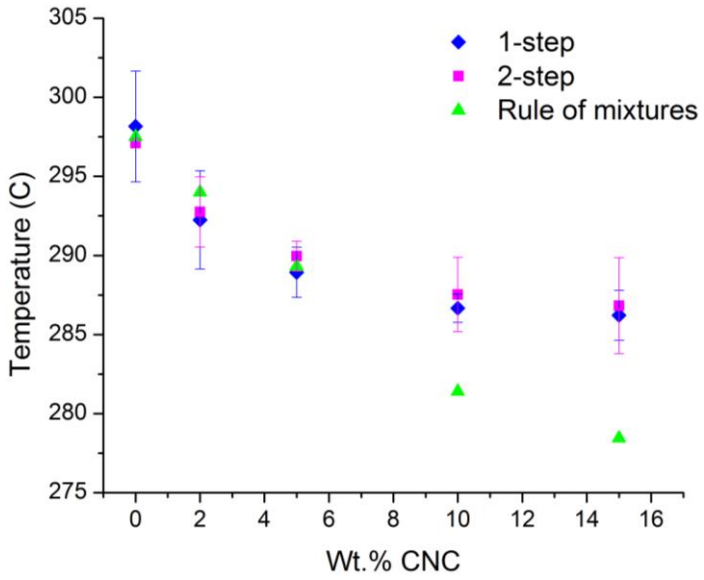

Figure 3.7: Onset temperature of thermal degradation as a function of CNC concentration.[15] Two-step mixing (♦), one-step mixing (■), rule of mixtures (▲).

The thermal degradation patterns of composites and neat epoxy occurred in two major steps, with the temperatures at maximum weight loss rates occurring at 335 °C and 385 °C. Processing conditions as well as CNC content had little to no effect on the degradation patterns observed here. The mixing method also had little to no effect on the water content of the samples, which was measured to be about 3 wt.% for all concentrations and processing methods tested here.

3.5.5 Mechanical Property of Nanocomposties

The thermomechanical performance of composites made by the two processing strategies was tested with DMA. The samples were tested in tension mode below and above T_g. Storage modulus (E') data are shown for samples made by one- and two-step mixing in Figure 3.8. These data suggested that the composites made by two-step mixing were reinforced more effectively than

composites made by one-step mixing in the glassy region of the storage modulus curve, with improvements of 49% for the 5 wt.% composite and 30% for the 10 wt.% composite at 40 °C. Comparing the composites to the neat matrix at 40 °C, the 5 wt.% sample made by one-step mixing had an increase in the storage modulus of 47% while the sample made by the two-step mixing method had an increase of 91%. Similarly, the 10 wt.% sample was increased by 60% for the one-step mixing case and 86% for the two-step mixing case when compared to the neat matrix at 40 °C. There were no significant differences in the rubbery modulus for composites made by either method. It is well known that CNCs can have profound effects on modulus, especially at temperatures greater than T_g.[82,89,109] Other work in CNC/epoxy composites has shown dramatic increases in storage modulus above T_g with respect to the neat polymer due to the formation of a network of mechanically percolated nanofibers. The ability of a fiber to form a percolated network and thus have substantial impacts on rubbery modulus is a function of the aspect ratio and the volume fraction. Generally, the critical volume fraction required to form a percolated network is given by: $X_c=0.7/AR$.[110] Results presented by Tang *et al.* showed a 70 X increase in the rubbery storage modulus for CNCs extracted from tunicate (AR=84) and a 12X increase for CNCs extracted from cotton fibers (AR=10) in epoxy composites at a 15 wt.% loading (12 vol.%), a CNC loading above the critical volume fraction of 0.8 vol.% for the tunicate CNCs and 7 vol.% for the cotton CNCs.[89] In the results presented here, much smaller gains in reinforcement were seen above T_g with respect to the neat polymer as compared to Tang *et al*. The different thermomechanical reinforcement trends were ascribed to differences in CNC network formation. In this work, a waterborne epoxy was used, and discrete birefringent domains of CNCs were observed in the composites with PLM. These results suggest large scale connectivity of individual nanofibers did

not occur in these composites, even though the CNC loadings used were above the critical volume fraction.

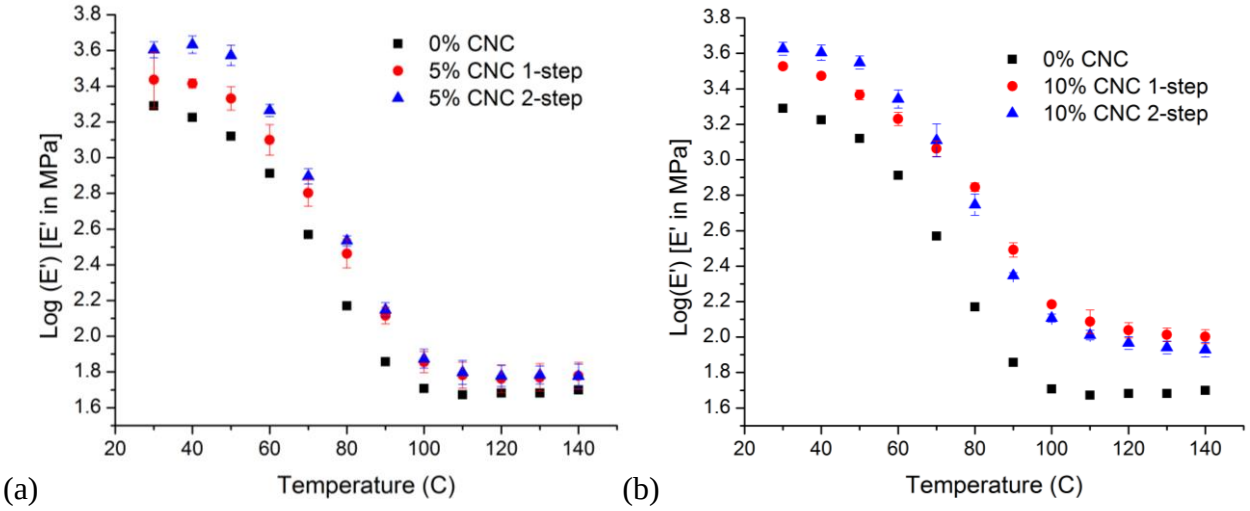

Figure 3.8: Storage modulus of (a) 5 wt.% and (b) 10 wt.% CNC composite made by one-(●) and two-(▲) step mixing. 0 wt.% CNC for comparison (■).[102] Error bars represent 95% confidence intervals.

While the processing method impacted the glassy mechanical properties preferentially, CNC addition had an effect on the storage modulus in the glassy and rubbery region when comparing the composites to the neat epoxy. As the temperature increased, the storage moduli for samples at different compositions began to deviate in the transition region at 50 °C, and this deviation continued into the rubbery region. The difference in the storage modulus values of the composites produced by both methods and the neat epoxy was greater with increasing CNC concentration, and these changes in rubbery storage modulus were similar for both mixing methods at a given CNC loading. For example, at a 5 wt.% CNC loading, the rubbery storage modulus was increased by 30 % at 120 °C, and for a 10 wt.% CNC loading, the rubbery storage modulus was increased by 70 % at 120 °C.

The loss modulus (E'') data comparing the two methods of preparation for a 5 and 10 wt.% composite are given in Figure 3.9. Generally, the value of loss modulus increased with increasing

CNC content, and the value of the loss modulus was similar for the composites of the same composition produced by the two methods, though there was some change in the magnitude of the loss modulus in the vicinity of the peak. However, these curves do not show significant differences in terms of peak shifts towards higher T_g with CNC content or processing method. The T_g values from DMA data would be most comparable to those obtained during the first heating cycle of the DSC measurements, where T_g was not different with processing or CNC concentration. Similar to the DSC data, there was a larger confidence interval in the measured value of the T_g for the samples made by the two-step mixing method.

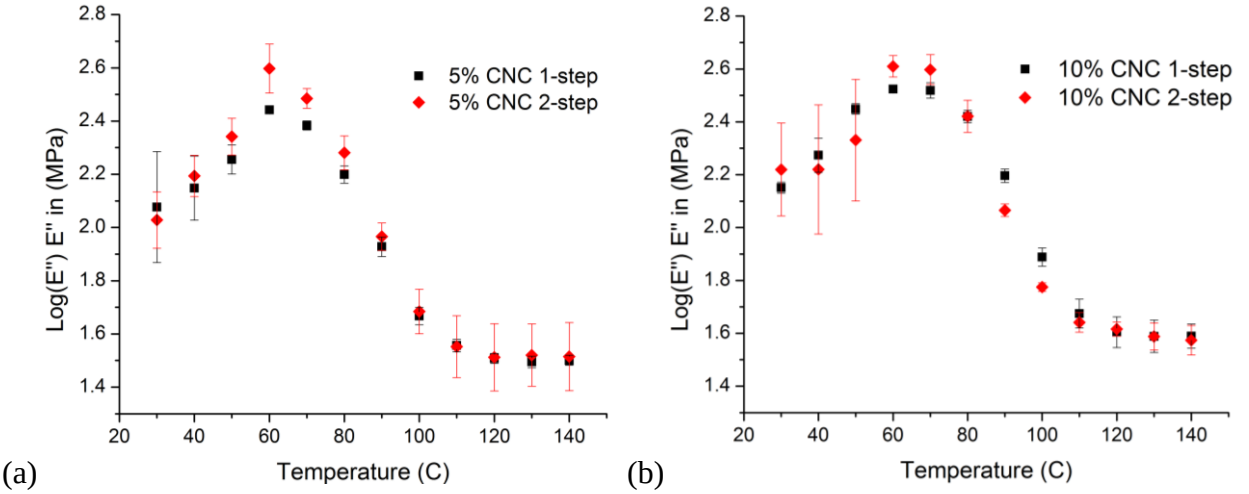

Figure 3.9: Loss modulus of (a) 5 wt.% and (b) 10 wt.% CNC composite made by one- (♦) and two-(■) step mixing.[102] Error bars represent 95% confidence intervals.

To understand more fully what these data trends indicated about the reinforcement mechanism provided by the CNCs, the ratio of the loss and storage moduli, tan delta, was also examined. The values of tan delta were similar for composites containing the same amount of CNCs (data not shown). Since tan delta, and as a result the phase angle, were similar, the reinforcement seen was largely a result of increased CNC dispersion. While the FT-IR data suggest that there is an association between the CNCs and the matrix when the two-step mixing processing

method is used, it does not appear to affect macroscale properties more than the differences in CNC dispersion since disproportionate changes in storage and loss modulus were not observed as a function of processing method.

Tensile testing also provided insight into the reinforcing effect of CNCs as well as the effect processing had on mechanical properties. The tensile strength and toughness from work of fracture data for 0, 5, and 10 CNC wt.% samples made by the two processing methods is given in Figure 3.10. The elongation at break was similar for all samples tested; therefore, the data are not shown. All samples experienced brittle fracture with an average elongation at break of about 4%.

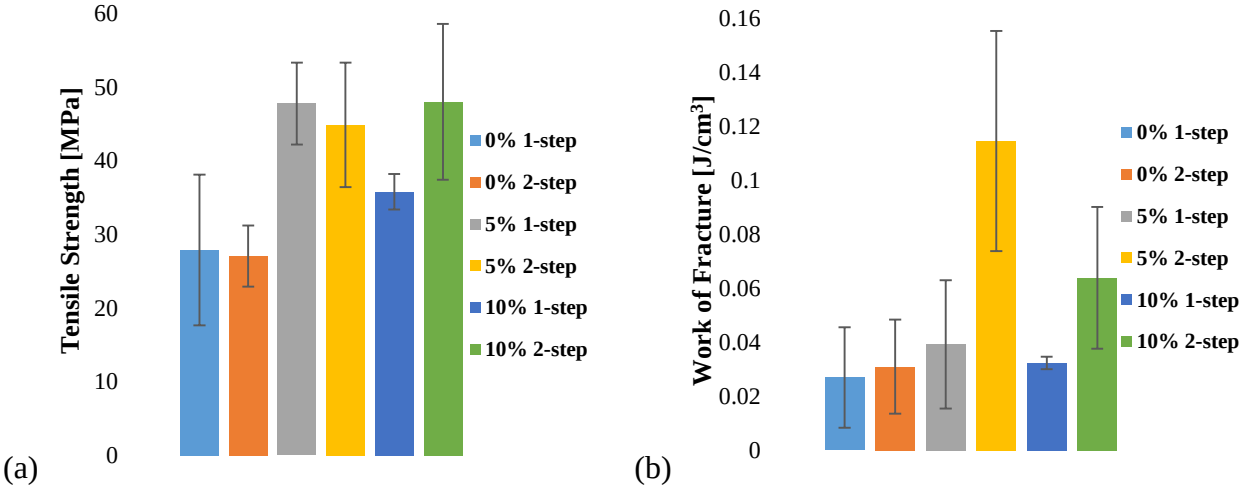

Figure 3.10: (a) Tensile strength and (b) work of fracture for 0, 5, and 10 wt.% CNC samples made by one- and two-step mixing. Error bars represent 95% confidence intervals.

Processing method was not found to affect the properties of the neat epoxy. Therefore, the delay in amine addition necessary for the CNC premixing step was not responsible for the changes observed in the composite samples, but rather the differences in morphology, level of CNC dispersion, and CNC-matrix interactions brought about by premixing the CNCs with the epoxy droplets before amine addition. The tensile strengths of the 5 and 10 wt.% CNC composites produced by one-step mixing were 47.7 ± 5.6 and 35.8 ± 2.4, respectively. The tensile strengths of

the 5 and 10 wt.% CNC composites produced by two-step mixing were 44.9 ± 8.5 and 48.0 ± 10.6, respectively. These values were greater than those obtained for the neat epoxy produced by one-step and two-step mixing, 27.9 ± 10.2 and 27.1 ± 4.1, respectively. The data showed that CNC addition improved tensile strength at both loadings and with both processing methods studied in this work, but the differences between the tensile strengths for the composite samples were not statistically significant when considering the calculated confidence intervals. The effect of processing was more evident when considering the work of fracture data. In general, the samples made by the one-step mixing method and the neat epoxy samples had similar values for the work of fracture, with no differences observed with increasing CNC concentration. Conversely, the CNC/epoxy composites made by the two-step method exhibited increases in work of fracture of 93% and 67% compared to the sample made by the one-step method at the same concentration for a 5 and 10 wt.% composite, respectively. The difference in toughness between the samples produced by the two methods likely resulted from better CNC dispersion in samples produced by the two-step processing method. However, it is important to note here that the confidence interval was large. In general, the error range was larger for samples made by the two step method. As mentioned earlier, a hypothesis for the larger variations in the data is the inhomogeneous fracture morphologies observed in SEM for the samples made by the two-step method.

3.6 Pot Life Extension

One potential application of the CNC-stabilized epoxide droplets was explored. In industrial applications, a practical concern is the large amount of water present in the CNC aqueous suspension. Addition of CNCs as a dry powder would be advantageous for practical reasons such as the avoidance of post-cure drying and reduced shipping costs for dry material. When 5 wt.% of the freeze dried CNC material was added to the epoxide suspension followed by amine addition,

the pot life of the nanocomposite mixture was extended by three orders of magnitude when compared to that of the neat epoxy-amine mixture (1 month versus 2 h). A substantially increased pot life enables the possibility of formulating one part waterborne epoxy coatings where the components are premixed and remain uncured for long periods of time until applied as a coating. In this scenario, the presence of the CNC particles that were premixed with the epoxide suspension appears to prevent the aggregation of the epoxide particles, even though the epoxide and amine reaction was occurring within them (confirmed by liquid ATR-FTIR indicating a decrease in 912 cm^{-1} peak, data not shown). The extension of the gel time (pot life) to 30 days may be a physical phenomenon resulting from the electrostatic stabilization conferred by the adsorbed CNCs. To explore this idea, we added NaCl to the CNC-stabilized epoxide/amine suspension. NaCl was added at 0.2 M to a stable mixture of freeze dried CNC, epoxide suspension and amine crosslinker prepared by the two-step method. Although the suspension was stable prior to salt addition, the system showed an immediate increase in viscosity (noted qualitatively) and eventually gelled after salt addition. These observations indicate flocculation of both CNCs and CNC-coated epoxy particles upon screening of the electrostatic charge imparted by the CNC particles to the epoxy particles.

3.7 Conclusions

In these CNC/epoxy composites, improved nanoparticle dispersion was achieved by a two-step procedure in which CNCs were premixed with the epoxy precursor, compared to the one-step mixing of the epoxy precursor, amine crosslinker, and CNCs. The stability of the waterborne system and resulting structure and properties are significantly improved by the pre-addition of CNCs. Improved dispersion was attributed to a more intimate association of CNC particles with the surfactant-stabilized epoxy precursor droplets allowed by the premixing step, similar to

stabilization mechanisms observed in colloidal haloing systems or Pickering emulsions. Evidence of the improved stability was supported by changes in the ATR-FTIR spectrum and zeta potential measurements of a CNC/epoxy mixture at various CNC concentrations. A change in the interfacial polymer morphology was observed with FE-SEM, with the improved dispersion composite featuring sphere-like structures consistent in size with the epoxy particles. The improved CNC dispersion observed in this study led to better mechanical performance in the glassy region of the storage modulus curve, increased work of fracture, and no changes in thermal stability. The CNC colloidal stabilization mechanism was expanded to incorporate freeze dried CNCs into the epoxy/crossliker formulation, resulting in an extension of the pot life by three orders of magnitude compared to the neat system; a result that could potentially enable the formulation of one part epoxies. Overall, these results highlight the importance of understanding processing-structure-property relationships in CNC-containing nanocomposites as they are considered for higher volume applications and provide a path forward for further processing optimization.

CHAPTER 4

INVESTIGATION OF CNCS AS EMULSIFIERS USING TENSIOMETRY

4.1 Overview

The stabilization of two or more immiscible fluid phases as an emulsion or foam is of great industrial interest. Common applications include pharmaceuticals, waste water treatment, construction, cosmetics, and food processing.[111–113] One route to stabilizing two immiscible phases involves the use of surfactants to lower the interfacial tension between oil and water or air and water.[114] By lowering interfacial tension, surfactants enable the formation of high surface area metastable emulsions and foams, and in some cases, stable microemulsions. However, environmental and practical considerations are driving the use of particles instead of surfactants in such applications. For example, surfactants readily adsorb and desorb from interfaces, thereby limiting the long term stability of the emulsion.[115] Additionally, many surfactants are known to be harmful contaminants when released to the environment.[116] These facts have motivated the substitution of surfactants with particles. The adsorption of particles with sufficient wettability at an interface is practically irreversible[115] and the particles can be chemically inert. Like surfactants, particles should meet a certain criteria to enable emulsions. For surfactants, the important parameter is the hydrophilic-lipophilic balance (HLB), a ratio of the hydrophilic molecular weight to the total molecular weight, and for particles the important parameter is wettability, where the particle should not be favorably wetted by either phase.[115] Often particles do not meet this criteria and surface modification is required to achieve a particle with amphiphilic properties. Emulsions stabilized by particles are referred to as Pickering emulsions for Spencer Pickering who reported on such systems in 1907,[117] although the discovery was first made by Ramsden in 1903.[118]

Examples of traditional materials for stabilizing foams and emulsions are low cost silica and carbon, however increasing environmental concern has led to the investigation of bio-based particles in such applications.[119] As such, cellulosic particles and their derivatives have been investigated as stabilizers for emulsions and solid porous foams.[37,119–122] Work by Capron *et al.* demonstrated hexadecane/water emulsions with bacterial cellulose nanocrystals (BCNs) produced by hydrochloric (HCl) acid hydrolysis. The HCl hydrolysis resulted in low surface charge density, which was in contrast to the typically high surface charge density imparted by the sulfate ester group via the more common extraction technique of sulfuric acid hydrolysis.[98] The authors attributed the BCN's ability to stabilize the o/w emulsions to their low surface charge density since high surface charge density particles have a stronger affinity to the aqueous phase and therefore did not partition at the o/w interface.[98] Similarly, Hu *et al.* investigated the emulsification behavior of anionic CNCs produced by sulfuric acid hydrolysis with two types of cationic surfactants. It was found that the CNCs associated with the cationic surfactants to synergistically stabilize Pickering emulsions with hexadecane as the oil phase.[120] However, due to the strong electrostatic interactions of the cationic and anionic species, more surfactant was required to achieve the same interfacial tension value when CNCs were present, leading to the conclusion that CNCs inhibited surfactant adsorption at the oil-water interface.[120] These studies examined slight modifications to the CNC surface with an uncharacteristically low CNC surface charge and with a surfactant that physically associated with, and neutralized, the negatively charged CNC surface. Alternative methods involved chemical modifications to the CNC surface with hydroxyl-reactive reagents. Tang *et al.* grafted Poly[2-(dimethylamino)ethyl methacrylate] (PDMAEMA) polymers on the CNC surface via free radical polymerization to enable toluene/water and heptane/water emulsions that were color-responsive to a change in pH.[123] It was found that the unmodified CNCs did not

result in stable emulsions and did not have a measureable influence on the surface tension of water, whereas the modified CNCs resulted in a decrease in the surface tension of water from 72 mN/m to 42 mN/m.[123] These three studies point to an underlying theme of the unmodified CNCs inability to stabilize high tension interfaces. These recent, impactful studies point to a growing area of developing the understanding of CNCs as Pickering emulsifiers. The choice of oil, physical or chemical modification to the CNCs, and the CNC surface charge are of critical importance to developing CNC stabilized emulsions and understanding the mechanism behind the resulting stabilization. The waterborne system studied in Chapters 2 and 3 present a new 'oil' and surfactant system that is yet to be studied with CNCs: epoxy and nonionic surfactant. The proprietary nature of the Air Products epoxide formulation prevented a complete understanding of the interfacial behavior of CNCs in the epoxy/water emulsion during the nanocomposite processing. Therefore, this Chapter aims to understand the effect of CNCs on the interfacial tension of an epoxy oil in water, as well as the interactions between CNCs and surfactants and CNCs and amine. This study can enable new waterborne epoxy emulsion formulations with cellulose nanoparticles which can have the practical and attractive benefits of long term emulsion stability and enhanced mechanical performance, as mentioned in Chapters 2 and 3.

Considering the commercial system used in Chapters 2 and 3 and the findings that hinted at CNC/polymer interactions, it was difficult to determine the specific components involved in facilitating increased CNC dispersion. The commercial system contained unknown additives and proprietary chemistry. Therefore, this Chapter will examine the individual component interactions of epoxy with CNCs, surfactants, and amines, using tensiometry. By monitoring a pure epoxy droplet in a continuous phase of water, the interfacial tension of epoxy and water can be determined by drop shape analysis. When CNCs, surfactant, or amine, and combinations thereof, are present

in the continuous aqueous phase, their effect on the dynamic interfacial tension can be measured. With this method, the individual components can be separated from one another or combined, thereby giving control of the experimental parameters. If the CNCs are located at the epoxy/water interface, as hypothesized in Chapter 3, this would be realized by a lowering of the interfacial tension of the epoxy/water interface. By considering the binary solutions of CNCs and surfactants, or CNCs and amine in the continuous aqueous phase, it can be determined whether the given components can act synergistically to lower the interfacial tension of epoxy. Additionally, if CNCs are located at the interface, when the internal pressure of the epoxy droplet is decreased the droplet will deform to an irregular shape (i.e. non-spherical) thus confirming the presence of CNCs at the interface. The irregular shape is caused by a rigid particle skin that deforms to accommodate the decreased interfacial area,[124] a phenomenon known as the crumpling effect. Such a deformation would not occur in the presence of small liquid molecules,[124] such as the surfactant or amine polymers.

4.2 Materials

Knowing the basic components that make up the Air Products formulation, an epoxy based on diglicidyl ether of bisphenol A (DGEBA) and a nonionic surfactant, the chemical components can be approximated by recognizing some common DGEBAs and nonionic surfactants used in epoxy polymer formulations.[32,62] Therefore, the nonionic surfactant Tergitol NP-9 was chosen, as well as a low molecular weight (EEW = 172) DGEBA, D.E.R. 332. D.E.R. 332 is a high-purity epoxy resin that has a very low level of production by-products.[125] The choice of a high purity epoxy resin eliminates the uncertainty associated with the commercial system, and is ideal for the tensiometry experiment-a technique that is sensitive to impurities. However, given the high purity and low molecular weight, this epoxy resin is prone to crystallization at or below room

temperature.[125] The melting point of crystalline DGEBA is 42 °C, therefore the DGEBA was held in a 50 °C convection oven prior to use.[125] The DGEBA and NP-9 were purchased from Sigma Aldrich and used without further purification. The amine hardener available from Air Products was diluted to a concentration of 4 wt.% and used as received. The amine was a mixture of low molecular weight, low weight fraction, amine compounds along with a 'polyamine polymer' which made up the bulk of the water soluble amine mixture at 40-70 wt.%. The polyamine polymer's specific chemical structure was proprietary, although it was likely to contain primary amines for the purpose of crosslinking the epoxy. Octanol was purchased from Sigma Aldrich and pre-contacted with water prior to measurement.

Aqueous based CNCs were used as received and the details of their chemistry vary only slightly from those used in Chapters 2 and 3. Specifically, the CNCs were derived from mixed southern yellow pine dissolving pulp via 64% sulfuric acid digestion as described elsewhere.[27] The CNCs were provided by the USDA Forest Products Laboratory at a 5.5 wt.% concentration, and were determined to contain 0.86 wt.% sulfur on a dry cellulose basis by ICP/MS. The counter ion on the CNCs was Na^+.

4.3 Tensiometry Measurements

The interfacial tension was measured via axisymmetric drop shape analysis of a pendant drop with a ramé-hart goniometer (model 100-25-A). An inverted pendant drop of DGEBA immersed in the aqueous phase was created by a syringe with a steel needle. A high speed CCD camera was programmed to capture the variation of drop shape with time in the DROPimage Advanced software. The interfacial tension was obtained by analyzing the contour shape resulting from the balance of gravitational forces and tension forces. All experiments were performed at room temperature.

For the measurement of the DGEBA/water interfacial tension, approximately 10 mL of DI water was poured into a glass box and the melted DGEBA was pipetted into the syringe. The DGEBA was allowed to cool for 10 minutes prior to measurement. An approximately 10 µL DGEBA droplet was formed in the aqueous phase and the dynamic interfacial tension was measured for 80 minutes. The data reported reflect the final interfacial tension value at 80 minutes. A similar procedure was followed when CNCs were added to the aqueous phase. Aqueous based CNCs were added to DI water and sonicated together for 1 hour using a 2510 Branson bath sonicator prior to the measurement. The CNC/water suspensions were 10 mL in volume and the CNC concentration was varied. After the CNC/water suspension was sonicated, a small amount of melted DGEBA was added to the syringe and both liquids were allowed to cool for 10 minutes prior to the measurement. Three measurements were repeated and error bars represent 95% confidence intervals.

For the measurements involving the nonionic surfactant, NP-9, a concentration of 1 mM surfactant was used and the CNC concentration was varied. The CNC/surfactant suspensions were sonicated together with DI water for 1 hour and cooled 10 minutes prior to the measurement. The total volume was 10 mL. For the measurements involving the amine corsslinker, a concentration of 0.15 g/L was used and the CNC concentration was varied. The CNC/amine suspensions were sonicated together with DI water for 1 hour and cooled 10 minutes prior to the measurement. The total volume was 10 mL. Three measurements were repeated and error bars represent 95% confidence intervals.

Each experiment was concluded by decreasing the droplet volume to zero, via the syringe, in order to determine if CNCs were present at the interface. If the droplet remained spherical during this step, it was concluded that CNCs were not present in a significant quantity at the interface,

and if the droplet was folded or irregular in shape, it was concluded that CNCs were present at the interface.

4.4 Zeta Potential Measurements

The zeta potentials of neat CNC, CNC/amine, and CNC/surfactant suspensions were measured. The concentration of each sample was 0.01 wt.%. The measurements were performed using a Malvern Zetasizer Nano ZS 90. Measurements were performed in triplicate at 25 °C, and the average values were reported.

4.5 Results

4.5.1 CNC Effect on DGEBA Interfacial Tension

The interfacial tension of DGEBA in water was measured to be 17.5 ± 0.1 mN/m. While a value for comparison was not found in literature, the surface tension of DGEBA (DGEBA in air) was measured to be around 46.1 ± 1.5 mN/m, which is close to the reported value of 44.2 mN/m;[126,127] therefore, the measurements were considered accurate. When CNCs were added to the aqueous phase, the interfacial tension was slightly lower compared to the neat value. However, the change in interfacial tension with CNC content was not appreciable, and fell within error of the neat value. From this data, it was determined that CNCs alone do not lower the interfacial tension of this DGEBA, and therefore were not located at the interface. The interfacial tension data of DGEBA as a function of CNC concentration is given in Figure 4.1.

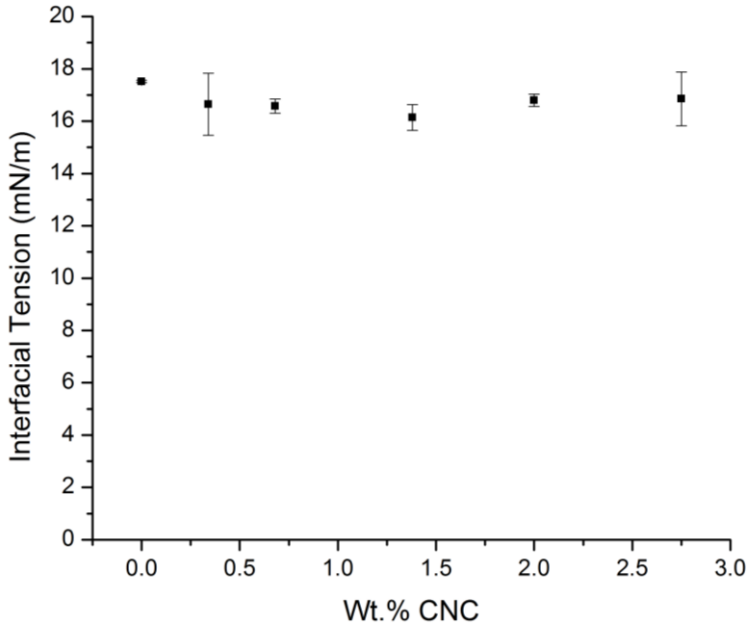

Figure 4.1: Interfacial tension of DGEBA and water as a function of CNC concentration. Error bars represent 95% confidence intervals.

Before considering the binary systems of CNC and surfactants or CNCs and amines, another parameter associated with the CNCs was tested to investigate whether CNCs could be used for the purpose of stabilizing oil/water emulsions. For example, previous studies have shown that the ionic strength will play an important role in a particle's ability to stabilize emulsions.[128] This phenomenon is known as the image charge effect where a charged particle creates an image of itself across an interface. The image force arises when an electric charge near an interface between dielectric media of different permittivity sets up a polarization field in which the charged particle experiences a force pointing toward the more polarizable medium.[128] The magnitude of the image charge is a function of the dielectric constant of the two fluids (oil and water) and is similar in magnitude to the actual charge when the oil has a low dielectric constant.[128] The image charge and the charged particle can repel each other, which would prevent particles from getting to the interface and thus prevent the particles from stabilizing o/w emulsions. The effects of the image charge can be mitigated by choosing a higher dielectric constant oil or by screening the

electrostatic charge of the particle with salt.[128] The dielectric constant of DGEBA is around ε = 4.8[129,130] whereas the dielectric constant for oils tested with CNCs in other publications, such a toluene or hexadecane,[98,120] is around ε = 2.[128] In order to test the image charge hypothesis, the interfacial tension of octanol (ε = 10.3) and water was tested and compared to the interfacial tension of octanol in a 1.38 wt.% aqueous CNC suspension. The dynamic interfacial tension curves are given in Figure 4.2.

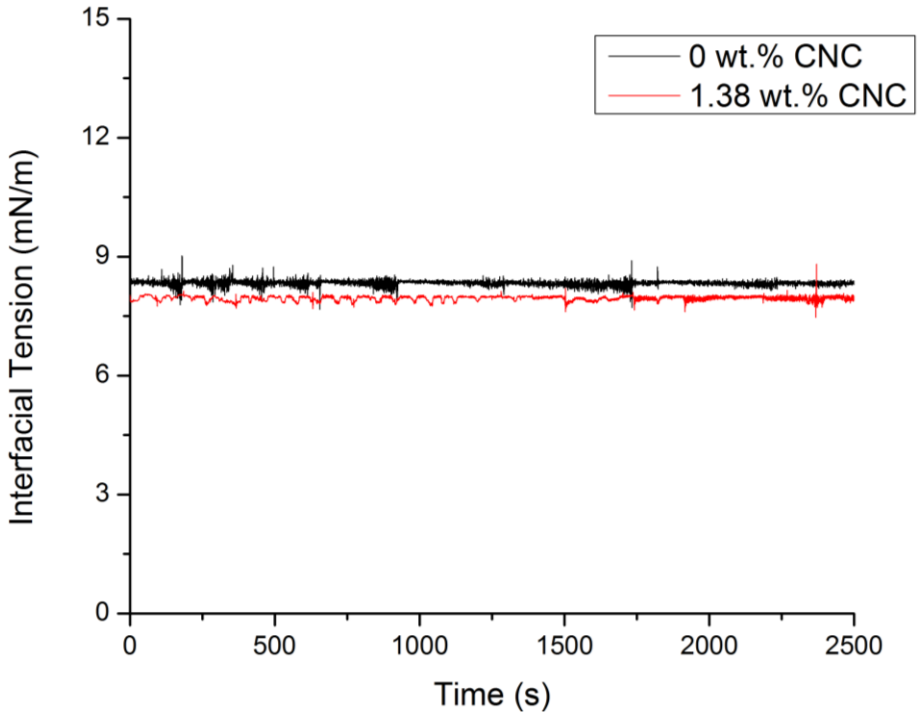

Figure 4.2: Interfacial tension of octanol and water with 0 wt.% CNC and 1.38 wt.% CNC.

The interfacial tension of octanol and water was measured to be 8.33 mN/m, the average value over the length of the experiment. This value was also consistent with the reported literature value of 8.5 mN/m.[131] The interfacial tension of octanol in a 1.38 wt.% aqueous CNC suspension was measured to be 7.95 mN/m, which was slightly lower than the neat octanol value. The interfacial tension of octanol in the 1.38 wt.% aqueous CNC suspension also remained at a relatively constant value during the time of the experiment (40 minutes), indicating that the CNCs

were not dynamically adsorbing at the interface on this time scale. While the CNCs slightly lowered the interfacial tension of octanol, the effect was not significant enough to conclude that the image charge would play a significant role in these CNCs' ability to stabilize emulsions.

4.5.2 CNC and Surfactant Effect on DGEBA Interfacial Tension

Since it was determined that CNCs do not significantly lower the interfacial tension of DGEBA, the interfacial tension of CNC/surfactant solutions was tested. The interfacial tension of DGEBA in a 1 mM NP-9 aqueous solution was 4.32 mN/m, considerably lower than the neat value of 17.5 mN/m, and the lowest value obtained with 0.34 wt.% CNCs, 16.6 mN/m. CNCs were added to 1 mM surfactant solutions and the interfacial tension was measured. It was found that the CNCs caused the interfacial tension to increase as more CNCs were added, as shown by Figure 4.3. At a CNC concentration of 1.38 wt.% and a surfactant concentration of 1 mM, the interfacial tension was increased to 6.2 mN/m. This result was counter intuitive to the hypothesis in Chapter 3 which presumed that the CNCs were associating with the surfactant stabilized epoxy droplet during the nanocomposite preparation involving the premixing step of CNCs with the epoxy emulsion. The increased interfacial tension with increasing CNC concentration implied that less surfactant was available to adsorb to the interface, thus, the surfactants were associating with the CNCs in the bulk solution. A similar result was encountered when CNCs were mixed with cationic surfactants.[120]

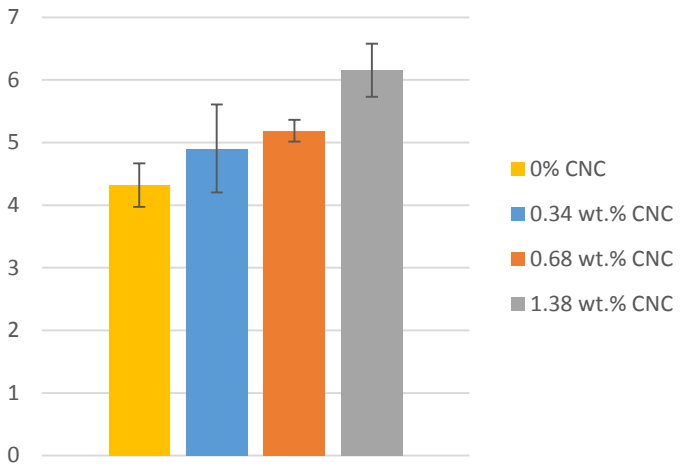

Figure 4.3: Interfacial tension values of DGEBA in water after 80 minutes with 1mM NP-9 and varied CNC concentration. Error bars represent 95% confidence intervals.

To verify whether the CNCs were associating with the nonionic surfactants, a step-wise experiment was conducted. First, the DGEBA droplet was equilibrated in a 1 mM NP-9 solution for 40 minutes, then that solution was exchanged for a 0.68 wt.% aqueous CNC solution and the interfacial tension was recorded for another 40 minutes. In this scenario, the surfactant and CNCs are not premixed and the surfactant stabilized DGEBA droplet can be introduced to CNCs where their interactions can be monitored via the dynamic interfacial tension. The dynamic interfacial tension curve of this experiment is given in Figure 4.4. During the 40 minute equilibration with the surfactant, the interfacial tension continuously decreased from 8.6 mN/m to 5.8 mN/m. When the surfactant solution is replaced by the CNC solution, there was a sharp increase in the interfacial tension from 5.8 mN/m to 6.9 mN/m. This confirmed the hypothesis that CNCs were causing the surfactants to desorb from the interface by associating with the surfactant molecules. However, the interfacial tension did not increase above the initial value of the experiment, where the final value was 7.5 mN/m after 40 minutes of equilibration with the CNC solution. Although the CNCs increased the DGEBA interfacial tension, previous work has shown that CNCs and surfactants can

stabilize o/w emulsions despite the fact that increased interfacial tension values were observed with CNC/surfactant mixtures compared to the surfactant only.[120]

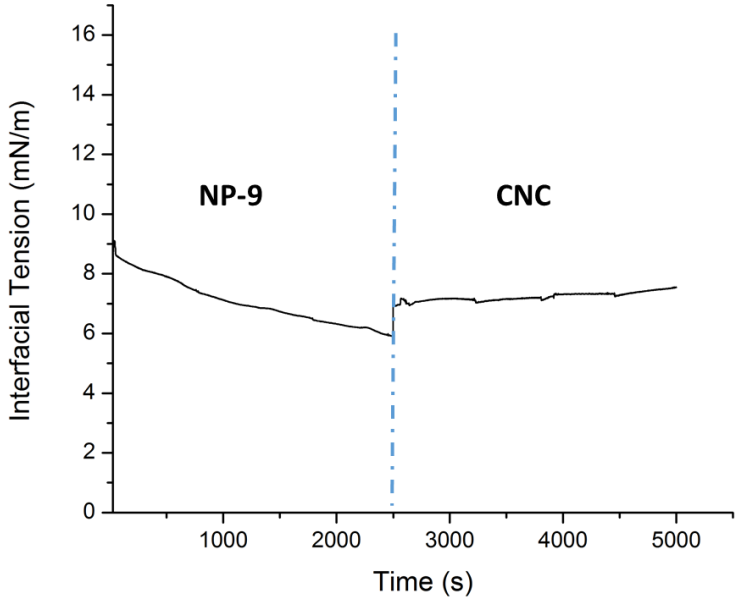

Figure 4.4: Dynamic interfacial tension curve for 1 mM NP-9 from t=0 to t=2500 s, and 0.68 wt.% CNC from t=2500 to t=5000 s. Vertical line denotes the step in the experiment when the 1 mM surfactant solution was exchanged for a 0.68 wt.% CNC suspension.

4.5.3 CNC and Amine Effect on DGEBA Interfacial Tension

Tensiometry experiments showed that CNCs alone do not lower the interfacial tension of DGEBA in water, and that CNCs facilitated the desorption of surfactants from the DGEBA/water interface, thereby increasing the interfacial tension to a value higher than the surfactant-only case. Considering the components involved in the nanocomposite preparation, another parameter that could have influenced the degree of CNC dispersion and interfacial associations was the amine crosslinker. The interfacial tension of DGEBA with CNC/amine suspensions was tested. The amine concentration was 0.15 g/L and the CNC concentration was varied. The interfacial tension of the DGEBA with 0.15 g/L amine was 3.7 ± 0.03, which indicated that amine molecule was adsorbing to the interface and was a good epoxy stabilizer. When 0.086 wt.% CNC was added to 0.15 g/L amine, the interfacial tension was increased to 12.4 ± 1.1 mN/m, a sign that the CNCs

were severely limiting amine adsorption to the interface. Similar to the CNC/surfactant case, the interfacial tension was further increased with increasing CNC content, where the interfacial tension of DGEBA in a 0.17 wt.% CNC and 0.15 g/L amine aqueous suspension was 13.0 ± 0.2 mN/m, and the interfacial tension of DGEBA in a 0.34 wt.% CNC and 0.15 g/L amine aqueous suspension was 13.6 ± 0.1 mN/m. The extent to which increasing CNC concentration increased the interfacial tension was more pronounced for CNC/amine suspensions than for the CNC/surfactant suspensions. For example, the interfacial tension of DGEBA was increased from 3.7 to 13.6 mN/m when 0.34 wt.% CNC was added to the 0.15 g/L amine suspension versus an increase of 4.3 to 4.9 mN/m when 0.34 wt.% CNC was added to the 1 mM surfactant suspension.

4.5.4 Crumple Test

Unlike the case with CNC-only or CNCs and surfactants, the CNC/amine suspensions had a distinct effect on the DGEBA droplet deformation during the crumple test. Figure 4.5 shows the evolution of the DGEBA drop shape as the internal pressure of the droplet is decreased, leading to a reduction in the volume and interfacial area. Figure 4.5(a) shows the DGEBA drop shape as a function of time for the 1.38 wt.% CNC-only case. From these images, it is clear that the droplet maintains a spherical shape throughout the test (phase I-V), reinforcing the conclusion that CNCs were not at the interface at the concentrations tested here (0.34 to 2.75 wt.%), and during the time allotted for equilibration (80 minutes). Figure 4.5(b) shows the DGEBA droplet deformation in the presence of 0.15 g/L amine. There are notable features of the droplet shape in the amine-only case. In phase III of Figure 4.5(b), the DGEBA droplet exhibited rounded corners near the edges of the steel needle. The non-spherical behavior continues through phase V, though the droplet surface remains smooth. Figure 4.5(c) shows the DGEBA drop shape as a function of time for the 0.15 g/L amine and 0.17 wt.% CNC suspension. There were significant differences when

comparing the DGEBA drop shape deformation of the CNC/amine suspension to the CNC-only and amine-only suspension. First, the droplet in phase II of Figure 4.5(c) began to show rounded corners near the edge of the needle, similar to the amine-only case. In the subsequent phases of droplet deformation of Figure 4.5(c), irregularities in the droplet shape can be noted where the droplet takes on a conical shape (phase III), then an oval shape (phase IV), and finally the droplet folds on itself (phase V). Additionally, in phases IV and V, creases in the droplet surface can be observed. These features were consistent with particles located at the interface.[124,132] It is important to note that the onset of crumpling occurred sooner for the lowest CNC concentration tested here (0.086 wt.%), and that the extent of crumpling observed was also qualitatively greater for the lowest CNC concentration sample. This observation suggested that lower CNC concentrations facilitated higher interfacial coverage of the DGEBA droplet surface by the CNCs. However, it was difficult to quantify the crumpling ratio for the amine/CNC suspension given that the DGEBA droplet was noticeably deformed when the CNC particles could not have influenced the droplet deformation behavior in the amine-only case.

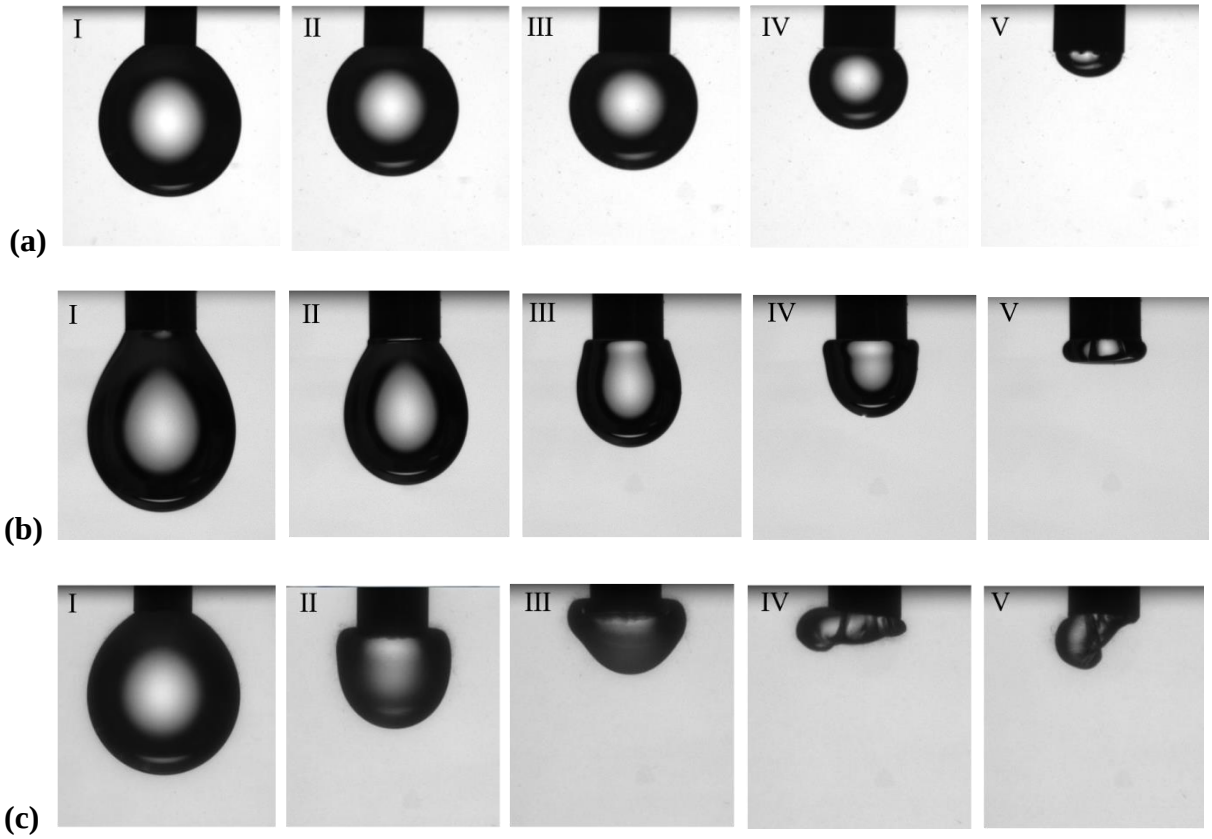

Figure 4.5: DGEBA drop shape as a function of time. (a) 1.38 wt.% CNC (b) 0.15 g/L amine (c) 0.17 wt.% CNC with 0.15 g/L Amine.

Although the amine molecule was responsible for CNC interfacial adsorption, the CNC/amine solutions still resulted in relatively high interfacial tension values of the DGEBA, around 12 to 13 mN/m depending on the CNC concentration. This would likely be insufficient to result in a stable emulsion, as the lowest interfacial tension value possible is optimal. In this regard, the CNC/surfactant combination would be more appropriate in an emulsion formulation since the DGEBA interfacial tension was reasonably low (4 to 5 mN/m) and was not a strong function of CNC concentration in that case.

4.5.5 Zeta Potential of CNC and CNC mixtures

Another interesting observation was made when mixing the CNC and amine suspensions. At moderate concentrations of CNC or amine, the solution was cloudy, which gave an indication

that the aggregation of either component was induced upon their addition. This observation, along with the interfacial tension data, implied an association between the CNC and amine, similar to the CNC and surfactant case, although this effect was greater for the CNC and amine case. To better understand these interactions, the zeta potential was measured for the CNCs as well as for the mixtures of CNC and surfactants, and CNC and amine. The summary of these results is given in Table 4.1. The zeta potential of neat CNC was -50.3 mV, indicating a stable suspension. In the binary mixtures, the ratio of the CNC/amine and CNC/surfactant samples were 5 times in excess of CNC by weight. This ratio reflected the lowest CNC concentrations used in the tensiometry experiments with amine and with surfactant, 0.086 wt.% and 0.34 wt.% CNC, respectively. Each zeta potential measurement showed a monomodal distribution of charges, indicating that the measurement reflected the zeta potential of a single species, rather than two distinct species. The zeta potential of the CNC and surfactant suspension was -54.6 mV, which was similar in magnitude the value obtained for neat CNC, indicating that the two species did not have significant interactions. Conversely, the zeta potential of the CNC and amine suspension was -19.1 mV, a much lower value compared to the neat CNC, indicating that the two species were associated in some manner that facilitated a modification of the CNC surface charge. The CNC/amine association was possibly due to the strongly negative CNCs interacting with a positively charged amine species, however, other possibilities exist. For example, Yang *et. al* observed an increase in the zeta potential of CNCs when the CNCs were mixed with polyethylene glycol (PEG) solutions.[133] The hypothesized interaction between the PEG and CNCs was attributed to hydrogen bonding,[133] thus hydrogen bonding was responsible for modifying the surface charge (zeta potential) of the CNCs. Considering the materials studied here, the amine polymer and CNCs could also participate in hydrogen bonding. Way *et. al* observed strong hydrogen bonded networks of

amine functionalized CNCs at high pH (8 to 13), and electrostatically repulsive CNCs at low pH (1 to 7) due to the protonation of the amine groups in acidic conditions.[134] The pH of the CNC/amine suspension at a 5:1 weight ratio was measured to be 10.21, where hydrogen bonding was likely to occur. However, protonation of the amine cannot be ruled out as it is possible that a small percentage of the amines were protonated, in which case, the positively charged amine group would have a strong electrostatic attraction to the negatively charged sulfate group. Given the proprietary nature of the amine polymer, it was difficult to determine the exact mechanism of the CNC and amine interaction.

In any case, these results help to explain the large increase in the interfacial tension of DGEBA when CNCs were added to the amine suspensions versus the slight increase of the interfacial tension when CNCs were added to the surfactant suspensions. In summary, the CNCs minimally interacted with the surfactant molecules and significantly interacted with the amine molecules, and in both cases the CNCs hindered their adsorption to the DGEBA interface.

Table 4.1: Zeta potential of neat CNC, CNC/amine, and CNC/surfactant mixtures.

Sample:	CNC	CNC:Amine 5:1	CNC:NP-9 5:1
Zeta Potential: (mV)	-50.3 ± 2.5	-19.1 ± 0.5	-54 ± 3.5

The zeta potentials of the binary mixtures also helps to explain the presence of CNCs at the interface when combined with the amine. For example, it was determined that the amine had a strong affinity for the DGEBA interface given the low interfacial tension value (3.73 mN/m) of the DGEBA in a weakly concentrated aqueous amine solution. The zeta potential measurements of the CNC and amine suspensions also suggested that the CNCs had a strong affinity for the

amine. Therefore, if an amine molecule adsorbed to the DGEBA interface, the CNCs electrostatically associated with the amine would also be adsorbed.

4.5.6 1-step and 2-step Mixing Mimicked with Tensiometry

The results from the CNC and amine interfacial tension measurements showed that the CNCs are located at the DGEBA interface when combined with the amine. Combining this observation with the findings from CNCs-only and CNCs and surfactants, it was concluded that the amine molecule was responsible for getting CNCs to the DGEBA/water interface.

In the aforementioned experiments, however, the individual components (CNC and amine or CNC and surfactant) were premixed together and then added to the DGEBA interface. This order of addition did not mimic the processing of the nanocomposites accurately since in the 1-step mixing composite case CNCs and amine were added to the surfactant stabilized epoxy droplets, and in the 2-step mixing composite case CNCs were added to the surfactant stabilized epoxy droplets and the amine was added some time later. To better reflect this reality, a similar step-wise experiment was conducted with tensiometry where in the 1-step mimic case an epoxy droplet was equilibrated for 40 minutes with a 1 mM surfactant solution and then that solution was exchanged for a solution containing 0.34 wt.% CNC and 0.15 g/L amine. Similarly, for the 2-step mimic, an epoxy droplet was equilibrated for 40 minutes with a 1 mM surfactant solution and then that solution was exchanged for a 0.34 wt.% CNC solution which was also equilibrated for 40 minutes. In the last step, 0.15 g/L of amine was added directly to the CNC suspension and the interfacial tension was recorded for another 40 minutes. These two experiments were concluded by monitoring the crumple point of the DGEBA droplet. The dynamic interfacial tension curves of the 1-step and 2- step mimic are given in Figure 4.6.

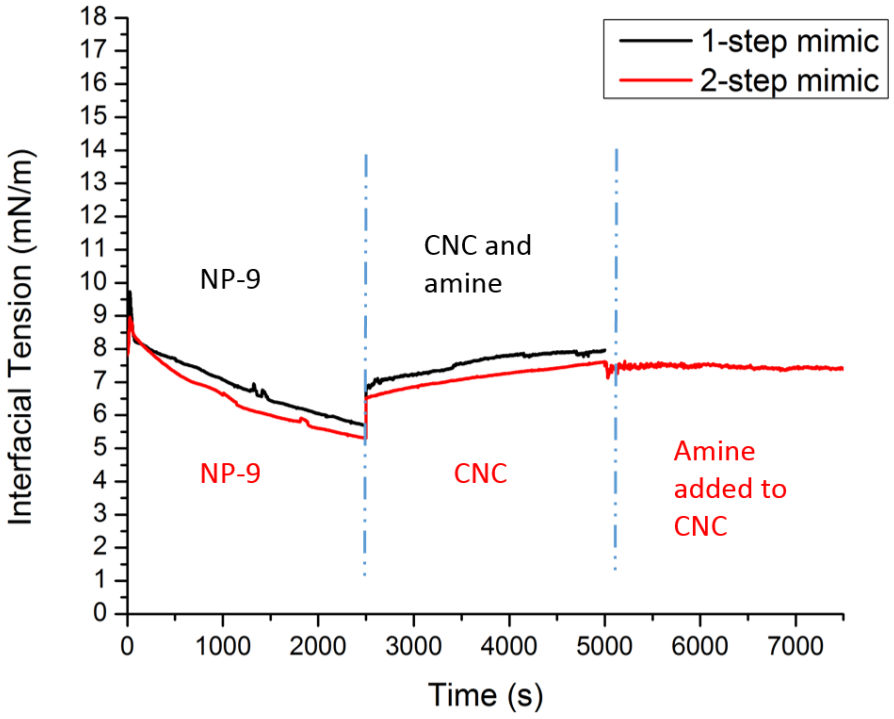

Figure 4.6: Dynamic interfacial tension curves for 1-step (black) and 2-step (red) tensiomety experiments. Vertical lines denote the steps of the experiment when the aqueous solution was exchanged or added to.

In the 1-step and 2-step mimic case dynamic interfacial tension curves, the interfacial tension continually decreased from 8.2 to 5.7 mN/m from t=0 to t=2500 s, the surfactant step. When the surfactant solution was replaced with either the CNCs or CNCs with amine, the interfacial tension was increased to 6.8 mN/m, and the magnitude of the increase was similar for the 1-step and 2-step mimic case. This result showed that whether the CNCs (2-step) or CNCs with amine (1-step) were added to the surfactant stabilized epoxy droplet, the interfacial tension would increase similarly. After CNC or CNC and amine addition, the dynamic interfacial tension values were again similar from t=2500 s to t=5000 s, indicating that either component did not have significant interactions with the surfactant stabilized epoxy droplet. Since a similar result was shown by Figure 4.4 when CNCs were added to a surfactant stabilized DGEBA drop, it was

concluded that the sharp increase in interfacial tension observed at t=2500 s was mostly due to the CNCs.

Next, the 2-step mimic experiment was continued where an aliquot of amine was added to the CNC solution surrounding the epoxy droplet. In this step at t=5000 s, the interfacial tension was unchanged and remained at a constant value of 7.4 mN/m until the conclusion of the experiment at t=7500 s. Again, this result implied that the amine did not have noticeable interactions with the DGEBA droplet.

The differences in these two experiments were realized during the crumple point test. The evolution of DGEBA droplet shape as a function of time for the 1-step and 2-step tensiometry mimics is given in Figure 4.7. Like the CNC-only case, the 1-step mimic case exhibited a spherical droplet shape during the crumple test and so it was concluded that CNCs were not located at the interface in a discernable quantity. Conversely, the 2-step mimic case exhibited an irregular droplet shape during deformation (phase III through V), indicating CNCs at the interface. Based on these experiments, the CNCs are more likely to be located at the epoxy/water interface when the CNCs are premixed with the epoxy and the amine added some time later (2-step), and the amine plays an important role in facilitating this effect.

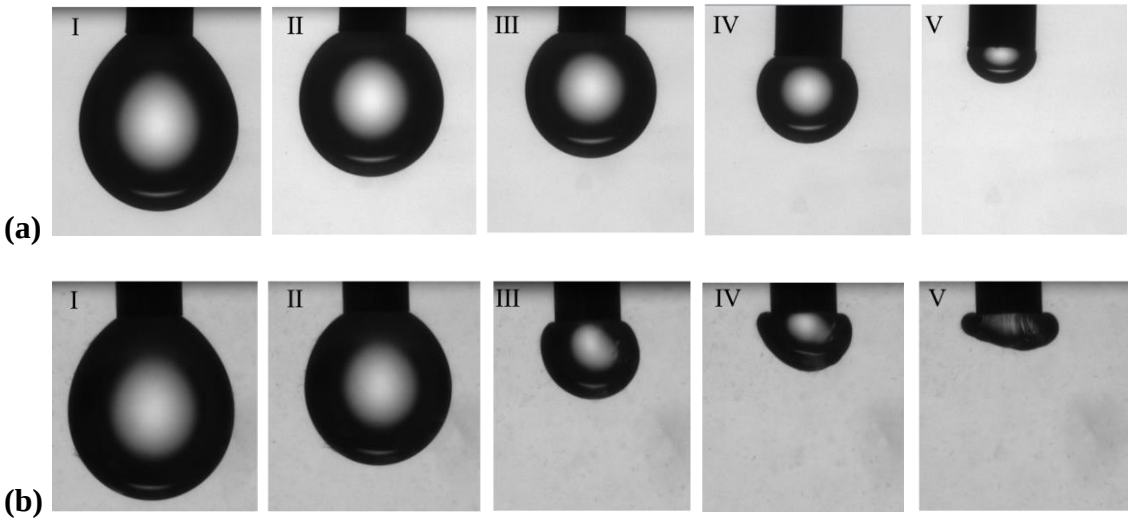

Figure 4.7: DGEBA drop shape as a function of time. (a) 1-step mimic (b) 2-step mimic.

While the greater component concentrations and mechanical agitation applied to the composite during processing would likely drive CNC particle adsorption to the epoxy interfaces, those parameters were impossible to study with tensiomerty given the inevitable viscosity increase accrued by higher CNC concentrations and the influence this would have on bulk fluid dynamics. In any case, thermodynamics of adsorption and electrostatic interactions were sufficient to understanding important colloidal behaviors of the CNCs with various components of interest using tensiometry.

4.6 Conclusions

The interfacial tension of an epoxy oil based on DGEBA was measured in a series of aqueous suspensions for the purpose of understanding the colloidal interactions present in a waterborne epoxy composite system involving a nonionic surfactant-stabilized epoxy droplet, a water soluble amine crosslinker, and CNC particles. First the interfacial tension of DGEBA and water was monitored as a function of CNC concentration. It was determined that the CNCs did not appreciably alter the interfacial tension of this DGEBA at the concentrations tested here. Therefore, the CNCs were combined with a 1 mM surfactant suspension and the interfacial tension

was measured. The interfacial tension was increased with increasing CNC concentration with respect to the surfactant-only case. Dynamic interfacial tension measurements confirmed that the CNCs facilitated surfactant desorption from the DGEBA interface, thereby leading to an increase in the interfacial tension. Finally, the amine crosslinker at a concentration of 0.15 g/L concentration was combined with varying CNC concentrations and the interfacial tension was measured. It was found that the interfacial tension was again increased with increasing CNC concentration with respect to the amine-only case, although the extent to which the interfacial tension was increased was greater for the CNC and amine case versus the CNC and surfactant case. Zeta potential measurements indicated a strong electrostatic association between the CNC and amine which was presumed to influence the CNC and amine interfacial tension values, as well as the localization of CNCs at the DGEBA interface; a feature that was noticeable only with the CNC and amine suspensions via the crumple point test. Although the amine molecule was responsible for CNC interfacial adsorption, the lowest DGEBA interfacial tension value obtained for the binary CNC mixtures occurred for the 1 mM surfactant with 0.34 wt.% CNC, therefore this combination was suggested to give the optimal emulsion formulation. This study highlights the importance of understanding individual component interactions for the purpose of formulating waterborne epoxy emulsions involving CNCs, and logically choosing processing strategies when formulating multi-component CNC composites.

CHAPTER 5

SITE SELECTIVE MODIFICATION OF CELLULOSE NANOCRYSTALS WITH ISOPHORONE DIISOCYANATE AND FORMATION OF POLYURETHANE-CNC COMOPSITES

A version of this Chapter was submitted for publication in the journal *ACS Applied Materials and Interfaces*:

Girouard N., Xu S., Schueneman G. T., Shofner M. L., and Meredith J. C., Site Selective Modification of Cellulose Nanocrystals with Isophorone Diisocyanate and Formation of Polyurethane-CNC Composites. *ACS Applied Materials and Interfaces*. (2015)

5.1 Overview

This Chapter will discuss a chemical modification of the CNC surface using isocyanate chemistry. There are many examples in literature of cellulose modification routes.[135] For example, poly[2-dimethylamino)ethyl methacrylate] (PDMAEMA) was grafted onto the CNC surface for the purpose of stabilizing o/w emulsions,[123] and silylation of the –OH surface with N-(β-aminoethyl)-γ-aminopropyltrimethoxysilane was used to improve the compatibility of CNCs with an unsaturated polyester resin.[136] The work presented here explored a modification route using hydroxyl/isocyanate chemistry with isophorone diisocyanate as the reactive monomer. Similarly, hexamethylene diisocyanate (HDI) was used to modify CNCs and then the modified nanoparticles were incorporated into the segmented thermoplastic polyurethane matrix.[66] The grafted HDI chains linked the CNCs together, e.g., chain extension, to form an interconnected network due to the in situ polymerization of the HDI, because both HDI isocyanate groups reacted with cellulose hydroxyl groups.[66] Alternatively, in this work, the proposed modification route did not lead to chain extension of the nanoparticles and offers a unique functionality for CNCs that opens the door for utilizing the isocyanate-modified CNCs in composites with many different polymer matrices.

The polyurethane industry is lucrative and diverse, with reported revenues in 2013 of $25.6 billion and finding end applications in appliance, automotive, building and construction,

electronics, footwear, and packaging industries.[137] The extensive choices available for isocyanates and polyols are responsible for polyurethane's wide range of properties and applications, where the physical properties of polyurethane are dependent upon the chemical structure of the starting reactants.[63] For example, the material properties of polyurethanes will depend on the extent of crosslinking as well as the chain length of the polyol where a high degree of crosslinking would yield a rigid polyurethane, and long chain polyols yield flexible polyurethanes. Of course there is a balance between choosing such chemistries for a given application without sacrificing additional mechanical properties, such as elongation at break. For this reason, many types of fillers have been incorporated into polyurethanes in order to improve their mechanical properties. These fillers include carbon nanotubes,[138,139] layered silcate clays,[140] and graphite oxide nanoplatelets.[141] Interest in the development of bio-based polyurethanes utilizing vegetable oils and sugars, suggest that reinforcements such as cellulosic nanoparticles would be better matches with polyurethane. The combination of cellulosic nanoparticles and polyurethane can aid in the development of bionanocomposites containing a significant amount of renewable carbon content.[64] However, as mentioned previously, current reports on CNCs in polyurethane formulations suffered from the undesirable chain extension and agglomeration of the CNCs which ultimately resulted in a decrease of the tensile strength, strain at break, and work of fracture in the final composites.[64,66] Given the diversity of isocyanate chemistries available to polyurethane formulations, it is prudent to investigate alternative isocyanate chemistries with the hydroxyl-decorated CNC surface.

Isophorone diisocyanate (IPDI) is part of a class of aliphatic isocyanates used in polyurethane coating applications. Aliphatic isocyanates make up a small percentage of the total isocyanate market, but are well known for their high abrasion resistance, and resistance to UV degradation.[142,143] These attributes makes these materials attractive for exterior coating

applications, such as airplanes. The two most common aliphatic isocyanates are IPDI and HDI. HDI has a linear hydrocarbon backbone with two terminating isocyanate groups on each end. IPDI is an aliphatic ring with one primary and one secondary isocyanate group. In HDI, the two isocyanate groups are of equal reactivity whereas the isocyanate groups in IPDI are of unequal reactivity.

In the IPDI molecule, the secondary isocyanate (the –NCO substituent directly connected to the ring) has a higher reactivity compared to the primary group (the $–CH_2NCO$ group), which is attributed to the primary group being more sterically hindered by the neighboring methyl group.[144] Moreover, the selectivity for the secondary isocyanate reaction can be enhanced by using dibutyl tin dilaurate (DBTDL) as the reaction catalyst, and can be inverted to be primary selective by using 1,4-Diazabicyclo[2.2.2]octane (DABCO).[144–147] By exploiting this unequal reactivity, it is possible to produce isolated CNCs decorated with IPDI monomers with a pendant isocyanate group that do not chain extend into isocyanate-linked CNC agglomerates. This reaction schematic is given in Figure 5.1.

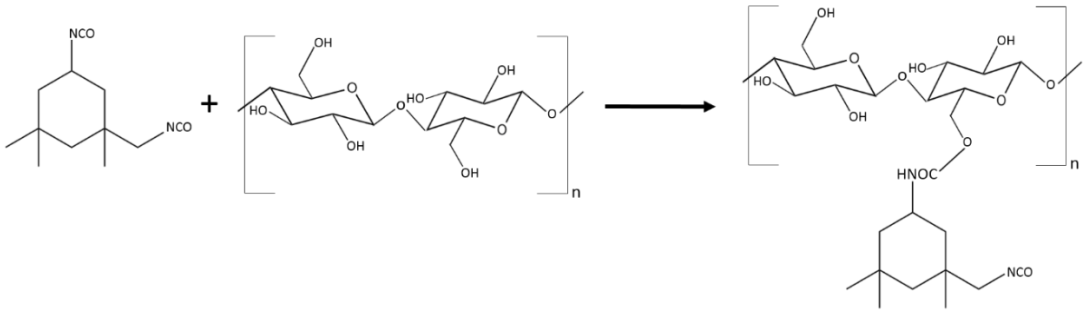

Figure 5.1: Illustration of IPDI/CNC reaction with the secondary NCO group on IPDI.

The surviving pendant isocyanate group is then available for reaction with additional monomers of interest, such as polyols commonly used in polyurethane formulations. This chemistry can facilitate covalent bonding between the CNC and polymer matrix, a feature that could offer desirable mechanical properties and new functionalities to CNC composites. Such

benefits could facilitate accelerated commercialization of these biobased nanomaterials. In this work, CNCs were successfully modified with IPDI, and for demonstrational and performance based-comparative purposes, modified CNC (m-CNC) and unmodified (um-CNC) particles were incorporated into a polyurethane elastomer using IPDI as the isocyanate-containing monomer and crosslinked with a polyether-based triol.

5.2 Materials and Methods

Freeze dried CNCs (FD-CNCs) were provided by the U.S.D.A. Forest Products Laboratory and used as received. The CNCs were freeze dried from an aqueous CNC suspension prepared from mixed southern yellow pine dissolving pulp via 64% sulfuric acid digestion as described in detail elsewhere.[27] The resulting CNCs had sulfate functionality due to residual sulfate esters on their surfaces. The CNCs were determined to contain 0.96 wt.% sulfur on a dry cellulose basis by inductively coupled plasma/optical emission spectroscopy (ICP/OES).[148] The counter ion on the nanocrystals was Na^+. IPDI was purchased from Sigma Aldrich at 98% purity and used as received. The IPDI was stored at 4 °C. The crosslinker used in polymer synthesis was a polyether polyol provided by Bayer MaterialScience (LHT-240, Molecular Weight=700 g/mol). Solvents of anhydrous dimethyl sulfoxide (DMSO) and toluene were purchased from Sigma Aldrich and used as received. Isocyante catalysts, DBTDL and DABCO, were purchased from Sigma Aldrich and used as received.

5.2.1 Surface Modification of CNCs

The FD-CNCs were first mixed with DMSO by magnetic stirring for 30 minutes. The concentration of CNC in DMSO was approximately 3 wt.%. This mixture was then sonicated for 1 hour with a 2510 Branson bath sonicator. A separate vessel partially submerged in an oil bath containing IPDI was heated to 60 °C under a flowing nitrogen atmosphere. The DBTL was then

added to the IPDI and allowed to stir for 5 minutes. The FD-CNC/DMSO suspension was added drop-wise to the stirring IDPI/DBTDL mixture with a separatory funnel. The reaction proceeded overnight in a flask with N_2 inlet and outlet ports. The reaction was run in excess of IPDI at a weight ratio of IPDI to CNC of 67:1. After the reaction, the mixture was washed with toluene and centrifuged at 2,800 RPM for 3 minutes, and repeated 3 times. The toluene was poured off, and the CNCs were either mixed with triol for composite synthesis, or allowed to dry in a vacuum oven overnight. An identical procedure was applied to produce the m-CNCs using DABCO as the reaction catalyst. All m-CNC characterizations were performed on samples that were synthesized using DBTDL as the reaction catalyst, with the exception of ^{13}C NMR which was employed to compare the selectivity of the two catalysts studied here.

5.2.2 Polyurethane Film Preparation

Composites were synthesized with both m-CNCs and um-CNCs at loadings of 1 and 5 wt.%, and DBTDL was used as the reaction catalyst for both the m-CNC preparation and the polyurethane film formulation. Elemental analysis was used to calculate the relative weight ratios of IPDI and CNC in the m-CNCs. This information was used to estimate the equivalent weight of CNC in the m-CNC sample, and all composite loadings were based on the weight of CNC only. All polymers were synthesized with a 1:1 stoichiometric ratio of –NCO from IPDI and –OH from triol. The concentration of –NCO groups on the modified CNCs was taken into account by the experimental values given by elemental analysis. The um-CNCs were first mixed with toluene and then sonicated. For both types of CNC composites, the CNC/toluene mixture was magnetically stirred with triol for 30 minutes and then vacuum oven dried until there was no mass change, indicating that the toluene had been removed. The CNC/triol mixture was then stirred with DBTDL for a few minutes. IPDI was added to the mixture was allowed to magnetically stir for 30 minutes.

The nanocomposite mixture was then poured onto a hydrophobic glass substrate and casted to the desired thickness with a doctor blade. The polymer was cured at 100 °C in a vacuum oven for 2 hours. For comparative purposes, a neat polyurethane polymer film was synthesized. The procedure for producing the neat polymer was identical to the procedure for the composite, except that in the step where the CNC/toluene mixture was added to the triol, here only toluene was added.

5.2.3 ATR-FTIR

The chemical structure of the um-CNCs, m-CNCs, and polymer films was analyzed with ATR-FTIR using an ATR accessory (Bruker Platinum ATR) with a Bruker Vertex 80V spectrometer. The ATR was equipped with a germanium crystal plate, which had a spectral range of 10,000 to 10 cm^{-1}. The spectra were corrected to subtract the background signals and flatten the baseline. The wavenumber scan range was 4000 to 600 cm^{-1} with a resolution of 4 cm^{-1} and a total of 64 scans. For the um-CNC/m-CNC comparison, the 1060 cm^{-1} band was chosen as the normalization wavenumber since this absorbance was associated with ether functional groups which were assumed to not participate in the reaction. Similarly, the composite spectra were normalized by a functional group assumed to not participate in the crosslinking reaction, the 1380 cm^{-1} peak[101] which was assigned to the dimethyl group on the C3 carbon of the aliphatic ring in the IPDI monomer.[146]

5.2.4 Elemental Analysis

Modified and unmodified CNC samples were sent to ALS Environmental in Tuscon, AZ for elemental analysis. The samples were analyzed for C, H, O and N content. The C, H, N analysis was performed on a Perkin Elmer 2400 Series II, and the O analysis was performed on a Leco Truspec Analyzer. The Perkin Elmer instrument was calibrated with acetanilide and the Leco Truspec was calibrated with benzylic acid. Approximately 2 to 5 mg of sample was weighed and

then held in the combustion chamber for about 5 minutes. The oxygen analyzer was held at 1000 °C and the C, H, N analyzer was held at 935 °C. The degree of substitution was calculated based on the nitrogen content.

5.2.5 Nuclear Magnetic Resonance Spectroscopy (NMR)

The selectivity for the primary/secondary isocyanate group using DABCO and DBTDL catalysts was verified with solid state ^{13}C NMR. Ca. 50 milligrams of um-CNC and m-CNC was packed into a 24 mm OD MAS rotor. CP-MAS spectra were recorded using a Bruker AV3-400 NMR spectrometer operating at a 1H frequency of 400 MHz. A dual channel BB-MAS probe was operated at a spinning speed of 10 kHz. Cross polarization was achieved with a trapezoidal shaped contact pulse for 1H varying in power from 70 to 100% and a length of 2 ms. Repetition delay between scans was 4s and at least 12,000 scans were acquired for each sample in order to measure spectra with an excellent signal to noise ratio. The spectra were normalized by the peak positioned at $\delta = 75$ ppm, an absorbance that was attributed to the C2, C3, and C5 carbons in the crystalline cellulose.[149] These groups were assumed to not participate in the reaction.

5.2.6 TGA

Thermal stability and changes in degradation patterns associated with the modification step were assessed with thermogravimetric analysis (TGA) (TA Instruments TGA Q5000). Samples were heated from room temperature to 600 °C at a rate of 5 °C/min under a flowing nitrogen atmosphere. The onset temperature (T-onset) and temperature at maximum weight loss rate (T-max) were determined with TA Universal Analysis software. The onset temperature of degradation was assessed by TA Universal analysis software by manually choosing a point before and after the sharp drop in mass loss on the weight loss curve. The temperatures at maximum weight loss were

determined for each event of degradation with TA Universal analysis software by manually selecting a point before and after the peak maximum on the derivative weight loss curve. Measurements were repeated three times, and average values were reported.

5.2.7 PLM

CNC dispersion in the polyurethane matrix was investigated qualitatively by the observation of birefringence with an optical microscope (Olympus BX51) equipped with two polarizers (Olympus U-AN360P). Images were captured with an Olympus camera (U-CMAD3) and processed with PictureFrame software. All films were imaged in transmission mode with a 20X objective and at full extinction of the polarizers.

5.2.8 Tensile Testing

Uniaxial tensile testing was performed using an Instron 5842. The samples were prepared by cutting the films with a dog bone die based on the ASTM standard D1708-13. The test section was approximately 22 mm long, and samples were approximately 0.6 mm thick. The testing speed used was 10 mm/min. Material properties associated with changes in tensile strength measured at break, % elongation, and work of fracture were reported. A minimum of four samples were tested for each material composition, and the average values were reported.

5.3 Results

5.3.1 Determining m-CNC Chemistry with ATR-FTIR, Elemental Analysis, and ^{13}C-NMR

In order to verify the attachment of the IPDI monomer to the CNC surface with pendant isocyanate groups, as illustrated in Figure 5.1, ATR-FTIR was used to characterize the m-CNCs and um-CNCs. The isocyanate functionality has an isolated and strong absorbance around 2240 cm^{-1},[101] thus evidence of its presence in any of the samples tested should be obvious. After the m-CNCs were washed with toluene 3 times, the supernatant of the third centrifuged product was

tested. The ATR-FTIR results indicated that a negligible amount of isocyanate was remaining from the reaction mixture after the toluene washing (data not shown), thus the isocyanate peak observed in the modified particles would be largely due to the presence of isocyanate on the CNC particles. Figure 5.2 shows the ATR-FTIR spectra for the um-CNC and m-CNC. The um-CNCs showed IR absorbances characteristic of cellulosic functional groups. There were strong absorbances around 3000-3550 cm^{-1} and 900-1100 cm^{-1}, the bands assigned to –OH and -C-O-C vibrations, respectively.[66,101] Changes across all regions of the spectra were observed for the m-CNCs; the most significant changes will be discussed. First, there was an apparent decrease in the –OH peak, which indicated that some of these functional groups were consumed. This decrease in the –OH peak coupled with the appearance of the isocyanate band at 2240 cm^{-1} gave a strong indication that the CNC surface was successfully modified. Additionally, there were significant increases in the absorbance of the carbonyl bond present in urethane groups at 1500-1750 cm^{-1}.[66,101] These results suggested that not only was the CNC surface successfully modified with the IPDI monomer, but that only some of the isocyanate groups were attached, thus demonstrating the unequal reactivity of the IPDI. The available isocyanate group from the m-CNC particles may facilitate a route for further CNC modifications and/or a covalent linkage with the polymer matrix.

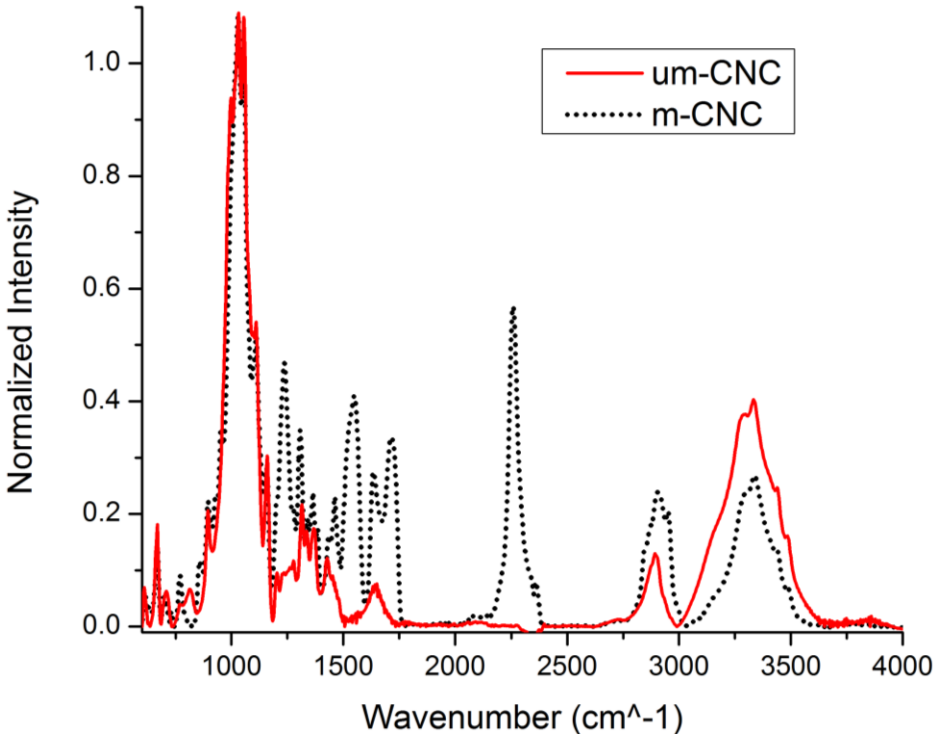

Figure 5.2: ATR-FTIR spectra of um-CNCs and m-CNCs.

The degree of substitution (DS) is a parameter used to describe the extent of modification and specifically translates to the number of hydroxyl groups that have been modified per one anhydroglucose unit (AGU). The results of the elemental analysis are given in Table 1 and this data was used to calculate the DS for the modification of CNCs with IPDI.

The unmodified cellulose contained a negligible amount of nitrogen, as expected. The modified CNCs contained 5.23 wt.% nitrogen, indicating that the IPDI was present. The DS was determined by considering the theoretical percentage of nitrogen that would be present in the modified CNCs if one IPDI monomer was attached to the 3 hydroxyl groups available in one AGU, the maximum DS.[150] The total molecular weight of such a structure would be 831 g/mol, and the % nitrogen would be 10%. Comparing the theoretical value, 10%, to the measured value of % nitrogen, 5.23%, the DS was approximately 0.52, which corresponds to 17% of the hydroxyls participating in the reaction. This value reflects the DS for bulk CNC, however not all of the CNC

hydroxyls are expected to react. Typically it is more appropriate to consider a DS for the surface since it is the surface hydroxyls that would participate in the reaction. Therefore, if only the surface hydroxyls of the CNC are considered, the DS would be higher. The DS for the surface is noted by DS_{surf}.

In their review article, Eyley *et al.* give an equation to calculate the number hydroxyl groups on the CNC surface in mol/g, a value that is then used in a separate equation to calculate DS_{surf}.[135] Using the dimensions of the CNCs used in this work, the CNC crystallographic parameters reported by Wu *et al.*,[151] and the elemental analysis data, the DS_{surf} was calculated to be 1.4. The DS_{surf} can be related to DS by the chain ratio parameter, R_c, which is the ratio of exposed cellulose chains to the total number of chains in a CNC.[135] Using the calculated value of DS_{surf} = 1.4, and the calculated R_c value for the CNCs used in this work, the DS was calculated to be 0.51. This value was similar to the DS calculated using the elemental analysis data and molecular weight arguments, and was therefore considered appropriate.

Eyley *et al.* noted that the maximum theoretical DS_{surf} is 1.5 due to the crystalline structure of CNCs where one C6, C3, and C2 hydroxyl group point out of the face of the crystal for every cellulose repeat unit (2 AGUs).[135] Given this information, the DS_{surf} calculated in this work was relatively high. The authors also noted that $DS_{surf} > 1$ was unlikely given the assumed lack of reactivity of the C3 hydroxyl group, and that $DS_{surf} > 1$ would disrupt the crystalline structure of cellulose.[135] The integrity of the crystalline structure after modification was qualitatively assessed with ^{13}C NMR, and is discussed below.

Table 5.1: Elemental composition of um-CNCs and m-CNCs.

	C	H	N	O
Unmodified CNC (%)	41.13	5.62	<0.05	44.43
Modified CNC (%)	50.33	7.04	5.23	30.95

In addition to characterizing the surface chemistry, the crystallinity of the CNCs was also characterized. There are many ways to determine the crystallinity of CNCs, the most common being the XRD peak height method, however this method often overestimates the crystallinity.[152] Other methods involving XRD include peak deconvolution or an amorphous peak subtraction method, each of which calculate a lower degree of crystallinity compared to the XRD peak height method.[152] Although it is a less common technique, ^{13}C NMR can also be used to determine CNC crystallinity.[152,153] The values mentioned here were used for comparing the degree of crystallinity of the um-CNC to the m-CNC products. In the NMR spectra, the C4 peak in the range of δ=93-87 ppm was assigned to the crystalline form of cellulose, and its shoulder peak at δ=86-80 ppm was assigned to the amorphous regions of cellulose.[152,153] The crystallinity index, CI, is computed with ^{13}C NMR by integrating the C4 crystalline peak and dividing that value by the total area of the C4 peak (δ=93-80).[152,153] Upon integration of these peaks, it was determined that the CI of um-CNC was 67%, and for both m-CNC products the CI was 66%. Although discrepancies are expected with CI values for CNCs given the variety of experimental techniques, cellulose sources, and CNC extraction methods available, the CI reported here fell within the range of the expected value for CNCs, which is 54-88% crystallinity.[18] In any case, these data show that it can be reasonably determined that the modification step did not result in a significant disruption of the CNC crystalline structure as suggested by Eyley *et al.* Possible explanations of the high DS_{surf} could be due to a lack of understanding of the CNC surface on the atomic scale. For example, the exact nature of the CNC crystal structure is not well understood, as some researchers have proposed a region in cellulose of intermediate order and mobility compared to the crystalline and amorphous domains.[154] If so, such a 'para-crystalline' region could accommodate additional IPDI groups and could result in a higher DS_{surf} than expected. Another possibility could be the method in which the

CNCs are modified, specifically with significant excess of the IPDI reactant, and with a CNC swelling solvent such as DMSO. When CNCs were modified in dimethylformamide (DMF) with HDI in a 5:1 excess of HDI, the DS was calculated to be 0.45 by elemental analysis, a similar value reported here.[66] The discussion presented here is meant to put into perspective the possibilities for the extent of surface coverage in CNC modifications, and highlight important considerations of such chemical modifications, specifically crystallinity. Although the DS_{surf} was higher than expected, it was difficult to say with certainty the extent of modification to the CNC surface given the assumptions of the number of hydroxyl groups on the surface and an incomplete picture of the CNC surface mobility and crystallinity. Therefore, it is perhaps more appropriate to report a range of DS from 0.5 to 1.4. Overall, these data indicated that the IPDI modification of CNCs resulted in good surface coverage without compromising the CNC crystallinity.

^{13}C NMR analysis also gave insight into the selectivity of two isocyanate catalysts, DBTDL and DABCO. The normalized spectra for the um-CNCs and m-CNCs modified using DBTDL and DABCO catalysts are given in Figure 5.3. The spectrum for the um-CNC represented a typical solid state ^{13}C NMR spectra for crystalline cellulose.[149] Major peaks in Figure 3 are labeled according to the corresponding 6 carbons in one AGU.[66,149] Changes to the NMR spectra associated with the IPDI modification were observed. In addition, it was possible to observe differences in the m-CNC spectra depending on the type of catalyst used for the preparation. First, both m-CNC spectra showed new peaks in the δ=160 to 120 ppm range, and in the δ=50 to 20 ppm range when compared to the um-CNCs. Peaks in the δ=50 to 20 ppm region were due the hydrocarbons present in the IPDI, specifically: $–CH_2–$ from the aliphatic IPDI ring (δ= 45.5 ppm), the tertiary carbon (δ=36.9 and δ=32.3 ppm), and the $–CH_3$ groups (δ=28.0 and δ=23.5 ppm). The peaks in the δ=160 to 120 ppm region represented the urethane (δ=158.0 – 156.8 ppm) and

isocyanate (δ=129.2 – 123.4 ppm) functionality on the CNC particle. All chemical shift values were consistent with previously established values. [66,101,155]

From solution NMR it is well known that the primary urethane linkage (δ = 157.13 ppm)[146] has a higher chemical shift than the secondary urethane linkage (δ = 155.99 ppm).[146] The observation of distinct peaks for the primary and secondary urethane assignment was less apparent due to the broader lines encountered in solid state NMR. However, the selectivity of the catalysts can be inferred by the apparent chemical shift of the single urethane peak, which in fact must be a superposition of two broader peaks. The urethane peak was positioned at δ=158 ppm for the DABCO catalyst, and at δ= 156.6 ppm for the DBTDL catalyst. Hence, the DABCO catalyst had a higher affinity for the primary isocyanate reaction site.

Alternatively, two distinct peaks were observed in the solid state NMR spectra for the assigned isocyanate absorbance. From solution NMR, it is known that the primary isocyanate group (δ = 122.22 ppm)[146] has a lower chemical shift compared to the secondary isocyanate site (δ = 122.98 ppm).[146] Similar results were found here when the neat IPDI was tested by solution ^{13}C NMR (data not shown). The primary isocyanate was positioned at 121.9 ppm and the secondary isocyanate at 123.8 ppm. The secondary peak also showed a stronger absorbance in this spectra, and the ratio of the secondary to primary peak intensity was 1.50. In order to compare the relative quantities of primary and secondary isocyanates in the solid state ^{13}C NMR spectra, however, the peak area should be considered.[149] This information was used to infer the selectivity of the two catalysts. First, the CNCs modified using the DABCO catalyst indicated two isocyanate peaks at 125.8 and 129.4 ppm, and the CNCs modified using the DBTDL catalyst indicated isocyanate peaks positioned at 123.5 and 129.2 ppm. Based on the values established by solution NMR for the assignment of primary and secondary isocyanate peaks, it was assumed that the peak

at approximately 124 ppm corresponded to the primary isocyanate, and that the peak at approximately 129 ppm corresponded to the secondary isocyanate. Given the relative area under the curve of the primary and secondary isocyanate peaks, it was apparent that the DABCO catalyst preferentially reacted the primary isocyanate. Specifically, the integrated peak area ratio of the secondary to primary isocyanate was 3.63 for the DABCO catalyst compared to 0.81 for the DBTDL catalyst. ^{13}C NMR suggested that the catalyst choice impacted the selectivity for an –OH cellulose reaction with either primary or secondary isocyanate groups. These results, along with the ATR-FTIR and elemental analysis data, confirmed that the m-CNCs had both isocyanate and urethane functionality.

Another qualitative difference between the two catalysts was revealed by the noticeable differences in intensity after the data was normalized to represent equivalent amounts of unmodified cellulose. The CNCs modified using the DBTDL catalyst showed peaks of higher intensity in the urethane region, and in the region representing the aliphatic carbons from the IPDI. This resulted indicated that the DBTDL catalyst facilitated a higher grafting density of IPDI molecules to the CNC surface when compared to the DABCO catalyst. It was determined that the DBTDL catalyst was more efficient than DABCO for the reaction studied here. Intuitively, this result was not surprising considering that the DABCO catalyst selects for the inherently less reactive isocyanate. Data reported by Speier *et. al.* indicated a similar conclusion with the calculated reaction rate constant for the secondary isocyanate using DBTDL occurring about twice as fast as the reaction rate for the primary isocyanate using DABCO.[147] Additionally, the authors reported that the reaction catalyzed by DBTDL reached 100% conversion sooner than the reaction catalyzed by DABCO, with a 2:1 NCO:OH stoichiometry and a temperature of 20 °C.[147]

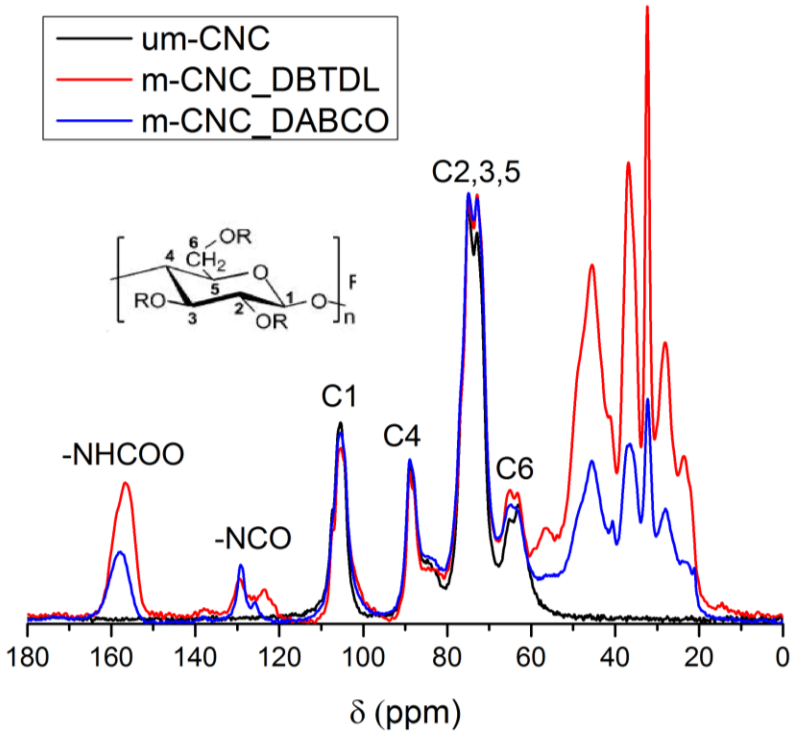

Figure 5.3: ^{13}C NMR spectra for um-CNCs and m-CNCs catalyzed with DBTDL and DABCO.

5.3.2 Thermal Degradation of um-CNC and m-CNC

To compare the thermal degradation behavior of the um-CNCs and m-CNCs, the materials need to be dried in a similar manner prior to TGA experiments since previous results have shown that the degradation behavior was related to the drying method used.[156] After the CNCs were functionalized with IPDI, the particles were washed with toluene to eliminate excess reactants, and allowed to dry in a vacuum oven at 80 °C. Thus, the um-CNCs were also wet with toluene and dried in a vacuum oven at 80 °C. When comparing the onset of degradation of freeze dried um-CNC to the m-CNC particles, there were appreciable changes. These changes are shown in the weight loss curves and derivative weight loss curves given in Figure 5.4. First, the onset of degradation for the m-CNCs was increased. A similar increase in the onset of degradation was also observed by Tang *et. al.* when wood based CNCs were chemically modified with PDMAEMA,[123]

and by Pereda *et. al.* when cotton CNCs and starch nanocrystals (SNC) were physically modified with PEO.[56] Here, the m-CNCs began to degrade at 300 °C, a 35 °C increase compared to the um-CNCs. The um-CNCs also began to lose weight much earlier in the heating process (around 35 to 100 °C) than the m-CNCs. This difference was attributed to a small amount (approximately 6 wt.%) of water associated with the um-CNC particles.[123] This moisture is likely not present for the modified particles due to the incorporation of organic molecules on the CNC surface. The m-CNCs also contained more char at the end of the run at 600 °C compared to the um-CNCs, 10 ± 1.8 wt.% and 2.3 ± 0.6 wt.%, respectively. This result also reflected the improved thermal stability of the m-CNC particles.

To gain insight into the events involved in the degradation process, the derivative TGA curve (Figure 5.4(b)) was considered. The degradation of the um-CNCs occurred in two major steps while the degradation of the m-CNCs occurred in three major steps. These steps were identified by the temperature associated with the maximum slope value in the weight loss signal, appearing as a peak in derivative signal. The first temperature at maximum weight loss rate (T-max 1) for both um-CNC and m-CNC was 280 °C. This peak signified the first degradation event for both particles, although this event was more significant for the um-CNCs. This process was attributed to the decomposition of the negatively charged sulfate ester groups on the CNC surface.[83,86] The um-CNCs continued to degrade more slowly with another event occurring at approximately 450 °C. This decomposition was attributed to the slower kinetic degradation of the crystalline interior[83] and also occurred for both types of particles. The m-CNCs exhibited an additional mode of degradation at 330 °C. This event was characteristic of hard segment polyurethane (-NHCOO) degradation and has been classified as the decomposition of a urethane group into an isocyanate and alcohol group.[157] These results provided further evidence of the

CNC/urethane functionality and demonstrated the improved thermal degradation behavior as a result of the modification.

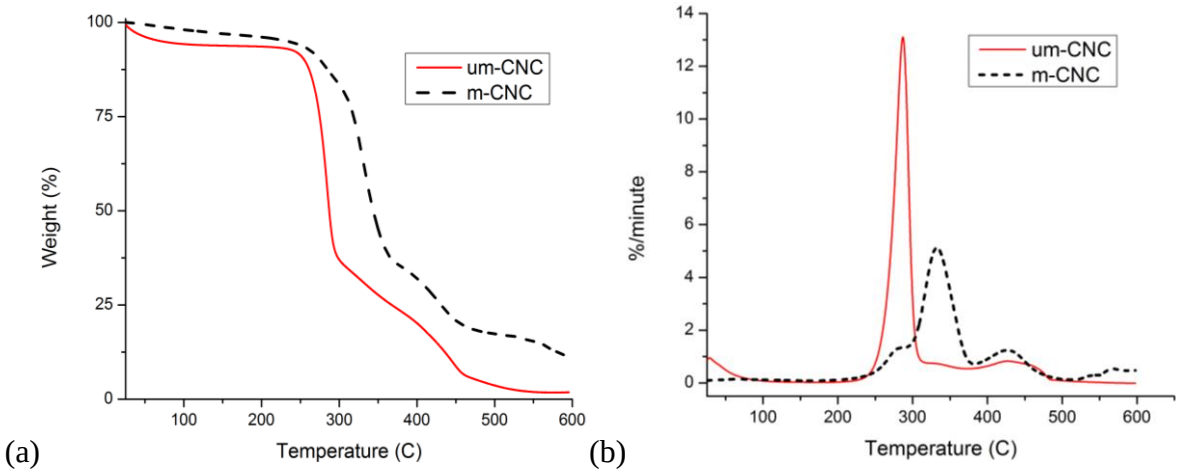

Figure 5.4: Weight loss curves (a) and (b) derivative weight loss curves for um-CNCs (——) and m-CNCs (- - -).

A summary of the thermal degradation data for the toluene treated um-CNC and m-CNCs, and freeze dried um-CNC is given in Table 5.2. Specifically, values for onset temperature of degradation (T-onset) and temperatures at maximum weight loss for each degradation process (T-max 1, T-max 2, and T-max 3) are shown. The freeze dried CNCs vacuum oven dried with toluene had a similar T-onset, T-max 1, and T-max 2 compared to the freeze dried um-CNCs, indicating that the additional washing and drying preparation steps did not have a significant impact on the degradation behavior of the particles. Therefore, it was concluded that the increase in the onset of degradation observed with the m-CNCs was solely due to the modification step and not the drying method or some combination of the two.

Table 5.2: Thermal degradation properties of CNC particles prepared by various methods. Error represents 95% confidence intervals.

Particle:	um-CNC	um-CNC	m-CNC
Drying method:	freeze dry from aqueous	vacuum oven (80 °C) from freeze dry	vacuum oven (80 °C) from freeze dry
T-onset (°C)	266 ± 3	265 ± 6	300 ± 1
T-max 1 (°C)	289 ± 0.5	287 ± 1	286 ± 10
T-max 2 (°C)	454 ± 0.1	433 ± 10	329 ± 2
T-max 3 (°C)	-	-	426 ± 4

5.3.3 Dispersion of CNCs in Polyurethane Composite

The um-CNC and m-CNC particles were incorporated into a polyurethane elastomer based on IPDI and triol according to the procedure outlined in the Materials and Methods section. The nanoparticle dispersion, polymer chemistry, and mechanical property were assessed with PLM ATR-FTIR, and tensile testing, respectively. PLM is a useful tool for analyzing CNC dispersions in transparent/amorphous media.[148,158] The CNC particles will appear polychromatic at certain concentrations if arranged in liquid crystalline domains, and as white/bright regions if they are randomly oriented and clustered.[18,102] The crystalline character of CNCs afford them an optical anisotropy, giving rise to obvious birefringence when viewed under cross polarizers. Conversely, if the PLM analysis yields uninteresting results (a dark image), it can be concluded that the CNCs are well dispersed at this length scale. Additionally, PLM can give an indication of the homogeneity of CNC dispersion at larger length scales when compared to electron microscopy techniques considering the viewing area offered by each method. While SEM or TEM may allow the user to see a few square nanometers or micrometers of the sample surface, optical microscopy images are on the order of mm^2 and represent a 3 dimensional distribution of the CNCs, thus providing a more complete picture of their dispersion. CNCs are also difficult to image with electron microscopes given their low stability in the electron beam, elemental similarity to most polymer matrices, and ~ 5 nm width. Viewing the um-CNC and m-CNC composites between

crossed polarizers gave information about the degree of CNC dispersion achieved in the polyurethane composites and these images are given in Figure 5.5(a). These images were qualitatively compared to the neat polyurethane matrix, in which no birefringence was observed, suggesting a completely amorphous material. The um-CNC composite appeared to have CNC aggregates present across a large area of the sample, while the m-CNC composite showed limited birefringence at identical CNC loadings. This result implied that the m-CNCs were dispersed in the polyurethane matrix on the micrometer scale. Similar results were achieved when CNCs were mixed with a waterborne epoxy system and filler-matrix compatibility was enhanced by physical polymer/nanoparticle interactions.[148] The m-CNCs were likely dispersed more homogeneously in the polyurethane matrix due to increased chemical compatibility with the monomeric components and the formation of urethane linkages. The m-CNC composite may have achieved better dispersion due to covalent linkage formation between the triol and the pendant isocyanate group on the m-CNC surface. The dispersion levels attained were likely related to the solvent used as well, toluene. Generally, toluene is a poor solvent for CNCs and was used as the dispersing solvent in both composite formulations, given its compatibility with the m-CNCs and volatility that facilitates film formation from solvent-based processing methods. The dispersion of the um-CNC particles in composites could be improved by using a better solvent for CNCs, like DMSO.

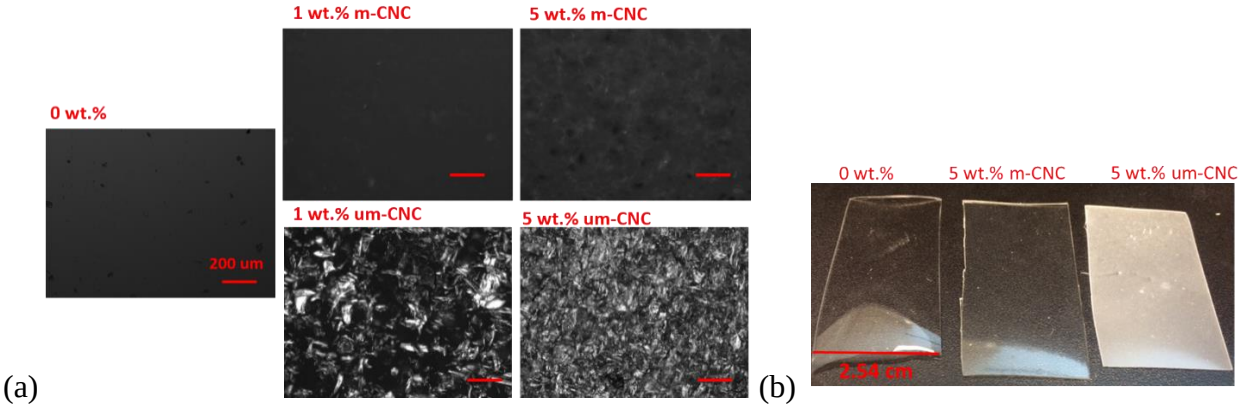

Figure 5.5: (a) PLM images of CNC-PU composites, and neat polyurethane. (b) Photographic image of cured polymers.

In addition to displaying a stark contrast in the amount of birefringence observed in the polyurethane composites, the bulk composites also had contrasting optical properties. These differences are highlighted by Figure 5.5(b). The sample containing um-CNCs took on the white color of the FD-CNC powders. Comparing the appearance of the m-CNC composite to the um-CNC composite, it was clear that the modified particles have less of an impact on the bulk optical property of the polyurethane sample. Coupling this observation with the polarized light micrographs, it was concluded that the modified CNCs were well dispersed in the polyurethane matrix and that the enhanced dispersion was due to the modification step.

5.3.4 Chemistry of CNC/Polyurethane Composites

To assess the effect that CNCs had on polyurethane chemistry, ATR-FTIR was used to characterize the functional groups present in the composites, and the results are summarized in Figure 5.6. For all concentrations tested here, there was no evidence of isocyanate absorption at 2240 cm^{-1}, thus indicating within the sensitivity of the measurement that all of the IPDI molecules reacted. The band at 1700 cm^{-1} represented the urethane linkage (-NHCOO), and the band at 3330 cm^{-1} represented the secondary amide (-CONH), which typically absorbs in the 3460-3400 cm^{-1} range but is lowered in the solid state and with hydrogen bonding.[101] Additional bands in the

fingerprint region (1500-600 cm^{-1}) were similar for all composites and represented a combination of ether, amine, and hydrocarbon bonds.[101] While their identification was not trivial, the CNC loadings used here did not create new bands, and intensities were comparable across all wavenumbers tested here. Therefore, it was assumed that all composites had similar chemistry, and similar concentrations of urethane linkages.

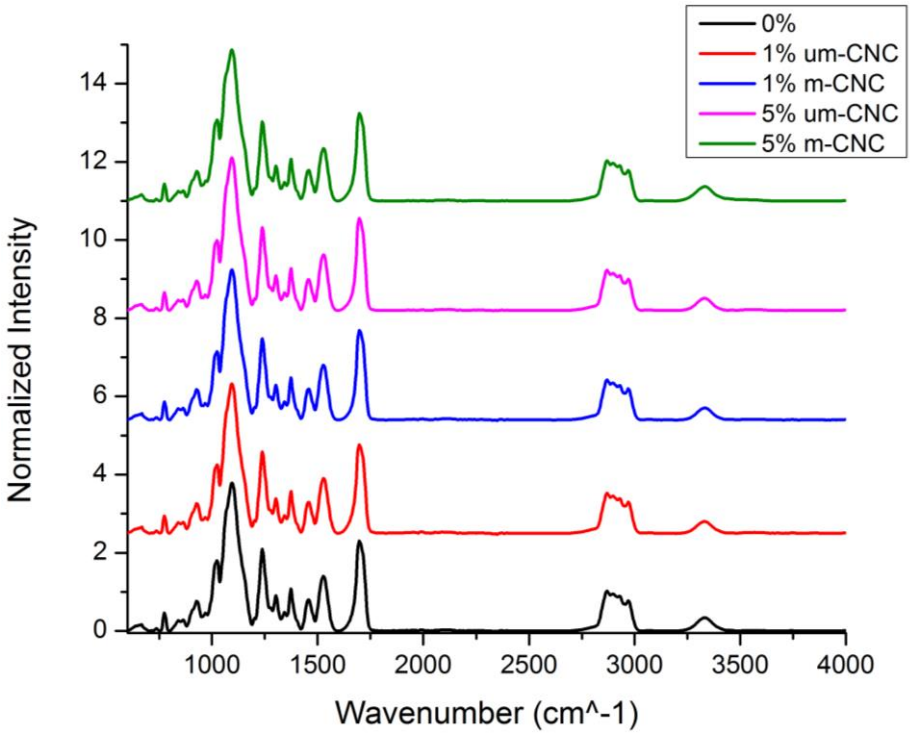

Figure 5.6: ATR-FTIR spectra for 0, 1, and 5 wt.% um-CNC and m- CNC polyurethane composites.

5.3.5 Mechanical property of CNC/Polyurethane Composites

The mechanical performance of the composites compared to the neat matrix was assessed with tensile testing. The elongation at break for all samples tested ranged from 160 to 190%, although all measurements fell within the error ranges of each other, so no change in this property was observed with CNC addition. The data for tensile strength at break and work of fracture is given in Figure 5.7, with error bars representing confidence intervals of 95%. As a general trend, the samples containing m-CNC performed better than samples containing um-CNC at the same

concentrations. For example, at a 1 wt.% concentration, the m-CNC composite had improved tensile strength and work of fracture by 42% compared to the um-CNCs. This trend was more apparent for the 5 wt.% samples, with a 163% increase in tensile strength, and a 132% increase in the work of fracture for the m-CNC composites. In fact, the 1 wt.% m-CNC samples performed better than the 5 wt.% um-CNC samples. Therefore, less of the modified material is needed to achieve a similar or improved mechanical performance when compared to the unmodified particles. Most significantly, the 5 wt.% m-CNC sample improved the tensile strength by 226%, and the work of fracture by 257% when compared to the neat matrix.

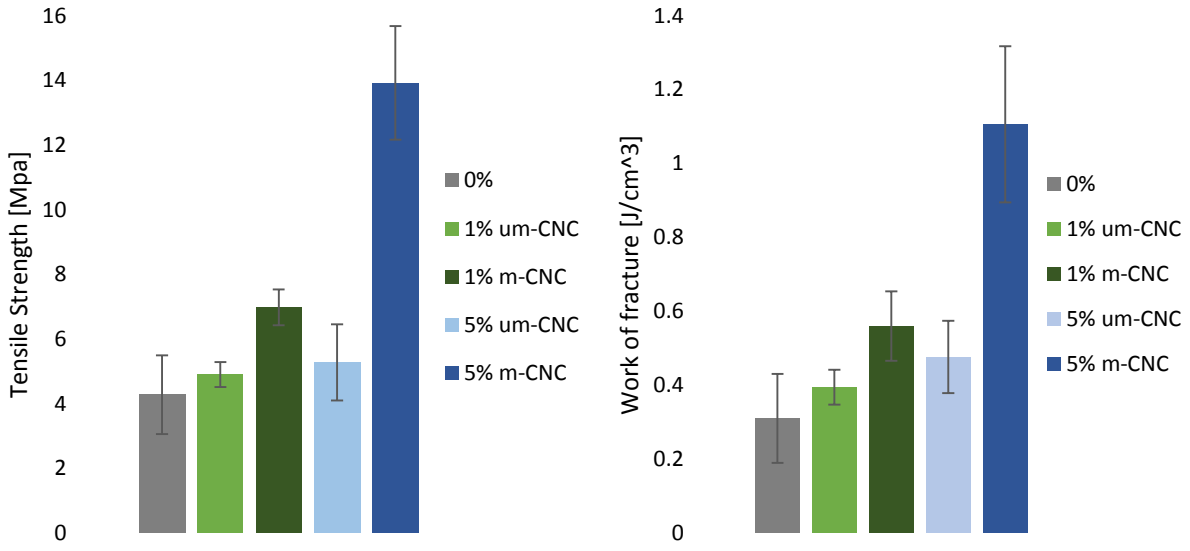

Figure 5.7: Tensile strength and work of fracture for um- and m-CNC composites and neat polyurethane. Error represents 95% confidence intervals.

Since the elongation at break was similar for all samples tested, it is possible that one of the mechanisms of reinforcement was due to the stiffening of the matrix by the CNC particles. While the tensile test standard chosen for this study did not allow for quantitative determination of elastic modulus, the initial slope of the stress-strain curves suggested that it was increased with increasing CNC loadings. This result was expected given that the CNCs were quite rigid compared

to the soft polyurethane matrix[38] ($E_{L\text{-}CNC}$ ~150 GPa, E_{PUE} ~ 0.025 GPa). However, the significant increase in the tensile strength and work of fracture suggested that there was more at work here than stiffening of the matrix. The factors affecting tensile strength and work of fracture include: particle size, particle loading, and the strength of the filler-matrix adhesion.[38] Assuming that for a given concentration of m-CNCs or um-CNCs the effective particle loading and particle size was similar, an increase in the tensile strength would imply good filler-matrix adhesion. The forces behind filler-matrix adhesion can range from physical (electrostatic, mechanical interlocking, van der Waals) to chemical (ionic, metallic, covalent).[159] These results, along with the FTIR and PLM, give evidence for strong m-CNC/polyurethane interactions such as chemical bonding.[159]

5.4 Conclusions

The reaction of freeze dried CNCs with IPDI was optimized to yield modified cellulose particles with a high surface coverage of the di-functional monomer. ATR-FTIR and ^{13}C NMR confirmed that the particles had both isocyanate and urethane functionality, and indicated that the DBTDL catalyst selectively reacted the secondary isocyanate. The pendant primary isocyanate group was then used as a route to facilitate covalent bond formation with a polyurethane elastomer, resulting in a significant improvement in the tensile properties at 5 wt.% m-CNC compared to the neat matrix. This study demonstrated a unique and versatile modification scheme not yet reported previously in the literature. Some advantages of this modification scheme were made apparent by a marked improvement in thermal degradation and nanoparticle dispersion in the selected polymer matrix, two highly sought after features concerning cellulose nanomaterials. Additionally, this functionalization method may serve as a platform for the addition of other desirable functional groups and/or as a means for increasing compatibility with a range of organic solvents and

polymers. Overall, the functionalization scheme presented is anticipated to be useful in a range of applications not limited to the composite application presented here.

CHAPTER 6

CONCLUSIONS AND RECOMMENDATIONS

6.1 Summary and Conclusions

This work provides a basis for designing two CNC/thermoset composites, specifically a waterborne epoxy and an elastomeric polyurethane. While the processing methods were specific to the polymer systems chosen in this work, the fundamental ideas are transferrable to other CNC/polymer composites. The results demonstrate the successful completion of the specific objectives outlined in Chapter 1. The key findings for each objective are summarized as follows:

6.1.1 Incorporation of CNCs into a commercial waterborne epoxy resin and optimizing CNC dispersion

CNCs were successfully used to improve the mechanical property of a waterborne epoxy resin. In Chapter 2, CNCs were mixed together with an epoxy emulsion and amine crosslinker with up to 15 wt.% CNCs in the cured composites. CNCs resulted in increased tensile modulus, storage modulus, and loss modulus. However, when considering the elementary upper and lower limits on the theoretical composite modulus, the enhancement was not optimized. Therefore, Chapter 3 investigated an alternate processing strategy for the CNC/epoxy composites. As learned here, when the CNCs were premixed with the epoxy emulsion, rather than added simultaneously with the amine, their dispersion in the cured polymer matrix was improved. By enhancing the CNC dispersion, the storage modulus, work of fracture, and tensile strength were improved compared to the neat matrix and compared to the less homogeneously dispersed composites at an identical CNC concentration. This study highlighted the importance of carefully choosing processing parameters when designing CNC composites, as processing will have a significant impact on mechanical properties and CNC dispersion.

6.1.2 Investigation of CNCs as Emulsifiers with Tensiometry

Chapter 4 details the first investigation of CNCs as interfacial tension modifiers using DGEBA as the oil phase, as well as the influence of a nonionic surfactant with CNCs, and an amine molecule with CNCs. Similar to other work involving the interfacial tension of dodecane and toluene, it was determined here that neat CNCs do not significantly lower the DGEBA/water interfacial tension, and that CNCs were not present at the interface in a significant quantity. The image charge effect was investigated for the first time with CNCs as a possible reason for the CNCs not partitioning at the oil/water interface, and it was concluded that the image charge did not play a significant role in hindering their interfacial adsorption. Also analogous to previous work, CNCs were found to facilitate surfactant desorption from the interface which was observed by an increase in the DGEBA interfacial tension in the aqueous CNC/surfactant mixtures compared to the surfactant-only case. CNCs also increased the DGEBA/water interfacial tension in the presence of amine with respect to the amine-only case, however, when the internal pressure of the DGEBA droplet was decreased, the droplet conformed to a non-spherical shape, indicating the presence of CNCs at the oil/water interface. Such a phenomenon is referred to as the crumpling effect. It was concluded that the amine was responsible for facilitating CNC adsorption to the DGEBA interface through visualization of droplet shape irregularity via the crumpling effect. Zeta potential measurements indicated an electrostatic association between the amine and CNCs, and it was hypothesized that this electrostatic attraction was responsible for facilitating CNC adsorption to the DGEBA interface. Another benefit to this study was the first visualization of CNCs at an oil/water interface using tensiometry, a method that is cheaper and more efficient than the labor and time intensive steps involved in electron and confocal microscope imaging, such as staining, freeze drying, and sputtering.

Overall this study looked at a new oil and water system not yet studied with CNCs to determine the ability of CNCs to act as emulsifiers. The important findings are that CNCs were not present at the oil/water interface unless coupled with the amine molecule, and that CNCs can be visualized at the interface via tensiometry.

6.1.3 Developing a Formulation for a Versatile CNC Surface Modification

A diisocyanate molecule with isocyanate groups of unequal reactivity was successfully used to modify the CNCs. ATR-FTIR, ^{13}C-NMR, and elemental analysis confirmed that the secondary isocyanate group preferentially reacted with CNCs hydroxyl groups and that the primary isocyanate group remained unreacted. Two appealing features of the IPDI functionalization were realized by an increase in the onset temperature of thermal degradation of the modified CNCs, and by the visual inspection of increased compatibility with organic solvents and the polyurethane matrix. The composites produced with modified CNCs present only one example of their application, however this was the first report of using IPDI to modify CNCs, which prevented the undesirable chain extension of the CNCs in the composites. Avoiding the chain extension, and resulting agglomeration, of the CNCs resulted in composites with improved tensile strength and work of fracture with respect to the neat matrix and with respect to the CNC composites produced with unmodified CNCs at the same loading.

The modification step outlined in Chapter 5 offers a versatile route to CNC composites with a wide range of polymer matrices with labile protons such as polyamines, polyols, and carboxylated polymers. The free isocyanate on the modified CNCs could also provide a route to additional functionalities such as acrylate or amine.

6.2 Recommendations and Future Work

Based on the findings of this work, a number of key scientific questions have been raised. The following section seeks to provide possible directions for furthering this work.

6.2.1 CNCs as emulsifiers

The tensiometry experiments discussed in Chapter 4 underlined some important considerations for designing waterborne epoxy emulsions using CNCs. If CNCs would be used in an emulsion formulation, the optimal concentration found here was 0.34 wt.% CNC with 1 mM surfactant, given that this combination of emulsifiers had the lowest DGEBA/water interfacial tension. The tensiometry experiments did not involve mechanical stirring or agitation of the mixture which could have a significant impact on the CNCs ability to stabilize emulsions by providing a mechanical driving force towards particle adsorption.[128] Therefore, determining an 'in-house' epoxy formulation using surfactant and CNCs would be useful to understanding if CNCs with nonionic surfactants can yield stable emulsions. If so, determining the long term stability and droplet size would be an important study to furthering CNC-stabilized emulsions and composite technologies.

Another interesting route to particle stabilized emulsions involves the use of CNCs with chitin nanofibers (ChNF). Chitin is the second most abundant biopolymer on the planet, and are derived from renewable sources such as crab and shrimp shells.[160] ChNFs are on the order of 5-50 nm in width and up to several micrometers in length.[160] ChNFs are stabilized by protonating its amine groups with a strong acid, and thus are positively charged.[160] CNCs and ChNFs would have a strong electrostatic attraction which could potentially result in emulsions stabilized by 100% bio-renewable particles, instead of the more common particle-surfactant mixtures.[161,162] Such an emulsion would be mechanically robust to particle coalescence, however, CNCs and ChNFs have

a tendency to severely aggregate and sediment when mixed together at alkaline pH.[163] Developing a strategy to maintain CNC/ChNF particle dispersion in the aqueous phase by adjusting pH or electrostatic charge would enable these particles to be used in novel ways not yet reported in literature. For more information refer to Appendix A.

Cellulose particle size, surface charge, and surface chemistry are variables that will also play a significant role in CNCs' ability to stabilize emulsions. Therefore, it is worthwhile to investigate the interfacial tension properties of cellulose nanofibers (CNFs), which typically have –COOH functionality instead of the sulfate ester ($-SO_3^-$) group on CNCs. CNFs are 4 to 40 times longer than CNCs[18] which may facilitate a higher degree of interfacial coverage, as suggested by previous work with BCNs.[34]

6.2.2 CNC/IPDI modifications

The modification scheme presented in Chapter 5 rendered the CNCs with reactive isocyanate groups, and in this regard several new possibilities for CNC functionality are available via isocyanate chemistry. A few possibilities will be presented here. The pendant isocyanate group on the modified CNCs would be reactive to monomers containing hydroxyl or amine functionality. The monomers 4-vinylaniline and 2-(hydroxylethyl) methacrylate (HEMA) contain one amine and one hydroxyl group, respectively. 4-vinylaniline contains an aromatic ring attached to a vinyl bond, this functionality could enable CNCs compatible with polystyrene. The HEMA monomer contains methacrylate functionality which could render CNCs to be more compatible with a number of vinyl polymers such as: polyvinyl alcohol (PVA), polyvinyl acetate (PVAc), and poly(methyl methacrylate) (PMMA). When the CNCs are modified with the monomers illustrated in Figure 6.1, after modification with the IPDI, then the CNCs would then be equipped with a new reactivity imparted by the vinyl bonds. The vinyl bonds on the CNCs could then participate in a

free radical polymerization, leading to CNCs covalently bonded to the polymer matrix. For more information on these modifications, refer to appendix A.

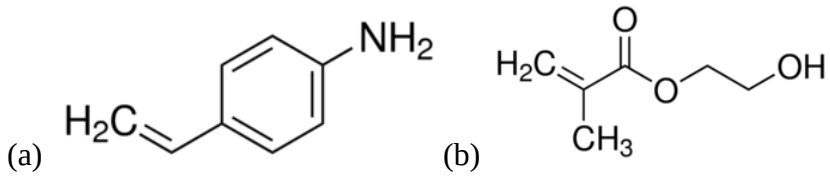

Figure 6.1: Chemical Structure of (a) 4-vinylaniline and (b) 2-(hydroxyethyl) methacrylate.

Another possibility for CNCs modifications could examine alternate isocyanate-containing molecules. For example, 2,4 toluene diisocyante (2,4-TDI) is also a difucntional isocyanate molecule with unequal reactivity of its isocyanate groups, but it is different from IPDI in that the central ring is aromatic instead of aliphatic. It has been reported that the para positioned isocyanate (*p-NCO*) was approximately 4 times as reactive as the ortho positioned isocyanate (*o-NCO*).[164] The o-NCO group is sterically hindered by the neighboring methyl group attached to the aromatic ring at the C1 position, although the relative reactivities changed with temperature. 2,4-TDI is used in higher volumes compared to IPDI in polyurethane production and could therefore present a higher volume market for use with CNCs. If CNCs were successfully modified with 2,4-TDI in a similar manner to the IPDI modified CNCs and incorporated into a polyurethane matrix, the aromatic ring on 2,4-TDI would facilitate a more rigid, rather than flexible polyurethane with a higher glass transition temperature. A short chain polyol could also facilitate more rigid composites. In this regard, several formulations could be developed to yield an extensive library of CNC/polyurethane composites with tailorable properties.

APPENDIX A

A.1 Interfacial Tension of DGEBA with CNCs and ChNFs

The interfacial tension of DGEBA was measured in an aqueous ChNF suspension of 0.25 wt.% chitin nanofibers (ChNF). Similar to the CNCs, it was determined that this concentration of ChNF (0.25 wt.%) was insufficient to lowering the interfacial tension of DGEBA with an interfacial tension value of 16.9 mN/m after 80 minutes of equilibration. However, when a much lower concentration of ChNFs were combined with CNCs in equal weight, (0.016 wt.% particles), the interfacial tension was decreased to 14.4 mN/m, a value lower than the interfacial tension of DGEBA in the presence of only CNC or only ChNF. This result showed that CNCs and ChNFs can synergistically lower the interfacial tension of an epoxy oil. However, at the CNC/ChNF concentration of 0.016 wt.%, the particles still appeared to be severely aggregated and settled out of solution, which was not ideal to measuring the interfacial tension. If the particles could be suspended in solution, their ability to lower the DGEBA interfacial tension could be further enhanced. Figure A.1 shows the dynamic interfacial tension curves of DGEBA with aqueous suspensions of 'highly concentrated' CNC (0.34 wt.%) and ChNF (0.25 wt.%) solutions versus the CNC/ChNF solution at 0.016 wt.%.

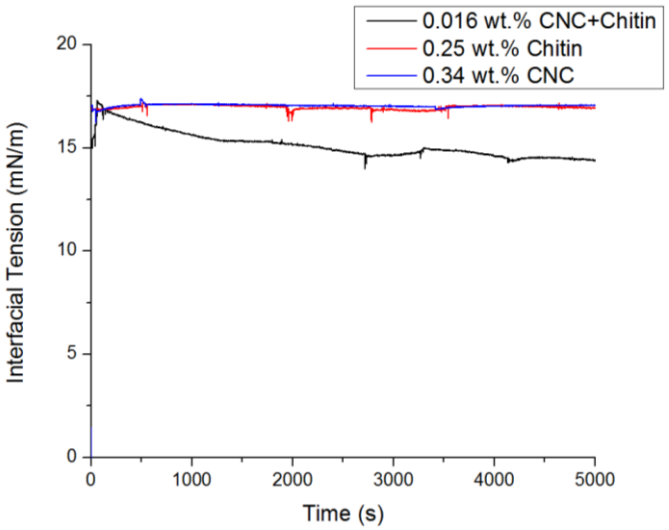

Figure A.1: Dynamic interfacial tension cuves for DGEBA in CNC, ChNF, and CNC/ChNF aqueous suspensions.

In addition to lowering the interfacial tension of DGEBA, the CNC/ChNF suspensions also gave visual confirmation of particles at the interface via the crumple test. Figure A.2 shows a deformed DGEBA droplet in the 0.016 wt.% CNC/ChNF suspension. Here, the crumpling was more severe compared to the CNC and amine case. Additionally, a particle halo can be observed surrounding the DGEBA droplet, and the sedimented particles can be observed at the bottom of the container.

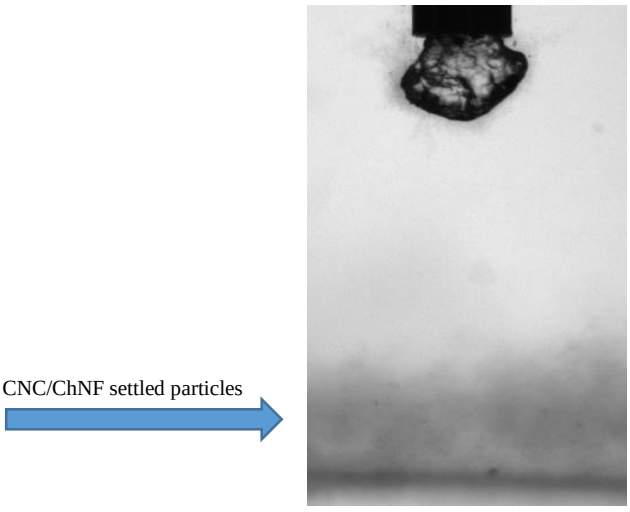

Figure A.2: Deformation of DGEBA droplet in 0.016 wt.% CNC/ChNF suspension. Note the particles surrounding the droplet and settled particles.

A.2 IPDI modified CNCs

The modification procedure to yield CNCs attached to one isocyanate group and having one free isocyanate group involved a purification step and separation step upon the completion of the reaction. Once the excess reactants were removed, the modified CNCs could then be mixed with an organic solvent, or incorporated with the polyurethane reactants. With this particular reaction, however, it was discovered that when the modified CNCs were allowed to sit in a DMSO suspension for a few days, the free isocyanate group was consumed. This was not unexpected given that isocyanates are highly reactive functional groups. The free isocyanate group could have reacted with unreacted hydroxyl groups on the CNCs, or with small amounts of water in the DMSO suspension. In any case, in order to successfully use the IPDI modified CNCs, it is prudent to quickly use them as this will ensure their best performance. Figure A.3 gives the ATR-FTIR spectra of modified CNCs tested immediately after synthesis and 8 days after synthesis. The disappearance of the band at 2240 cm^{-1} indicated the lack of isocyanate functionality.

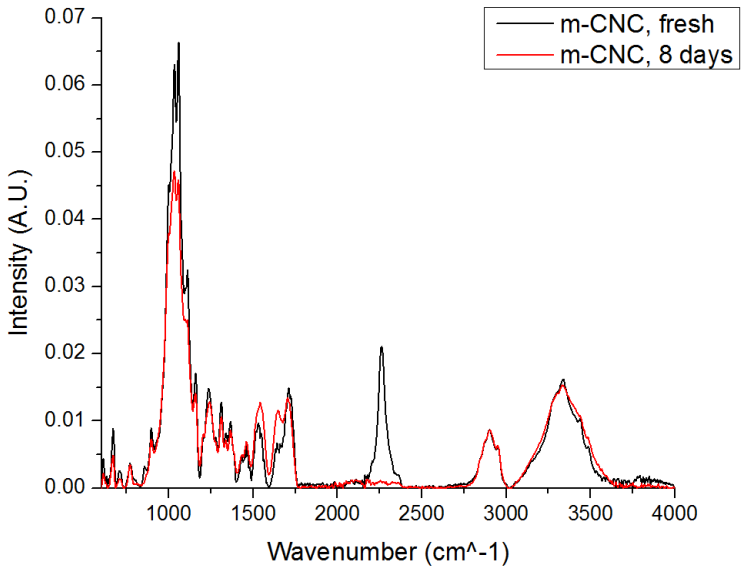

Figure A.3: ATR-FTIR spectra of m-CNC measured immediately after synthesis and 8 days after synthesis.

The utility of the IPDI modification was demonstrated by the enhanced mechanical performance of the modified CNC polyurethane composites. This example illustrated a manner in which the modified CNCs could be used in a polymer composite. Another way to demonstrate the utility of the IPDI modification was to incorporate new monomers on the CNC surface via the unreacted isocyanate group in a second modification step. After the CNCs were functionalized with IPDI and washed with toluene, the product was re-dispersed in tetrahydrofuran (THF) and added to a round bottom flask heated to 60 °C and purged with nitrogen. 1 gram of 2-(hydroxylethyl) methacrylate (HEMA) was added to the flask, along with 0.05 grams of the DABCO catalyst, and the reaction proceeded overnight with a nitrogen purge. Although a condenser was attached to the round bottom flask, a considerable amount of THF was evaporated throughout the reaction given its low boiling point. Therefore, the particles were taken directly from the reaction flask and dried in a vacuum oven. Figure A.4 shows the ATR-FTIR spectra of unmodified CNCs, CNCs modified with IPDI, and CNCs modified with HEMA after the IPDI modification. Evidence of the successful IPDI modification is shown by the isocyanate band at 2240 cm^{-1} for the IPDI modified CNCs, and an increase in the urethane band at 1725 cm^{-1}. When the CNCs were modified with HEMA after the IPDI modification, the isocyanate band was consumed and the urethane band intensity was increased. This indicated that the isocyanate was consumed by the hydroxyl group on the HEMA molecule, and that higher quantities of urethane were present through the hydroxyl/isocyanate reaction.

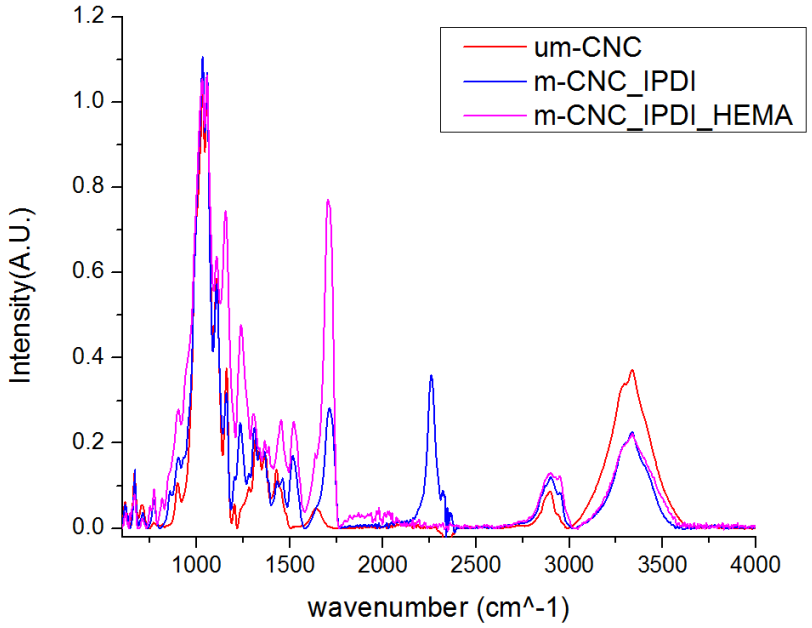

Figure A.4: ATR-FTIR spectra of unmodified CNCs (um-CNC), modified CNCs with IPDI (m-CNC_IPDI), and modified CNCs with IPDI and HEMA (m-CNC_IPDI_HEMA).

A.3 Onset of Thermal Degradation of Polyurethane/CNC Composites

The thermal degradation behavior for the polyurethane/CNC composites was tested with TGA. Approximately 7 mg of the polymer samples was added to the platinum TGA pan and heated to 600 °C at a rate of 10 °C/minute. The onset of thermal degradation was automatically determined by the TA Universal Analysis software by selecting a point before and after the onset of degradation. The data is given in Figure A.5 for the 5 wt.% um-CNC and m-CNC composites, and the neat matrix. The onset of degradation for the neat polyurethane occurred at 260 °C, which was consistent with previous reports. When 5 wt.% un-CNC was added to the polyurethane, the onset of thermal degradation was slightly increased to 267 °C, although this result did not appear to be statistically significant. A larger difference was observed for the 5 wt.% m-CNC composite, with an onset of thermal degradation of 287 °C. The improvement in the thermal degradation was likely

due to the improved thermal degradation of the m-CNCs compared to the um-CNCs. This data highlights an additional benefit to the polyurethane matrix imparted by the m-CNCs.

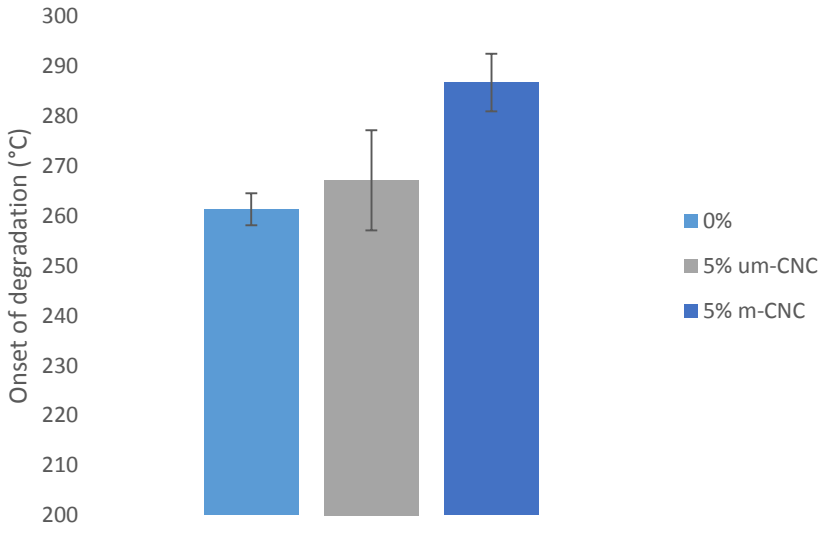

Figure A.5: Onset of Thermal degradation for the neat polyurethane and composites containing 5 wt.% um-CNC and 5 wt.% m-CNC.

REFERENCES

1. ASTM International. D883-12 Standard Terminology Relating to Plastics. 16 (2012). doi:10.1520/D0883-12.2

2. Xanthos, M., Gmbh, W. V. & Isbn, W. in *Handb. Fill.* 1–18 (ChemTech Publishing, 2010). doi:978-3-527-32361-6

3. *High_Performance_Fillers_2005*. (Rapa Technology, 2005).

4. Hancock, M. & Rothon, R. N. *Principal Types of Particulate Fillers*. (Smithers Rapra Technology, 2000).

5. Poland, C. a, Duffin, R., Kinloch, I., Maynard, A., Wallace, W. a H., Seaton, A., Stone, V., Brown, S., Macnee, W. & Donaldson, K. Carbon nanotubes introduced into the abdominal cavity of mice show asbestos-like pathogenicity in a pilot study. *Nat. Nanotechnol.* **3,** 423–8 (2008).

6. McClory, C., McNally, T., Brennan, G. P. & Erskine, J. Thermosetting polyurethane multiwalled carbon nanotube composites. *J. Appl. Polym. Sci.* (2007). doi:10.1002/app.26144

7. Hammel, E., Tang, X., Trampert, M., Schmitt, T., Mauthner, K., Eder, a. & Pötschke, P. Carbon nanofibers for composite applications. *Carbon N. Y.* **42,** 1153–1158 (2004).

8. Ghose, S. Fabrication and Characterization of High Temperature Resin/Carbon Nanofiber Composites. *High Perform. Polym.* **18,** 527–544 (2006).

9. LichaoFeng, E., NingXie, E. & Zhong, J. Carbon Nanofibers and Their Composites: A Review of Synthesizing, Properties and Applications. *Materials (Basel).* **7,** 3919–3945 (2014).

10. Martone, a., Formicola, C., Giordano, M. & Zarrelli, M. Reinforcement efficiency of multi-walled carbon nanotube/epoxy nano composites. *Compos. Sci. Technol.* **70,** 1154–1160 (2010).

11. Meador, M. a. DRAFT Nanotechnology Roadmap Technology Area 10. (2010).

12. Lam, C., James, J. T., McCluskey, R., Arepalli, S. & Hunter, R. L. A Review of Carbon Nanotube Toxicity and Assessment of Potential Occupational and Environmental Health Risks. *Crit. Rev. Toxicol.* **36,** 189–217 (2006).

13. Obama, P. WHAT IS THE CLEAN POWER PLAN ? 1–8

14. DOE. Renewable Low-Cost Carbon Fibers: a Proposal for a DOE Workshop. *Igarss 2014* 1–5 (2014). doi:10.1007/s13398-014-0173-7.2

15. Chatterjee, S., Jones, E. B., Clingenpeel, A. C., McKenna, A. M., Rios, O., McNutt, N. W., Keffer, D. J. & Johs, A. Conversion of lignin precursors to carbon fibers with nanoscale graphitic domains. *ACS Sustain. Chem. Eng.* **2,** 2002–2010 (2014).

16. Ma, A., Zhou, L. & Chang, J. Conversion of Lignin-Nanofibers to CNFs. *Nano* **10,** 1550092 (2015).

17. Tashiro, K. & Kobayashi, M. Theoretical evaluation of three-dimensional elastic constants of native and regenerated celluloses: role of hydrogen bonds. *Polymer (Guildf).* **32,** 1516–1526 (1991).

18. Moon, R. J., Martini, A., Nairn, J., Simonsen, J. & Youngblood, J. *Cellulose nanomaterials review: structure, properties and nanocomposites. Chem. Soc. Rev.* **40,** (2011).

19. Habibi, Y., Lucia, L. A. & Rojas, O. J. Cellulose Nanocrystals : Chemistry , Self-Assembly , and Applications. **d,** 3479–3500 (2010).

20. Gardner, D. J., Oporto, G. S., Mills, R. & Azizi Samir, M. A. S. Adhesion and surface issues in cellulose and nanocellulose. *J. Adhes. Sci. Technol.* **22,** 545–567 (2008).

21. *Agenda 2020 Technology Alliance Critical Nanotechnology Needs in the Forest Products Industry White Paper*. (2009).

22. Klemm, D., Heublein, B., Fink, H.-P. P. & Bohn, A. Cellulose: fascinating biopolymer and sustainable raw material. *Angew. Chemie - Int. Ed.* **44,** 3358–93 (2005).

23. Saito, T., Nishiyama, Y., Putaux, J. L., Vignon, M. & Isogai, A. Homogeneous suspensions of individualized microfibrils from TEMPO-catalyzed oxidation of native cellulose. *Biomacromolecules* **7,** 1687–1691 (2006).

24. Zimmermann, T., Bordeanu, N. & Strub, E. Properties of nanofibrillated cellulose from different raw materials and its reinforcement potential. *Carbohydr. Polym.* **79,** 1086–1093 (2010).

25. Stelte, W. & Sanadi, A. R. Preparation and characterization of cellulose nanofibers from two commercial hardwood and softwood pulps. *Ind. Eng. Chem. Res.* **48,** 11211–11219 (2009).

26. Iwamoto, S., Nakagaito, a. N. & Yano, H. Nano-fibrillation of pulp fibers for the processing of transparent nanocomposites. *Appl. Phys. A Mater. Sci. Process.* **89,** 461–466 (2007).

27. Beck-Candanedo, S., Roman, M. & Gray, D. G. Effect of reaction conditions on the properties and behavior of wood cellulose nanocrystal suspensions. *Biomacromolecules* **6,** 1048–1054 (2005).

28. Ranby, B. G. the Colloidal Properties. *Discuss. Faraday Soc.* **11,** 158–164 (1951).

29. Mukherjee, S. M. & Woods, H. J. X-ray and electron microscope studies of the degradation of cellulose by sulphuric acid. *Biochim. Biophys. Acta* **10,** 499–511 (1953).

30. Karlson, P. 1959 Nature Publishing Group. *Nature* (1959). at <http://www.mendeley.com/research/pheromones-new-term-class-biologically-active-substances-2/>

31. Ganster, J. & Fink, H. P. Novel cellulose fibre reinforced thermoplastic materials. *Cellulose* **13,** 271–280 (2006).

32. Matos Ruiz, M., Cavaillé, J. Y., Dufresne, a., Gérard, J. F. & Graillat, C. Processing and characterization of new thermoset nanocomposites based on cellulose whiskers. *Compos. Interfaces* **7,** 117–131 (2000).

33. Marcovich, N. E., Auad, M. L., Bellesi, N. E., Nutt, S. R. & Aranguren, M. I. Cellulose micro/nanocrystals reinforced polyurethane. *J. Mater. Res.* **21,** 870–881 (2006).

34. Kalashnikova, I., Bizot, H., Cathala, B. & Capron, I. Modulation of cellulose nanocrystals amphiphilic properties to stabilize oil/water interface. *Biomacromolecules* **13,** 267–275 (2012).

35. Kalashnikova, I., Bizot, H., Bertoncini, P., Cathala, B. & Capron, I. Cellulosic nanorods of various aspect ratios for oil in water Pickering emulsions. *Soft Matter* **9,** 952 (2013).

36. Liu, A. & Berglund, L. a. Fire-retardant and ductile clay nanopaper biocomposites based on montmorrilonite in matrix of cellulose nanofibers and carboxymethyl cellulose. *Eur. Polym. J.* **49,** 940–949 (2013).

37. Hu, Z., Patten, T., Pelton, R. & Cranston, E. D. Synergistic Stabilization of Emulsions and Emulsion Gels with Water-Soluble Polymers and Cellulose Nanocrystals. *ACS Sustain. Chem. Eng.* (2015). doi:10.1021/acssuschemeng.5b00194

38. Fu, S. Y., Feng, X. Q., Lauke, B. & Mai, Y. W. Effects of particle size, particle/matrix interface adhesion and particle loading on mechanical properties of particulate-polymer composites. *Compos. Part B Eng.* **39,** 933–961 (2008).

39. Tjong, S. C. & Xu, S. a. Ternary polymer composites: PA6,6/maleated SEBS/glass beads. *J. Appl. Polym. Sci.* **81,** 3231–3237 (2001).

40. Amdouni, N., Sautereau, H. & Gerard, J. F. Epoxy composites based on glass beads. II. Mechanical properties. *J. Appl. Polym. Sci.* **46,** 1723–1735 (1992).

41. Dekkers, M. E. J. & Heikens, D. Journal of Applied Polymer Science Volume 28 issue 12 1983 [doi 10.1002_app.1983.070281220] M. E. J. Dekkers; D. Heikens -- The effect of

interfacial adhesion on the tensile behavior of polystyrene–glass-bead composite.pdf. **28,** 3809–3815 (1983).

42. Mishra, S., Sonawane, S. H. & Singh, R. P. Studies on characterization of nano CaCO3 prepared by thein situ deposition technique and its application in PP-nano CaCO3 composites. *J. Polym. Sci. Part B Polym. Phys.* **43,** 107–113 (2005).

43. Douce, J., Boilot, J.-P., Biteau, J., Scodellaro, L. & Jimenez, A. Effect of filler size and surface condition of nano-sized silica particles in polysiloxane coatings. *Thin Solid Films* **466,** 114–122 (2004).

44. Ji, X. L., Jing, J. K., Jiang, W. & Jiang, B. Z. Tensile modulus of polymer nanocomposites. *Polym. Eng. Sci.* **42,** 983–993 (2002).

45. He, J., Yang, C., Xiong, X. & Jiang, B. Preparation and characterization of monodisperse porous silica microspheres with controllable morphology and structure. *J. Polym. Sci. Part A Polym. Chem.* **50,** 2889–2897 (2012).

46. Adam, N. K. & Livingston, H. K. Nature - contact angle and work of adhesion.pdf.

47. Khoshkava, V. & Kamal, M. R. Effect of surface energy on dispersion and mechanical properties of polymer/nanocrystalline cellulose nanocomposites. *Biomacromolecules* (2013). doi:10.1021/bm400784j

48. Mittal, K. L. in *Adhes. Sci. Technol. SE - 9* (ed. Lee, L.-H.) **9,** 129–168 (Springer US, 1975).

49. Kovacevic, V., Lucic, S., Hace, D. & Cerovecki, Z. Tensile properties of calcium carbonate-reinforced poly(vinyl acetate). *J. Adhes. Sci. Technol.* **10,** 1273–1285 (1996).

50. Lucic, S., Kovacevic´, V. & Hace, D. Mechanical properties of thin films. *Mt* **20A,** 2217–2245 (1989).

51. Kalin, M. & Polajnar, M. The Effect of Wetting and Surface Energy on the Friction and Slip in Oil-Lubricated Contacts. *Tribol. Lett.* **52,** 185–194 (2013).

52. Bedair, T. M., Yu, S. J., Im, S. G., Park, B. J., Joung, Y. K. & Han, D. K. Effects of interfacial layer wettability and thickness on the coating morphology and sirolimus release for drug-eluting stent. *J. Colloid Interface Sci.* **460,** 189–199 (2015).

53. Lee, J. H., Thio, B. J. R., Bae, T. H. & Carson Meredith, J. Role of Lewis Basicity and van der Waals Forces in Adhesion of Silica MFI Zeolites (010) with Polyimides. *Langmuir* **25,** 9101–9107 (2009).

54. Fumagalli, M., Sanchez, F., Boisseau, S. M. & Heux, L. Gas-phase esterification of cellulose nanocrystal aerogels for colloidal dispersion in apolar solvents. *Soft Matter* **9,**

11309–11317 (2013).

55. Junior de Menezes, A., Siqueira, G., Curvelo, a. a S. & Dufresne, A. Extrusion and characterization of functionalized cellulose whiskers reinforced polyethylene nanocomposites. *Polymer (Guildf).* **50,** 4552–4563 (2009).

56. Pereda, M., Kissi, N. El & Dufresne, A. Extrusion of polysaccharide nanocrystal reinforced polymer nanocomposites through compatibilization with poly(ethylene oxide). *ACS Appl. Mater. Interfaces* **6,** 9365–9375 (2014).

57. Strong, B. A. in *Fundam. Compos. Manuf. Mater. methods Appl.* 543–578 (2008).

58. May, C. A. *Epoxy Resins: Chemistry and Technology*. (New York: Dekker, M., 1988).

59. Petrie, E. M. Epoxy Adhesive Formulations. (2006).

60. Air Products. *Epoxy Curing Agents and Modifiers, AR555 Waterborne Epoxy Resin*.

61. Waterborne Epoxy Curatives. High performance. Low emissions. Cost-effective. (2008).

62. Ruiz, M. M., Cavaille, J. Y., Dufresne, A., Graillat, C. & Gerard, J.-F. New waterborne epoxy coatings based on cellulose nanofillers. *Macromol. Symp.* **169,** 211–222 (2001).

63. Kresta, J. in 26–29 (University of Detroit Mercy, 1998).

64. Saralegi, a., Rueda, L., Martin, L., Arbelaiz, a., Eceiza, a. & Corcuera, M. a. From elastomeric to rigid polyurethane/cellulose nanocrystal bionanocomposites. *Compos. Sci. Technol.* **88,** 39–47 (2013).

65. Rueda, L., Saralegui, a., Fernández D'Arlas, B., Zhou, Q., Berglund, L. a., Corcuera, M. a., Mondragon, I. & Eceiza, a. Cellulose nanocrystals/polyurethane nanocomposites. Study from the viewpoint of microphase separated structure. *Carbohydr. Polym.* **92,** 751–757 (2013).

66. Rueda, L., Fernández d'Arlas, B., Zhou, Q., Berglund, L. A., Corcuera, M. A., Mondragon, I. & Eceiza, A. Isocyanate-rich cellulose nanocrystals and their selective insertion in elastomeric polyurethane. *Compos. Sci. Technol.* (2011). doi:10.1016/j.compscitech.2011.09.014

67. Pei, A., Malho, J. M., Ruokolainen, J., Zhou, Q. & Berglund, L. a. Strong nanocomposite reinforcement effects in polyurethane elastomer with low volume fraction of cellulose nanocrystals. *Macromolecules* **44,** 4422–4427 (2011).

68. McGovern, M. E., Kallury, K. M. R. & Thompson, M. Role of Solvent on the Silanization of Glass with Octadecyltrichlorosilane. *Langmuir* **10,** 3607–3614 (1994).

69. Kulkarni, S. a., Mirji, S. a., Mandale, a. B., Gupta, R. P. & Vijayamohanan, K. P. Growth

kinetics and thermodynamic stability of octadecyltrichlorosilane self-assembled monolayer on Si (100) substrate. *Mater. Lett.* **59,** 3890–3895 (2005).

70. Cha, K.-H. & Kim, D.-E. Investigation of the tribological behavior of octadecyltrichlorosilane deposited on silicon. *Wear* **251,** 1169–1176 (2001).

71. Liu, Y., Wolf, L. K. & Messmer, M. C. A Study of Alkyl Chain Conformational Changes in Self-Assembled n -Octadecyltrichlorosilane Monolayers on Fused Silica Surfaces. *Langmuir* **17,** 4329–4335 (2001).

72. Araki, J., Wada, M., Kuga, S. & Okano, T. Flow properties of microcrystalline cellulose suspension prepared by acid treatment of native cellulose. *Colloids Surfaces A Physicochem. Eng. Asp.* **142,** 75–82 (1998).

73. Pullawan, T., Wilkinson, A. N. & Eichhorn, S. J. Influence of magnetic field alignment of cellulose whiskers on the mechanics of all-cellulose nanocomposites. *Biomacromolecules* **13,** 2528–2536 (2012).

74. Yano, H., Sugiyama, J., Nakagaito, A. N., Nogi, M., Matsuura, T., Hikita, M. & Handa, K. Optically Transparent Composites Reinforced with Networks of Bacterial Nanofibers. *Adv. Mater.* **17,** 153–155 (2005).

75. Liao, Y. T. A Study of Glass Fiber-Epoxy Composite Interfaces. *Polym. Compos.* **10,** (2000).

76. Grande, C. J., Torres, F. G., Gomez, C. M., Troncoso, O. P., Canet-Ferrer, J. & Martínez-Pastor, J. Development of self-assembled bacterial cellulose–starch nanocomposites. *Mater. Sci. Eng. C* **29,** 1098–1104 (2009).

77. Liang, C. Y. & Marchessault, R. H. Infrared spectra of crystalline polysaccharides. III. Mercerized cellulose. *J. Polym. Sci.* **43,** 85–100 (1960).

78. Composites, F., Chiang, C. & Koenig, J. L. Chemical Reactions Occurring at the Interface of Epoxy Matrix and Aminosilane Coupling Agents in. **1,** (1980).

79. Scherzer, T. Rheo-optical FTIR spectroscopy of amine cured epoxy resins. *J. Mol. Struct.* **348,** 465–468 (1995).

80. Anirudhan, T. S., Rejeena, S. R. & Tharun, A. R. Preparation, characterization and adsorption behavior of tannin-modified poly(glycidylmethacrylate)-grafted zirconium oxide-densified cellulose for the selective separation of bovine serum albumin. *Colloids Surf. B. Biointerfaces* **93,** 49–58 (2012).

81. Yue, Y., Zhou, C., French, A. D., Xia, G., Han, G., Wang, Q. & Wu, Q. Comparative properties of cellulose nano-crystals from native and mercerized cotton fibers. *Cellulose* **19,** 1173–1187 (2012).

82. Azizi Samir, M. A. S., Alloin, F., Dufresne, A. & Samir, M. A. S. A. Review of recent research into cellulosic whiskers, their properties and their application in nanocomposite field. *Biomacromolecules* **6,** 612–626 (2005).

83. Rämänen, P., Penttilä, P. a., Svedström, K., Maunu, S. L. & Serimaa, R. The effect of drying method on the properties and nanoscale structure of cellulose whiskers. *Cellulose* **19,** 901–912 (2012).

84. George, J., Ramana, K. V., Bawa, A. S. & Siddaramaiah. Bacterial cellulose nanocrystals exhibiting high thermal stability and their polymer nanocomposites. *Int. J. Biol. Macromol.* **48,** 50–57 (2011).

85. Tonoli, G. H. D., Teixeira, E. M., Corrêa, a. C., Marconcini, J. M., Caixeta, L. a., Pereira-Da-Silva, M. a. & Mattoso, L. H. C. Cellulose micro/nanofibres from Eucalyptus kraft pulp: Preparation and properties. *Carbohydr. Polym.* **89,** 80–88 (2012).

86. Kargarzadeh, H., Ahmad, I., Abdullah, I., Dufresne, A., Zainudin, S. Y. & Sheltami, R. M. Effects of hydrolysis conditions on the morphology, crystallinity, and thermal stability of cellulose nanocrystals extracted from kenaf bast fibers. *Cellulose* **19,** 855–866 (2012).

87. Wang, N., Ding, E. & Cheng, R. Thermal degradation behaviors of spherical cellulose nanocrystals with sulfate groups. *Polymer (Guildf).* **48,** 3486–3493 (2007).

88. Johnson, D. J., Compton, D. A. C., Cass, R. S. & Canale, P. L. The characterization of amine-activated function of cure by using TGA / FT-IR epoxies as a. **230,** 293–308 (1993).

89. Tang, L. & Weder, C. Cellulose whisker/epoxy resin nanocomposites. *ACS Appl. Mater. Interfaces* **2,** 1073–1080 (2010).

90. Šturcová, A., Davies, G. R. & Eichhorn, S. J. Elastic modulus and stress-transfer properties of tunicate cellulose whiskers. *Biomacromolecules* **6,** 1055–1061 (2005).

91. Rusli, R. & Eichhorn, S. J. Determination of the stiffness of cellulose nanowhiskers and the fiber-matrix interface in a nanocomposite using Raman spectroscopy. *Appl. Phys. Lett.* **93,** 033111 (2008).

92. Halpin, J. C. & Kardos, J. L. The Halpin-Tsai equations: A review. *Polym. Eng. Sci.* **16,** 344–352 (1976).

93. Srivastava, V. K. Modeling and mechanical performance of carbon nanotube / epoxy resin composites. *Mater. Des.* **39,** 432–436 (2012).

94. Diddens, I., Murphy, B. & Krisch, M. Anisotropic elastic properties of cellulose measured using inelastic X-ray scattering. *Macromolecules* 9755–9759 (2008). doi:10.1021/ma801796u

95. Watt, J. P. & Peselnick, L. Clarification of the Hashin-Shtrikman bounds on the effective elastic moduli of polycrystals with hexagonal, trigonal, and tetragonal symmetries. *J. Appl. Phys.* **51,** 1525 (1980).

96. Christensen, R. M. in *Mech. Compos. Mater.* (DOVER PUBLICATIONS, INC., 1979).

97. van Krevelen, D. W., and te Nijenhuis, K. in (Elsevier Science & Technology, 2009).

98. Kalashnikova, I., Bizot, H., Cathala, B. & Capron, I. New pickering emulsions stabilized by bacterial cellulose nanocrystals. *Langmuir* **27,** 7471–7479 (2011).

99. Tohver, V., Smay, J. E., Braem, a, Braun, P. V & Lewis, J. a. Nanoparticle halos: a new colloid stabilization mechanism. *Proc. Natl. Acad. Sci. U. S. A.* **98,** 8950–8954 (2001).

100. Zhang, F., Long, G. G., Jemian, P. R., Ilavsky, J., Milam, V. T. & Lewis, J. A. Quantitative Measurement of Nanoparticle Halo Formation around Colloidal Microspheres in Binary Mixtures. *Langmuir* **24,** 6504–6508 (2008).

101. Miller, A. P. Lange's Handbook of Chemistry. *Am. J. Public Heal. Nations Heal.* **31,** 1324 (1941).

102. Xu, S., Girouard, N., Schueneman, G., Shofner, M. L. & Meredith, J. C. Mechanical and thermal properties of waterborne epoxy composites containing cellulose nanocrystals. *Polymer (Guildf).* **54,** 6589–6598 (2013).

103. Landry, Veronic, Alemdar, Ayse, Blanchet & Pierre. Nanocrystalline Cellulose: Morphological, Physical, and Mechanical Properties. *For. Prod. J.* **61,** 104–112 (2011).

104. Cranston, E. D. & Gray, D. G. Birefringence in spin-coated films containing cellulose nanocrystals. *Colloids Surfaces A Physicochem. Eng. Asp.* **325,** 44–51 (2008).

105. Augerson, C. C. & Messinger II, J. M. Controlling the refractive index of epoxy adhesives with acceptable yellowing after aging. *J. Am. Inst. Conserv.* **32,** 311–314 (1993).

106. Yeo, G. A. & Ford, T. A. Ab initio molecular orbital calculations of the infrared spectra of hydrogen bonded complexes of water, ammonia, and hydroxylamine. Part 6. The infrared spectrum of the water-ammonia complex. *Can. J. Chem.* **69,** 632–637 (1991).

107. Ben Mabrouk, A., Rei Vilar, M., Magnin, A., Belgacem, M. N. & Boufi, S. Synthesis and characterization of cellulose whiskers/polymer nanocomposite dispersion by mini-emulsion polymerization. *J. Colloid Interface Sci.* **363,** 129–36 (2011).

108. Cui, Z. G., Cui, C. F., Zhu, Y. & Binks, B. P. Multiple phase inversion of emulsions stabilized by in situ surface activation of CaCO \n3 nanoparticles via adsorption of fatty acids. *Langmuir* **28,** 314–320 (2012).

109. Ansari, F., Galland, S., Johansson, M., Plummer, C. J. G. & Berglund, L. A. Cellulose nanofiber network for moisture stable, strong and ductile biocomposites and increased epoxy curing rate. *Compos. Part A Appl. Sci. Manuf.* **63,** 35–44 (2014).

110. Capadona, J. R., Van Den Berg, O., Capadona, L. A., Schroeter, M., Rowan, S. J., Tyler, D. J. & Weder, C. A versatile approach for the processing of polymer nanocomposites with self-assembled nanofibre templates. *Nat. Nanotechnol.* **2,** 765–769 (2007).

111. Mezzenga, R., Schurtenberger, P., Burbidge, A. & Michel, M. Understanding foods as soft materials. *Nat. Mater.* **4,** 729–740 (2005).

112. Fennel, Evans D., Wennerström, H. *The colloidal domain : where physics, chemistry, biology, and technology meet*. (VCH Publishers, 1994).

113. Hiernenz, P. *Principles of Colloid and Surface Chemistry*. (M. Dekker, 1986).

114. Zhang, Y., Wu, J., Wang, H., Meredith, J. C. & Behrens, S. H. Stabilization of Liquid Foams through the Synergistic Action of Particles and an Immiscible Liquid**. doi:10.1002/anie.201405816

115. Binks, B. P. Particles as surfactants—similarities and differences. *Curr. Opin. Colloid Interface Sci.* (2002). doi:10.1016/S1359-0294(02)00008-0

116. Calvo, E., Bravo, R., Amigo, A. & Gracia-Fadrique, J. Dynamic surface tension, critical micelle concentration, and activity coefficients of aqueous solutions of nonyl phenol ethoxylates. *Fluid Phase Equilib.* **282,** 14–19 (2009).

117. Pickering, S. U. Emulsions. *J. Chem. Soc.* 2001–2021 (1907).

118. Ramsden, W. Separation of Solids in the Surface-Layers of Solutions and 'Suspensions' (Observations on Surface-Membranes, Bubbles, Emulsions, and Mechanical Coagulation)-- Preliminary Account. *Proc. R. Soc. London* **72,** 156–164 (1903).

119. Tasset, S., Cathala, B., Bizot, H. & Capron, I. Versatile cellular foams derived from CNC-stabilized Pickering emulsions. *RSC Adv.* **4,** 893–898 (2014).

120. Hu, Z., Ballinger, S., Pelton, R. & Cranston, E. D. Surfactant-enhanced cellulose nanocrystal Pickering emulsions. *J. Colloid Interface Sci.* **439,** 139–148 (2015).

121. Lif, A., Stenstad, P., Syverud, K., Nydén, M. & Holmberg, K. Fischer-Tropsch diesel emulsions stabilised by microfibrillated cellulose and nonionic surfactants. *J. Colloid Interface Sci.* **352,** 585–92 (2010).

122. Zoppe, J. O., Venditti, R. A. & Rojas, O. J. Pickering emulsions stabilized by cellulose nanocrystals grafted with thermo-responsive polymer brushes. *J. Colloid Interface Sci.* **369,** 202–209 (2012).

123. Tang, J., Lee, M. F. X., Zhang, W., Zhao, B., Berry, R. M. & Tam, K. C. Dual responsive pickering emulsion stabilized by poly[2-(dimethylamino) ethyl methacrylate] grafted cellulose nanocrystals. *Biomacromolecules* (2014). doi:10.1021/bm500663w

124. Gao, S., Moran, K., Xu, Z. & Masliyah, J. Role of bitumen components in stabilizing water-in-diluted oil emulsions. *Energy and Fuels* **23,** 2606–2612 (2009).

125. DOW. *Crystallization of Liquid Epoxy Resins*. (2007).

126. Surface and Interfacial Tension of Liquids Exponential Business and Technologies Company. 1–2 at <www.ebatco.com>

127. Abbott, J. R. & Higgins, B. G. Surface tension of a curing epoxy. *J. Polym. Sci. Part A Polym. Chem.* (1988). doi:10.1002/pola.1988.080260724

128. Wang, H., Singh, V. & Behrens, S. H. Image charge effects on the formation of pickering emulsions. *J. Phys. Chem. Lett.* (2012). doi:10.1021/jz300909z

129. Shanmugam Nagendiran, Muthukaruppan Alagar, I. H. Octasilsesquioxane reinforced DGEBA and TGDDM epoxy nanocomposites: Characterization of Thermal, Dielectric and Morphological properties Shanmugam. **XXXIII,** 81–87 (2012).

130. Liming Zong, Rensheng Sun, Leo C. Kempel, and M. C. H. Dielectric Properties of Epoxy Resins at Different Extents of Cure at 2.45 GHz. 3–6

131. Davarpanah, L. & Vahabzadeh, F. Formation of oil-in-water (O/W) pickering emulsions via complexation between b-cyclodextrin and selected organic solvents. *Starch/Staerke* **64,** 898–913 (2012).

132. Alvarez, G., Poteau, S., Argillier, J. F., Langevin, D. & Salager, J. L. Heavy oil-water interfacial properties and emulsion stability: Influence of dilution. *Energy and Fuels* **23,** 294–299 (2009).

133. Yang, J., Zhao, J. J., Han, C. R., Duan, J. F., Xu, F. & Sun, R. C. Tough nanocomposite hydrogels from cellulose nanocrystals/poly(acrylamide) clusters: Influence of the charge density, aspect ratio and surface coating with PEG. *Cellulose* **21,** 541–551 (2014).

134. Way, A. E., Hsu, L., Shanmuganathan, K., Weder, C. & Rowan, S. J. PH-responsive cellulose nanocrystal gels and nanocomposites. *ACS Macro Lett.* **1,** 1001–1006 (2012).

135. Eyley, S. & Thielemans, W. Surface modification of cellulose nanocrystals. *Nanoscale* **6,** 7764–7779 (2014).

136. Kargarzadeh, H., M. Sheltami, R., Ahmad, I., Abdullah, I. & Dufresne, A. Cellulose nanocrystal: A promising toughening agent for unsaturated polyester nanocomposite. *Polymer (Guildf).* **56,** 346–357 (2015).

137. Moore, M. G. The Economic Benefits of the U.S. Polyurethanes Industry 2013. (2014).

138. Sen, R., Zhao, B., Perea, D., Itkis, M. E., Hu, H., Love, J., Bekyarova, E. & Haddon, R. C. Preparation of single-walled carbon nanotube reinforced polystyrene and polyurethane nanofibers and membranes by electrospinning. *Nano Lett.* **4,** 459–464 (2004).

139. Xia, H. & Song, M. Preparation and characterization of polyurethane–carbon nanotube composites. *Soft Matter* **1,** 386 (2005).

140. Liff, S. M., Kumar, N. & McKinley, G. H. High-performance elastomeric nanocomposites via solvent-exchange processing. *Nat. Mater.* **6,** 76–83 (2007).

141. Cai, D., Yusoh, K. & Song, M. The mechanical properties and morphology of a graphite oxide nanoplatelet/polyurethane composite. *Nanotechnology* **20,** 085712 (2009).

142. Meier-Westhues, U. in 52–55 (Vincentz Network, 2007).

143. *Wood Floor Coating Technology Comparison Bayer MaterialScience publication #20937*. (Bayer MaterialScience, 2012).

144. Ono, H.-K., Jones, F. N. & Peter, S. Relative Reactivity of Isocyanate Groups of Isophorone Diisocyanate. Unexpected High Reactivity of the Secondary Isocyanate Group. *J. Polym. Sci. Polym. Lett. Ed.* **23,** 509–515 (1985).

145. Götz, H., Beginn, U., Bartelink, C. F., Grünbauer, H. J. M. & Möller, M. Preparation of isophorone diisocyanate terminated star polyethers. *Macromol. Mater. Eng.* (2002). doi:10.1002/1439-2054(20020401)287:4<223::AID-MAME223>3.0.CO;2-Z

146. Marschner, M. & Ritter, W. 13C NMR studies on the relative reactivity of isocyanate groups of isophorone diisocyanate isomers. **1852,** 1843–1852 (1990).

147. Lomölder, R., Plogmann, F. & Speier, P. Selectivity of isophorone diisocyanate in the urethane reaction influence of temperature, catalysis, and reaction partners. *J. Coatings Technol.* (1997). doi:10.1007/BF02696250

148. Girouard, N., Schueneman, G. T., Shofner, M. L. & Meredith, J. C. Exploiting colloidal interfaces to increase dispersion, performance, and pot-life in cellulose nanocrystal/waterborne epoxy composites. *Polymer (Guildf).* **68,** 111–121 (2015).

149. Gårdebjer, S., Bergstrand, A., Idström, A., Börstell, C., Naana, S., Nordstierna, L. & Larsson, A. Solid-state NMR to quantify surface coverage and chain length of lactic acid modified cellulose nanocrystals, used as fillers in biodegradable composites. *Compos. Sci. Technol.* **107,** 1–9 (2015).

150. Abdalla, A. I. & Ragab, Y. A. Esterification of Shambat Cotton Cellulose by (octanoyl (C8), decanoyl (C10) and lauroyl (C12) acid chlorides using N,N-Dimethyl Acetamide/

Lithium Chloride Solvent System. **1,** 101–112 (2014).

151. Wu, X., Moon, R. J. & Martini, A. Crystalline cellulose elastic modulus predicted by atomistic models of uniform deformation and nanoscale indentation. *Cellulose* **20,** 43–55 (2013).

152. Park, S., Baker, J. O., Himmel, M. E., Parilla, P. A. & Johnson, D. K. Cellulose crystallinity index: measurement techniques and their impact on interpreting cellulase performance. *Biotechnol. Biofuels* **3,** 10 (2010).

153. Park, S., Johnson, D. K., Ishizawa, C. I., Parilla, P. a. & Davis, M. F. Measuring the crystallinity index of cellulose by solid state 13C nuclear magnetic resonance. *Cellulose* **16,** 641–647 (2009).

154. Larsson, P. T., Wickholm, K. & Iversen, T. A CP / MAS 13C NMR investigation of molecular ordering in celluloses. *Carbohydr. Res.* **302,** 19–25 (1997).

155. Cho, G., Natansohn, A., Ho, T. & Wynne, K. J. Phase Structure of Poly (dimethylsiloxane-urea-urethane) - Segmented Copolymers as Observed by Solid-State Nuclear Magnetic Resonance Spectra. *Macromolecules* 2563–2569 (1996).

156. Peng, Y., Gardner, D. J., Han, Y., Kiziltas, A., Cai, Z. & Tshabalala, M. a. Influence of drying method on the material properties of nanocellulose I: Thermostability and crystallinity. *Cellulose* **20,** 2379–2392 (2013).

157. Rao, Y., Munro, J., Ge, S. & Garcia-Meitin, E. PU elastomers comprising spherical nanosilicas: Balancing rheology and properties. *Polymer (Guildf).* (2014). doi:10.1016/j.polymer.2014.09.065

158. Cheng, Q., Wang, S. & Rials, T. G. Poly(vinyl alcohol) nanocomposites reinforced with cellulose fibrils isolated by high intensity ultrasonication. *Compos. Part A Appl. Sci. Manuf.* **40,** 218–224 (2009).

159. Chen, Y., Zhou, S., Yang, H. & Wu, L. Structure and properties of polyurethane/nanosilica composites. *J. Appl. Polym. Sci.* **95,** 1032–1039 (2005).

160. Wu, J., Zhang, K., Girouard, N. & Meredith, J. C. Facile Route to Produce Chitin Nano fi bers as Precursors for Flexible and Transparent Gas Barrier Materials. *Biomacromolecules* (2014).

161. Pérez-Gramatges, A., Matheus, C. R. V, Lopes, G., Da Silva, J. C. & Nascimento, R. S. V. Surface and interfacial tension study of interactions between water-soluble cationic and hydrophobically modified chitosans and nonylphenol ethoxylate. *Colloids Surfaces A Physicochem. Eng. Asp.* **418,** 124–130 (2013).

162. Yu, L. Yu., Shen, H. M. & Xu, Z. L. Interfacial Properties of Chitosan and Nonylphenol

Polyoxyethylene Ether. *J. Appl. Phys.* **113,** 1763–1772 (2009).

163. Liu, P., Sehaqui, H., Tingaut, P., Wichser, A., Oksman, K. & Mathew, A. P. Cellulose and chitin nanomaterials for capturing silver ions (Ag+) from water via surface adsorption. *Cellulose* **21,** 449–461 (2014).

164. Dubois, C., Desilets, S., Ait-Kadi, A. & Tanguy, P. Bulk polymerization of hydroxyl terminated polybutadiene (HTPB) with tolylene diisocyanate (TDI): a kinetics study using 13C-NMR spectroscopy. *J. Appl. Polym. Sci.* **58,** 827–834 (1995).